Interaction of sialylated glycans with Siglec receptors on suppressive myeloid cells

Inauguraldissertation

zur

Erlangung der Würde eines Doktors der Philosophie

vorgelegt der

Philosophisch-Naturwissenschaftlichen Fakultät

der Universität Basel

von

Ronja Wieboldt

Basel, 2023

Genehmigt von der Philosophisch-Naturwissenschaftlichen Fakultät auf Antrag von

Erstbetreuer: Prof. Dr. Heinz Läubli

Zweitbetreuer: Prof. Dr. Christoph Hess

Externer Experte: Dr. Matthew Macauley

Basel, den 19.09.2023

Prof. Dr. Marcel Mayor

Dekan der Philosophisch-Naturwissenschaftlichen Fakultät

SUMMARY

In spite of the impressive advances in cancer immunotherapy that have entered the clinics, only a subset of patients benefits from current treatment strategies and many fail to achieve a durable response. Most treatment regimens are T cell-centric and neglect the role of the suppressive tumor microenvironment (TME) that drives various resistance mechanisms. Myeloid cells are the most abundant immune cells found in the TME and include immunosuppressive subsets such as myeloid-derived suppressor cells (MDSCs). In addition, overexpression of sialoglycans within the TME can drive tumor progression via various mechanisms. Hypersialylation can, for example, enhance immune evasion via interaction with sialic acid-binding immunoglobulin-like lectin (Siglec) receptors on tumor-infiltrating immune cells. Here, we tested the role of sialic acid on MDSCs and their interaction with Siglec receptors. We found that MDSCs derived from the blood of lung cancer patients and tumor-bearing mice strongly express inhibitory Siglec receptors. In murine cancer models of emergency myelopoiesis, Siglec-E knockout on myeloid cells resulted in prolonged survival and increased infiltration of activated T cells. Targeting suppressive myeloid cells by blocking Siglec receptors or desialylation led to a strong reduction of their suppressive potential. We further identified CCL2 as a mediator involved in T cell suppression upon the interaction of sialoglycans and Siglec receptors on MDSCs. Our results provide mechanistic insights into how sialylated glycans inhibit anti-cancer immunity by facilitating CCL2 expression. This interaction marks a new potential target to limit the suppressive capacity of the TME and induce anti-tumor response.

TABLE OF CONTENTS

1 INTRODUCTION

1.1 Cancer immunology

Cancer is defined as the uncontrolled growth of abnormal cells and represents one of the most prevalent causes of death worldwide (Hassanpour & Dehghani, 2017). This genetic disease is caused by an accumulation of genetic changes that can affect tumor suppressor genes, proto-oncogenes, and DNA repair genes, leading to malignant transformation of normal cells (Hassanpour & Dehghani, 2017). Although tumorigenesis is highly diverse between tumor types and patients, it relies on common capabilities of cells necessary for malignant transformation, which are summarized as hallmarks of cancer (Hanahan, 2022). These include the evasion of immune destruction and tumor-promoting inflammation, which on first glance seem to be contradictory characteristics of immune cells during tumorigenesis. The research field of cancer immunology studies the interaction between the immune system and cancer cells.

1.1.1 Immunosurveillance and immunoediting

Even though alterations in the genome and epigenome of cells can support malignant transformation, they can also increase recognition by immune cells by marking them as foreign. The immune system plays a key role in protecting the host against infections by distinguishing "self" from "non-self", but its relevance in cancer has been controversial for decades given the fact that most cancers are inherent "self" and can grow in the presence of the immune system (Schreiber et al., 2011a). More than 60 years ago, Burnet and Thomas hypothesized that there must be an immunological mechanism that monitors and protects organisms against neoplastic diseases (Burnet, 1957). This led to the concept of tumor immunosurveillance, but experimental proof was lacking. It was only in the 1990s, when the usage of genetically modified mouse strains in combination with tumor transplantation and carcinogen-induced tumor models highlighted the importance of the immune system for tumorigenesis. Various publications demonstrate the enhanced susceptibility of immunodeficient mice to tumor formation. For example, a lack of interferon-γ (IFN-γ), perforin, or lymphocytes increased the appearance of chemically induced and spontaneous tumor formation (Dighe et al., 1994; Shankaran et al., 2001; Street et al., 2001).

In humans, supporting evidence for the existence of immunosurveillance was observed in patients with primary immunodeficiencies and after transplantation. Both showed a higher risk to develop cancers, including Kaposi's sarcoma, non-Hodgkin's lymphoma and cutaneous squamous cell carcinomas (Chockalingam et al., 2015; Hernández-Ramírez et al., 2017; Vajdic & Van Leeuwen, 2009). Nevertheless, these cancers are often virally-induced

and can arise from a lack of viral-control rather than defects in immunosurveillance of malignant cells (Vajdic & Van Leeuwen, 2009). Additionally, the presence of infiltrating lymphocytes such as CD8+ T cells, dendritic cells (DCs) and natural killer (NK) cells can be a good prognostic marker for survival of cancer patients indicating a role for innate and adaptive immunity in tumorigenesis (Galon et al., 2006; Pagès et al., 2010; Senovilla et al., 2012).

Based on the immunosurveillance theory, the broader concept of immunoediting was elucidated in 2002, which describes the paradox role of the immune system in defeating and promoting cancer growth. Immunoediting consists of 3 phases: elimination, equilibrium, and escape (Dunn et al., 2002) (Fig. 1.1).
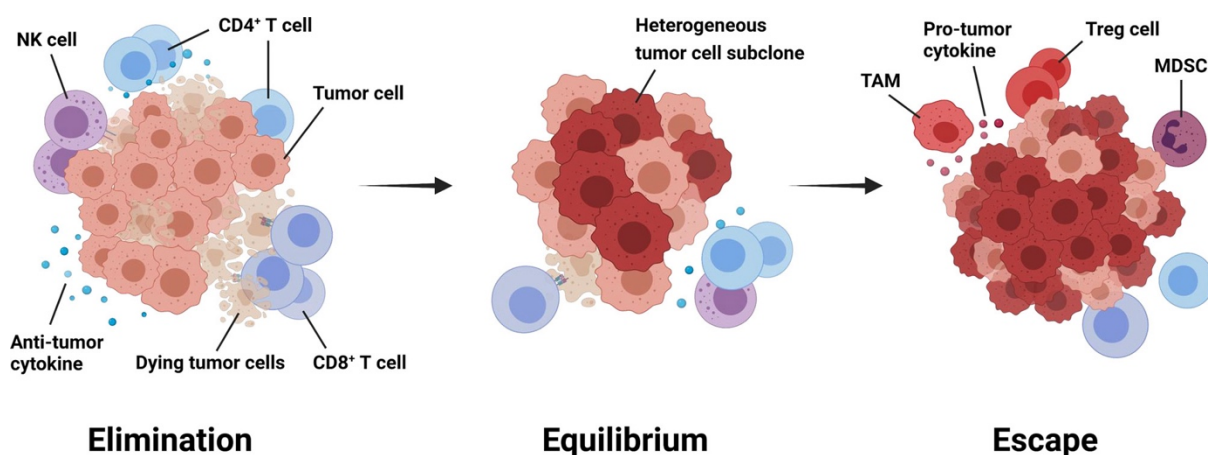

Figure 1.1: Principle of immunoediting

Immunoediting is divided into three phases: elimination, equilibrium, and escape. The immune system can detect and destroy cancer cells by immunosurveillance (=elimination). Immune pressure can lead to immune editing and generation of clones that avoid immune detection in the equilibrium phase. During the escape phase, less immunogenic clones can grow out and completely evade immunosurveillance. From (Zhu & Yu, 2022), based on (Schreiber et al., 2011b)

In the elimination phase, tumor cells are detected and destroyed by the adaptive and innate immune system, including NK and T cells, before clinical detection of the tumor. During the equilibrium phase, immune pressure can lead to immune editing of cancer cells, resulting in new tumor cell subclones that can be less tumorigenic or more resistant to immune destruction. This can be facilitated by major histocompatibility complex (MHC) molecules or antigen loss, secretion of immune-suppressive cytokines (e.g., TGF-β, Interleukin-10 (IL-10)) or upregulation of inhibitory receptors and ligands (e.g., PD-1/PD-L1) (Mittal et al., 2014; Schreiber et al., 2011b). In the escape phase, tumor growth is no longer restricted by the immune system. Subclones with strong immune escape capability can prevent recognition and destruction by the immune system. In addition, suppressive cells in the tumor

microenvironment (TME), including tumor-associated macrophages (TAMs), myeloid-derived suppressor cells (MDSCs), and regulatory T cells (Treg), can further hinder immune cell response and favor cancer growth (Mittal et al., 2014). Hence, a high abundance of these cells has a negative prognostic value for cancer patients (Senovilla et al., 2012).

This concept of immunoediting is observed in various patients and preclinical models. For example, tumors from immunocompetent wild type and immunodeficient mice showed qualitative differences when tumor cell lines generated from primary tumors were transplanted into naïve recipients (Schreiber et al., 2011b; Shankaran et al., 2001). Tumors from immunodeficient mice were highly immunogenic ("unedited") upon transfer and could be eliminated by immunocompetent mice. However, tumors from wild type mice were less immunogenic ("edited") and grew in all recipients, indicating that the immune system controls immunogenicity and tumor quality. Exploiting the dynamics of immunoediting by shifting from tumor escape to tumor detection and destruction is a promising approach that has given rise to many immune-based cancer treatments.

1.1.2 Cancer immunotherapy and resistance mechanisms

Various strategies aim to exploit the patient's immune system to treat cancer, including monoclonal antibodies, small molecules, cancer vaccines, oncolytic viruses, and adoptive cell transfer (Liu et al., 2022). In 1996, it was first described that blockade of cytotoxic T lymphocyte-associated protein 4 (CTLA-4) using an antibody could eliminate tumors in mice (Leach et al., 1996). CTLA-4 as well as programed death 1 (PD-1) are important inhibitory receptors on T cells maintaining peripheral self-tolerance and activating immune response. The discovery of these immune checkpoints led to the development and commercialization of various monoclonal antibodies targeting CTLA-4 and the PD-1/PD-L1 axis, which were successfully used to treat a variety of tumor types (e.g., advanced melanoma) and led to a durable response in a subset of patients (Couzin-Frankel, 2013) (Fig. 1.2).

Although cancer immunotherapy is a promising treatment frequently used in the clinic, only a subset of patients responds and many relapse over time (Liu et al., 2022). Factors influencing therapy success include patient characteristics (age, gender, hormones and the gut microbiome), genomic factors (tumor mutation burden, microsatellite instability), and tumor heterogeneity (Dobosz et al., 2022). An important hurdle in cancer immunotherapy is initial (primary) and acquired therapy resistance, which is facilitated via tumor intrinsic and extrinsic mechanisms (Sharma et al., 2017). Tumor cell intrinsic mechanisms include the loss of antigen presentation and antigens as well as resistance to T cells (Sharma et al., 2017). The TME shapes and influences tumor cell extrinsic factors such as the presence of immunosuppressive

cells, upregulation of inhibitory immune checkpoints (CTL-4, PD-1) and lack and exhaustion of T cells. The TME plays an important role in tumor progression and resistance to immunotherapy (Kirchhammer et al., 2022). Cancer cells are surrounded by various other cell types including innate and adaptive immune cells, fibroblasts, cell matrix components, and vascular cells (Labani-Motlagh et al., 2020). These cells produce various soluble factors such as cytokines, chemokines, growth factors, reactive oxygen, and nitrogen species. Additionally, the TME can induce hypoxic conditions and a low pH value, which can favor tumor growth (Labani-Motlagh et al., 2020).
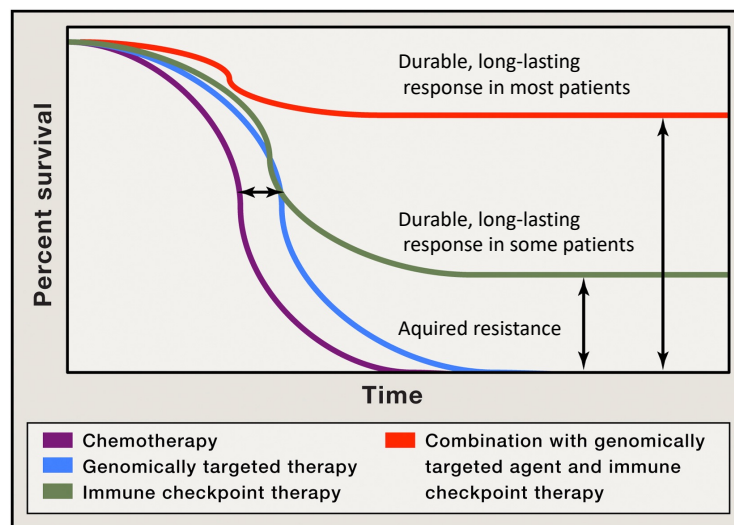

Figure 1.2: Predicted response to immunotherapy

A simplified view of cancer patient survival curves upon different cancer treatment regimes. Genomically targeted agents (blue) can prolong median overall survival compared to conventional therapies like chemotherapy (purple) but lack a durable response. Immune checkpoint blockade and other immunotherapies can not only lead to prolonged survival but also induce lasting responses in a subset of patients (green). A combination of therapies might increase the response rate by synergistic activity (red). Adapted from (Sharma & Allison, 2015a)

The TME is a complex and heterogenous milieu that is made up of plastic cells that frequently change their phenotype and function (Greten & Grivennikov, 2019). Depending on the composition, the TME can be classified as hot, excluded, immunosuppressed, and cold (Galon & Bruni, 2019). On one hand, hot tumors are highly infiltrated by T cells, have high immunogenicity, high mutational burden, high PD-1/PD-L1 expression, and are often good responders to immune checkpoint inhibitor therapy. Excluded and immunosuppressed tumors are altered, intermediate tumor types that have moderate numbers of mutations, T cells at the periphery of the tumor, and are surrounded by suppressive cells. On the other hand, cold tumors show no T cell infiltration, have a low mutational burden, and are poor immune checkpoint responders.

Thus, the composition of the TME influences therapy success and should be considered before choosing a treatment regime (Galon & Bruni, 2019). Understanding current limitations is essential to improve treatment regimens and increase response rates to cancer immunotherapy. Combination of immunotherapy with other treatment regimens including modulators of the TME might lead to prolonged survival (Kirchhammer et al., 2022; Sharma & Allison, 2015b) (Fig. 1.2).

1.1.3 Myeloid-derived suppressor cells

Myeloid cells are the most abundant immune cells found in the TME. This heterogenous and plastic family of cells includes closely related cells that differentiate from common myeloid progenitors and can change their phenotype and function due to stimuli from the surrounding microenvironment (Fig. 1.3) (Goswami et al., 2023).
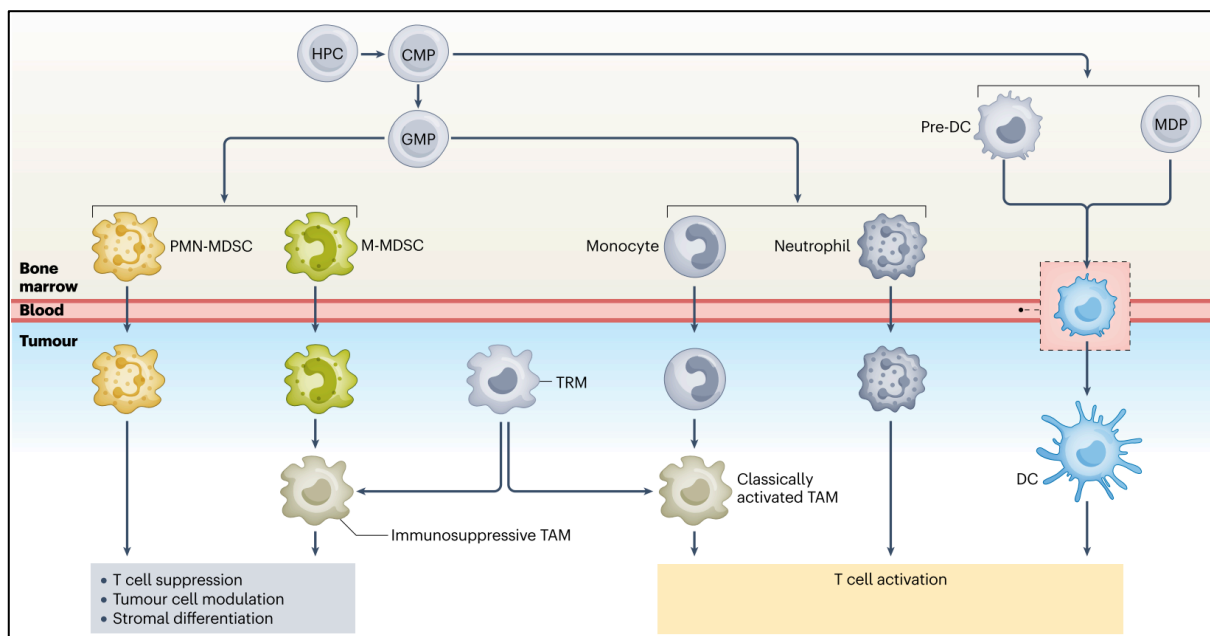
Figure 1.3: Myeloid cells in cancer

Myeloid cells are closely related and stem from common myeloid precursors (CMP) which can give rise to granulocyte–macrophage progenitors (GMPs) and monocyte dendritic cell precursors (MDPs). In normal conditions, myeloid cells mainly consist of dendritic cells (DCs), neutrophils and monocytes, which are involved in T cell activation. In the context of cancer, myeloid cells can be pathologically activated, giving rise to myeloid-derived suppressor cells (MDSCs) and tumor-associated macrophages (TAMs) which are involved in T cell suppression and tumor cell modulation. MDSCs can be subdivided into monocytic myeloid-derived suppressor cells (mMDSCs) and polymorphonuclear myeloid-derived suppressor cells (PMN-MDSCs). From (Barry et al., 2023). *HPC, hematopoietic progenitor cell; TRM, tissue-resident macrophages*

Under healthy conditions, myeloid cells consist of macrophages, monocytes, DCs, and granulocytes (e.g., neutrophiles, eosinophiles, basophiles and mast cells) and drive innate immune response including T cell activation (Deng & Fleming, 2022). Upon stimulation (e.g., by malignant cells, pathogens, tissue damage), myeloid cells can be activated and expanded. This process is called emergency myelopoiesis and allows a quick immune response that can drive tumor and pathogen detection and tissue repair (Yang et al., 2020). Persistent stimulation and myeloid growth factor signaling can lead to aberrant myelopoiesis in the context of chronic infection, autoimmunity, and cancer causing accumulation of different types of myeloid cells. Under pathological conditions, granulocytic and monocytic precursors can give rise to immature immunosuppressive cells and tumor cells can recruit myeloid cells to the TME via direct and indirect interactions. Pathologically activated myeloid cells include tumor-promoting TAMs, DCs, tumor-associated neutrophils (TANs), and MDSCs and convey immune suppression via inhibition of T cells and modulation of tumor cells (Fig. 1.3).

The term "myeloid-derived suppressor cell" was first proposed in 2007 to describe a heterogenous group of immature cells from the myeloid lineage that conveys immunosuppression and favors cancer growth (Gabrilovich et al., 2007). MDSCs are found in a variety of diseases including chronic infections and inflammations, autoimmune diseases, and cancer (Yang et al., 2020). For example, MDSCs were significantly increased in the blood of solid cancer patients compared to healthy controls (Cassetta et al., 2020). Across various solid tumors, increased numbers of MDSCs in patients correlated with reduced survival, poor outcome, and therapy resistance, making MDSCs an interesting prognostic biomarker (Ai et al., 2018; Law et al., 2020; Zhang et al., 2016).

MDSCs can be subdivided into monocytic MDSCs (mMDSCs) and granulocytic or polymorphonuclear MDSCs (gMDSCs or PMN-MDSCs), which are classified according to their monocytic or granulocytic myeloid cell lineage markers, respectively (Cassetta et al., 2019). First guidelines that aimed to harmonize the nomenclature and identification of MDSCs were published in 2016 by Bronte et al. but up to date no specific human MDSC marker is known (Bronte et al., 2016). Predominantly, human MDSCs are phenotypically identified as $CD33^+CD11b^+HLA-DR^{low/-}$ which can be further subdivided into $CD15^+CD14^-$ gMDSCs, $CD15^-CD14^+$ mMDSCs and $CD15^-CD14^-$ early-stage MDSCs (eMDSCs) (Cassetta et al., 2019; Vanhaver et al., 2021). All murine MDSCs express Gr1 and CD11b and can be further subdivided into $Ly6G^+Ly6C^{low}$ gMDSCs and $Ly6C^{high}$ mMDSCs (Bronte et al., 2016). In addition, recent publications highlight the possible relevance of other phenotypic markers including CD84 to identify human and murine MDSCs (Alshetaiwi et al., 2020; Vanhaver et al., 2021). Nevertheless, MDSCs are closely related to other myeloid cells and share the same

expression markers, which makes the identification of MDSCs based on their phenotypic characteristics alone impossible (Dysthe & Parihar, 2020). In order to reliably identify MDSCs, it is necessary to assess their immunosuppressive potential via additional functional analysis (Cassetta et al., 2019).

Although the phenotypic markers differ, murine and human MDSCs have similar functions. Most relevantly, MDSCs are involved in immunosuppression of innate and adaptive cells and help to generate a suppressive TME. Various different mechanisms of immunosuppression are described, including cell-to-cell contact, soluble mediators, and metabolites (Fig. 1.4) (Yang et al., 2020).
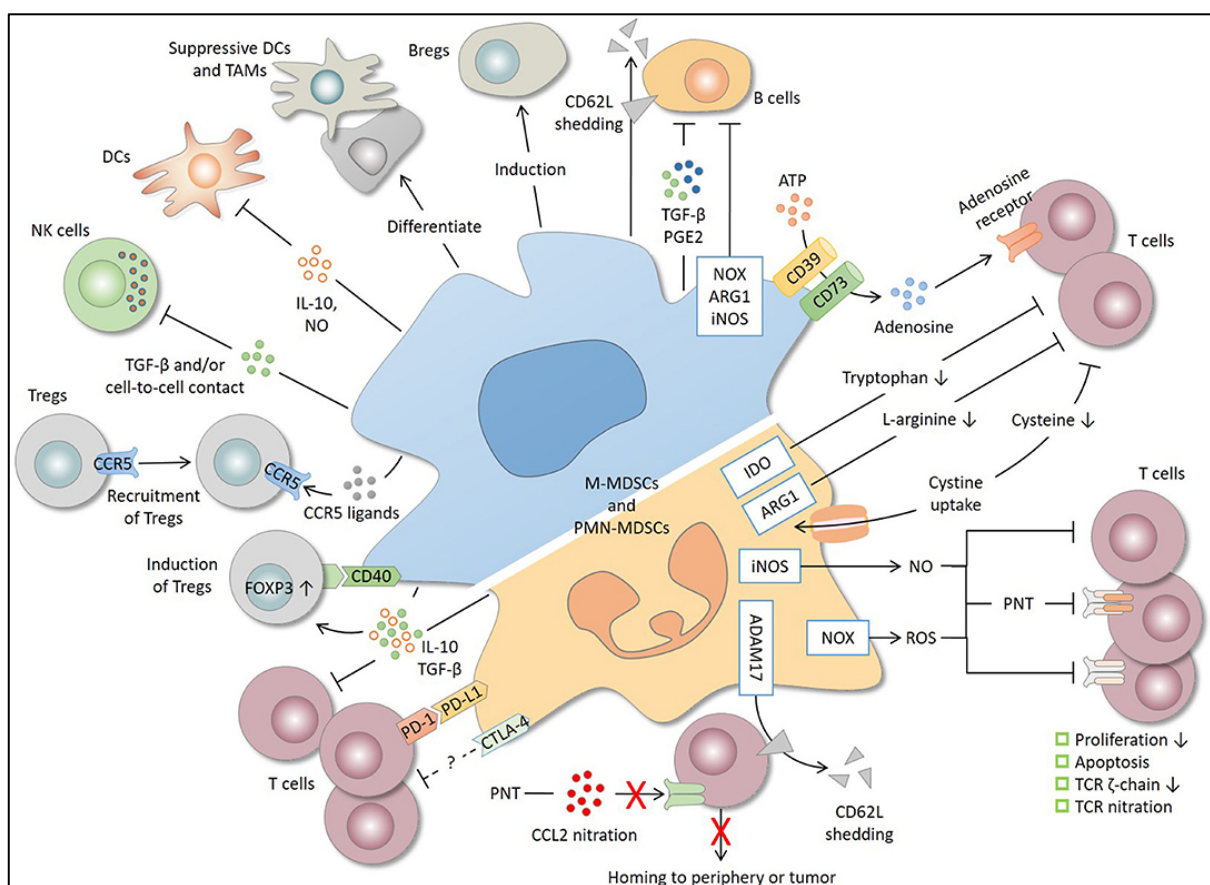
Fig. 1.4: Suppressive mechanisms of MDSCs
Overview of mechanisms and target cells of M-MDSCs and PMN-MDSCs to generate immunosuppression in the tumor microenvironment. From (Yang et al., 2020).

The mechanism of immunosuppression is highly context- and cancer-dependent and can affect various immune cell types including NK cells, DCs, B cells, and cytotoxic T cells. In the periphery, MDSCs mainly act via antigen-specific and contact-dependent interactions. Among others, this results in the release of reactive oxygen species (ROS), nitric oxide (NO), and immunosuppressive cytokines (IL-10, IL-6), inhibition of T cell activity and induction of

Tregs (Kumar et al., 2016). Within the TME, MDSCs are more potent and induce nonspecific suppression by creating an inflammatory and hypoxic environment via ROS and NO production, upregulation of inhibitory ligands (e.g., PD-L1) and release of chemoattractants for Tregs (CCR5 ligands) (Kumar et al., 2016; Yang et al., 2020). In addition to their immunosuppressive function, MDSCs can directly drive tumor progression by influencing neovascularization, invasion and metastasis via secretion of Vascular Endothelial Growth Factor (VEGF), matrix metalloproteinases (MMPs), and transforming growth factor β (TGF-β) (Umansky et al., 2016). Although MDSCs are involved in various pro-tumorigenic mechanisms, a key feature is their ability to inhibit T cell response which is currently the gold standard to assess MDSC function (Bronte et al., 2016). The effects on cytotoxic T cells are vast. For example, MDSCs can cause (i) deprivation of amino acids (arginine, cysteine) necessary for T cell proliferation and activity, (ii) nitration of T cell receptors (TCRs) and apoptosis initiation via NO and ROS, (iii) a downregulation of TCR ζ-chains and (iv) an increased expression of ligands and cytokines downregulating T cell proliferation and homing (Umansky et al., 2016). MDSCs can not only inhibit the function of cytotoxic T cells, but also limit their accumulation within the TME (Zhang et al., 2016).

MDSCs greatly contribute to the suppressive TME, hindering immune infiltration and therapy success. Thus, targeting MDSCs is a promising approach for cancer therapy to generate a more permissive TME (T. Li et al., 2021; Wu et al., 2022). Various strategies aim to target MDSCs, including (i) inhibition of MDSC immunosuppression, (ii) blockade of migration and accumulation, (iii) differentiating MDSCs and (iv) depletion of MDSCs (Barry et al., 2023; Umansky et al., 2016). For example, MDSCs can be directly eliminated by low-dose chemotherapy (gemcitabine, 5-fluorouracil), leading to an increased anti-tumor effect *in vivo* and a reduction of MDSCs in colon cancer patients (Eriksson et al., 2016; Vincent et al., 2010). Administration of the small molecule tyrosine kinase inhibitor Sunitinib was shown to efficiently target STAT3 dependent MDSC signaling, resulting in a reduction of circulating MDSCs and increased numbers of intratumoral T cells (Guislain et al., 2015; Ko et al., 2010). Various approaches that entered clinical trials focus on inhibition of chemokines to prevent MDSC recruitment to the tumor including inhibitors against CXC-chemokine receptor 2 (CXCR2) (AZD5069, Reparicin, SX-682), CCR5 (Maraviroc) and CC-chemokine receptor 2 (CCR2) and are currently under investigation (Barry et al., 2023; Law et al., 2020; Noel et al., 2020). All-trans-retinoic acid (ATRA) was successfully used to differentiate MDSCs *in vitro* and showed a reduction of circulating MDSCs in cancer patients (Kusmartsev et al., 2008; Mirza et al., 2006). Many more approaches are under current investigation, including downregulation of NOS and ROS by disruption of COX-2/PGE2 (Celecoxib) signaling (Veltman et al., 2010).

Nevertheless, due to heterogeneity, plasticity, and context-dependent functions of MDSCs, therapeutic options targeting MDSCs remain a challenge. Current therapies targeting myeloid cells in cancer fail to show robust clinical activity and the selection of suitable patients and combinational therapies remains unclear (Barry et al., 2023). Thus, it is necessary to better understand the mechanisms involved in MDSC function and activation in order to develop strategies to overcome immunosuppression and boost anti-cancer immunotherapy using combinational approaches.

1.2 Glycobiology

The human cell surface is covered with a dense and complex layer of carbohydrate structures (glycans) called glycocalyx. Glycans can be free or covalently attached to proteins and lipids, forming complex structures that are named according to their linkage to lipid, glycan, or protein moiety (Reily et al., 2019). The major glycan types found in the glycocalyx of vertebrates are glycoproteins, glycosaminoglycans (GAGs), and glycosphingolipids (Fig. 1.5) (Pinho & Reis, 2015).
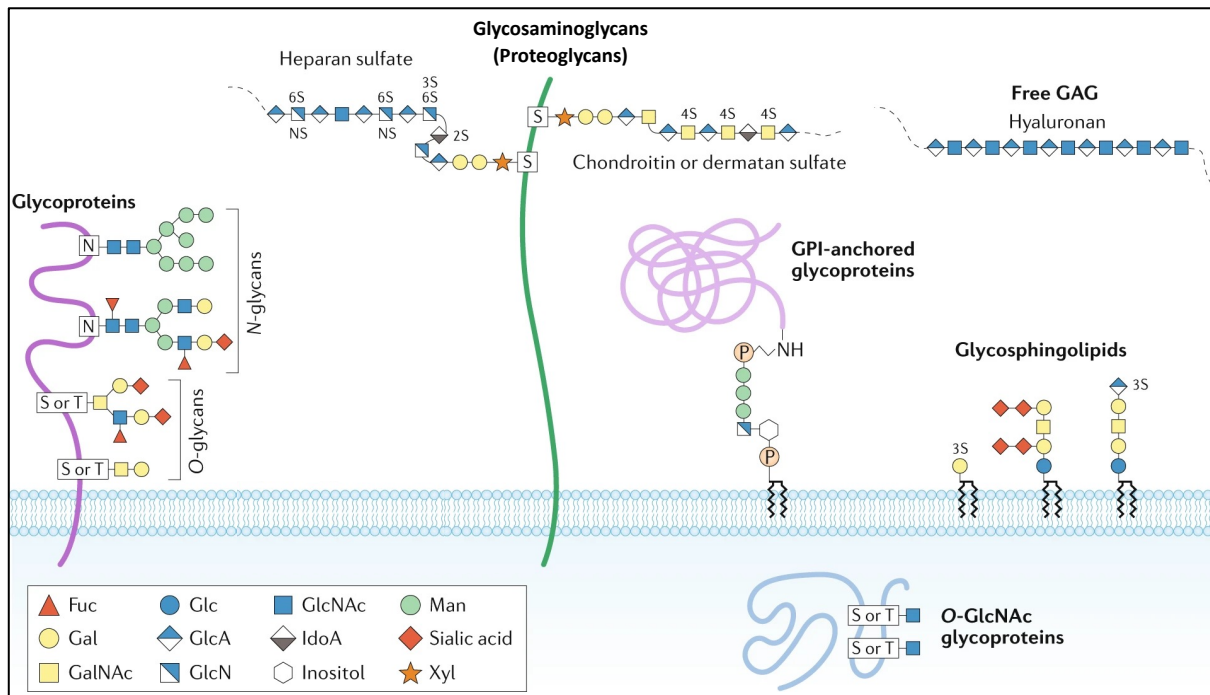

Fig. 1.5: Common classes of glycans in humans

Glycans can be classified into 3 common classes called glycoproteins, glycosaminoglycans (GAGs) and glycosphingolipids. Glycosylation is highly diverse and can vary in monosaccharide compounds, linkage, branching structure and bound protein/lipid, resulting in a variety of glycosylation patterns. In humans, glycans mainly consists of 10 different monosaccharides called glucose (Glc), galactose (Gal), N-acetylglucosamine (GlcNAc), N-acetylgalactosamine (GalNAc), fucose (Fuc), xylose (Xyl), sialic acid (Neu5Ac), glucuronic acid (GlcA), mannose (Man) and iduronic acid (IdoA). Adapted from (Reily et al., 2019). *GPI, glycosylphosphatidylinositol*

Glycosylation is the most common and diverse posttranslational modification of membrane-bound proteins (Schjoldager et al., 2020). While protein and nucleic acid synthesis is template-driven, glycosylation is a dynamic process that depends on the presence of substrates and enzymes responsible for the addition and removal of glycan moieties. Protein glycosylation mainly occurs in the endoplasmic reticulum and Golgi apparatus as a sequential multistep process including more than 200 glycosyltransferase enzymes that are responsible for the attachment site and glycan structure added to the selected protein (e.g., cytokines and

ECM components) (Schjoldager et al., 2020). Glycoproteins are highly diverse and can vary depending on the cell origin and cell type as well as the differentiation and activation status of the cell. Internalization and degradation of surface glycoproteins allows fast changes of the glycocalyx due to cues from the environment (Dennis et al., 2009). Thus, it is not surprising that glycans play a crucial role in various biological processes including cell structure, communication, and function by facilitating the interaction of cells and the surrounding extracellular matrix (ECM) and shaping protein stability, trafficking, and folding (Peixoto et al., 2019; Reily et al., 2019). The three main functions of glycosylation include (i) structure and physical properties, (ii) functional modulation, and (iii) ligands for carbohydrate-specific receptors (Smith & Bertozzi, 2021).

An in-depth view on GAGs, changes in the TME and their role in cancer therapy are part of my published review article, which can be accessed online: https://journals.physiology.org/doi/epdf/10.1152/ajpcell.00063.2022

REVIEW

Deciphering the Role of Proteoglycans and Glycosaminoglycans in Health and Disease

Glycosaminoglycans in cancer therapy

Ronja Wieboldt[1] and Heinz Läubli[1,2]

[1]Laboratories for Cancer Immunotherapy and Immunology, Department of Biomedicine, University Hospital and University of Basel, Basel, Switzerland and [2]Division of Oncology, Department of Theragnostics, University Hospital Basel, Basel, Switzerland

Abstract

Glycosaminoglycans (GAGs) are an important component of the tumor microenvironment (TME). GAGs can interact with a variety of binding partners and thereby influence cancer progression on multiple levels. GAGs can modulate growth factors and chemokine signaling, invasion, and metastasis formation. Moreover, GAGs are able to change the physical property of the extracellular matrix (ECM). Abnormalities in GAG abundance and structure (e.g., sulfation patterns and molecular weight) are found across various cancer types and show biomarker potential. Targeting GAGs, as well as the usage of GAGs and their mimetics, are promising approaches to interfere with cancer progression. In addition, GAGs can be used as drug and cytokine carriers to induce an antitumor response. In this review, we summarize the role of GAGs in cancer and the potential use of GAGs and GAG derivatives to target cancer.

cancer therapy; heparin; hyaluronidase; nanoparticles; proteoglycans

My thesis is focusing on the role of cancer-associated changes in glycosylation, in particular in sialylation, the engagement of sialoglycans by inhibitory Siglec receptors and its role in anti-cancer immunity.

1.2.1 Cancer-associated changes in glycosylation

Composition and changes in the glycocalyx are important indicators for the physiological state of cells. Altered glycosylation is a common characteristic of cancer cells and can contribute to malignant transformation and cancer progression (Pinho & Reis, 2015). Cancer-associated alterations in glycosylation include increased branching of complex N-glycans, truncation of O-glycans, and changes in sialylation and fucosylation patterns as well as changes in GAGs and glycosphingolipids (Fig. 1.6) (Mantuano et al., 2020; Pinho & Reis, 2015). These alterations are cancer-dependent and can be driven by genetic and epigenetic changes in glycan-modifying enzymes or enzymes involved in glycan synthesis, including glycosyltransferases, glycosidases, and monosaccharide transporters (Mereiter et al., 2019; Pearce & Läubli, 2015). For example, upregulated expression of β1,6N-acetylglucosaminyltransferase V, which modulates N-glycan branching, can lead to an increase of N-glycans on α3β1 integrin and is associated with metastasis and migration (Bellis et al., 2022). Truncated O-glycans and synthesis of glycoantigens (e.g., Tn and sialyl-Tn antigen) can be driven by mutations or loss of the chaperone enzyme core 1 β3-galactosyltransferase Specific Molecular Chaperone (COSMC). COSMC is critical for proper synthesis of O-glycans by affecting the enzymatic activity of β1-3 galactosyltransferase necessary for subsequent O-glycan branching (Mantuano et al., 2020). For instance, increased levels of Sialyl Tn antigen can increase invasion (Bellis et al., 2022). Changes in fucose-containing glycans can further drive tumorigenesis and cancer progression. For example, increased expression of fucosyltransferases 8, which facilitates the transfer of fucose to N-glycans, is overexpressed in various tumor entities (Bellis et al., 2022; Pinho & Reis, 2015).

Additionally, malignant glycosylation includes alteration and increase of sialic acid containing glycans (sialoglycans). Upregulation of sialoglycans called hypersialylation is associated with cancer progression, metastasis, and poor survival rates and shapes various tumor traits (Pearce & Läubli, 2015). The sialic acid family consists of over 50 members of negatively charged carbohydrates that harbor a nine-carbon backbone and are incorporated on the terminal site of many glycans (Varki et al., 2015). The most commonly found sialic acid in humans is N-acetyl-neuraminic acid (Neu5Ac), which contains an acetyl group at its amino site and is synthesized via UDP-N-acetylglucosamine 2-epimerase/N-acetylmannosamine kinase (GNE) (Varki et al., 2015). Because of an evolutionary mutation of the *CMAH* gene, humans can not synthesize N-glycolyl-neuraminic acid (Neu5Gc) and rely on the uptake of Neu5Gc from food sources (Varki, 2001). The addition of sialic acid to glycans is facilitated by various sialyltransferases at the Golgi apparatus, resulting in a huge amount of sialic acid containing glycans with α2,3/ α2,6/ and α2,8-linkage (Pearce & Läubli, 2015). Aberrant

sialylation in cancer can be driven by enzymatic changes including sialyltransferases, sialic acid-synthesizing enzymes and sialidases, which remove sialic acid from glycans (Pearce & Läubli, 2015). For example, overexpression of glycosyltransferase ST6Gal-1, an enzyme adding α2,6-linked sialic acid, is found across various cancer types and is associated with poor prognosis (Bärenwaldt & Läubli, 2019). Various sialylated glycans can serve as a biomarker, including sialyl-Tn (STn), sialic acid-containing disialyl gangliosides (GD3), sialyl-Lewis x (Le^x) and Lewis a (Le^a) and are known to interact with carbohydrate-specific receptors involved in immunomodulation (Bellis et al., 2022) (Fig. 1.6). In addition, increased incorporation of Neu5Gc is observed in cancer-related glycans and can lead to inflammation driven by an immune response against Neu5Gc (Pearce & Läubli, 2015).
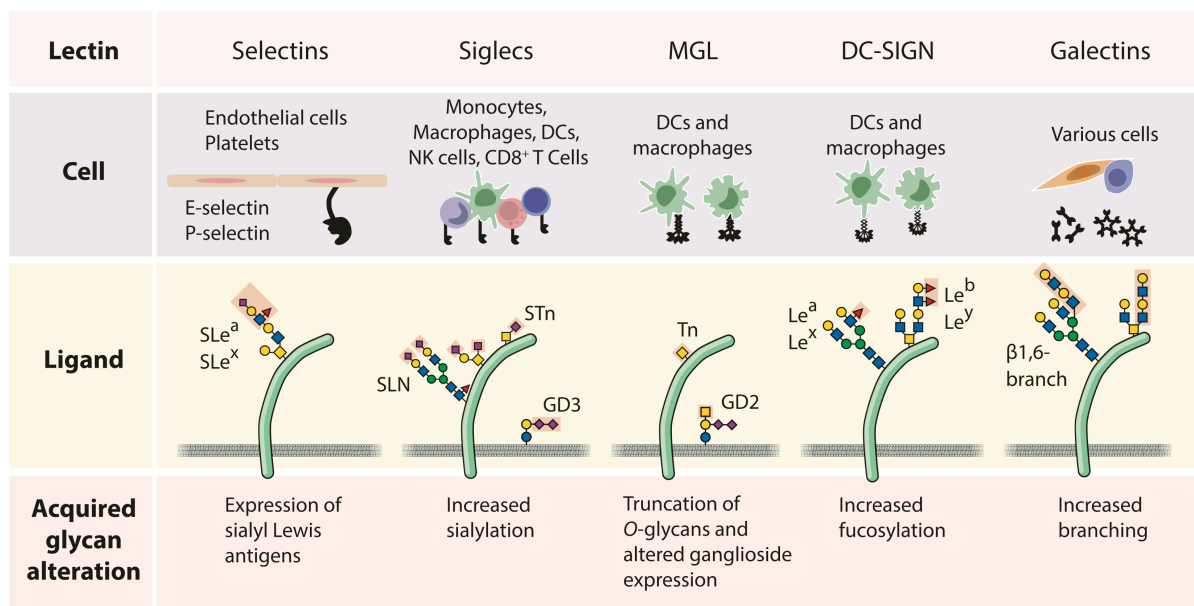

Figure 1.6: Cancer-associated glycan alterations can act as ligands for carbohydrate-specific receptors

Major alterations in glycosylation in cancer include increased branching of N-glycans, truncation of O-glycans, and changes in fucosylation and sialylation patterns. These changes can serve as ligands for lectin families, namely selectins, Siglecs and galectins. Specific lectins include macrophage galactose-specific lectin (MGL) and dendritic cell-specific ICAM-3-grabbing non-integrin 1 (DC-SIGN). Carbohydrate-specific receptors are expressed by a range of cells and major populations involved in the indicated glycan interaction are depicted (Mereiter et al., 2019).

The effects of altered glycosylation in cancer are broad and integral for various aspects of cancer formation and progression which led to the proposal to add aberrant glycosylation to the hallmarks of cancer (Peixoto et al., 2019; Vajaria & Patel, 2017). Cancer-associated changes in glycans can be used as clinical biomarker for early diagnosis, prognosis, and therapy outcome (Mereiter et al., 2019). Additionally, cancer-associated glycosylation patterns can be a promising therapeutic target for cancer therapy (Mantuano et al., 2020; Smith &

Bertozzi, 2021). On a functional level, aberrant glycosylation can influence cell adhesion, receptor dimerization, and effector function, e.g., of adhesion molecules (integrins) and tyrosine kinases and can serve as ligands for carbohydrate-specific receptors such as galectins, selectins, and sialic acid-binding immunoglobulin-type lectins (Siglecs) (Fig. 1.6).

Hypersialylation is involved in metastasis, inflammation, survival, immunosurveillance, and modulation of the TME (Rodrigues & Macauley, 2018). Sialoglycans can directly promote tumor growth by enhancing migration and invasion capabilities regulating tumor cell interactions with the TME (Peixoto et al., 2019). For example, increased binding of α2-6-sialylated β1 integrin to collagen I facilitates migration and invasion by modulating integrin-mediated adhesion (Bellis et al., 2022). Hypersialylation can also influence the stability of surface receptors on cancer cells, including Fas receptor and tumor necrosis factor receptor. As a result, these cell death receptors evade internalization and inhibit activation of cell death pathways (Dobie & Skropeta, 2021). Additionally, sialoglycans can indirectly favor tumor growth via modulation of immune cells and thereby impact anti-cancer immunity. Thus, sialoglycans can be recognized by carbohydrate-specific receptors called lectins, which harbor carbohydrate-recognition domains and are classified according to their glycan binding specificity and domains (Mereiter et al., 2019). (Fig. 1.6). Sialic acid-binding lectins include Siglecs and selectins. Selectins are important modulators of lymphocyte trafficking and can influence metastasis (Smith & Bertozzi, 2021).

1.2.2 Siglecs

Siglecs belong to the family of immunoglobulin (I)-type lectins and can bind to various terminal sialylated moieties (Mereiter et al., 2019). Siglecs are mainly expressed by immune cells and are involved in immune-modulatory functions. The Siglec family comprises 14 family members in humans and 8 in mice, which can be subdivided into highly conserved Siglecs and rapidly evolving CD33-related Siglecs (Fig 1.7) (Duan & Paulson, 2020). Conserved Siglecs include sialoadhesin (Siglec-1), CD22 (Siglec-2), MAG (myelin-associated glycoprotein, Siglec-4), and Siglec-15, which are evolutionary highly conserved in mammals but relatively distinct from other Siglec family members (Varki, 2013). CD33-related Siglecs show low evolutionary conservation leading to differences between species but share high sequence similarity. All genes encoding for CD33-related Siglecs are found on chromosome 19 and are derived by gene duplication (Cao & Crocker, 2011). In humans, CD33-related Siglecs include Siglec-3 (CD33), Siglec-5, Siglec-6, Siglec-7, Siglec-8, Siglec-9, Siglec-10, Siglec-11, Siglec-14 and Siglec-16 (Fig. 1.7). Upon human evolution, Siglec-12 lost its ability to bind sialic acid and Siglec-13 was deleted (Varki, 2013). Murine CD33-related Siglecs are mostly named alphabetically and include Siglec-E, Siglec-F, Siglec-G, Siglec-H, and Siglec-3

(Varki, 2013). Based on their sequence, function and structure, some murine Siglecs are thought to be human functional paralogs/orthologs, like human Siglec-9 and murine Siglec-E (Smith & Bertozzi, 2021).
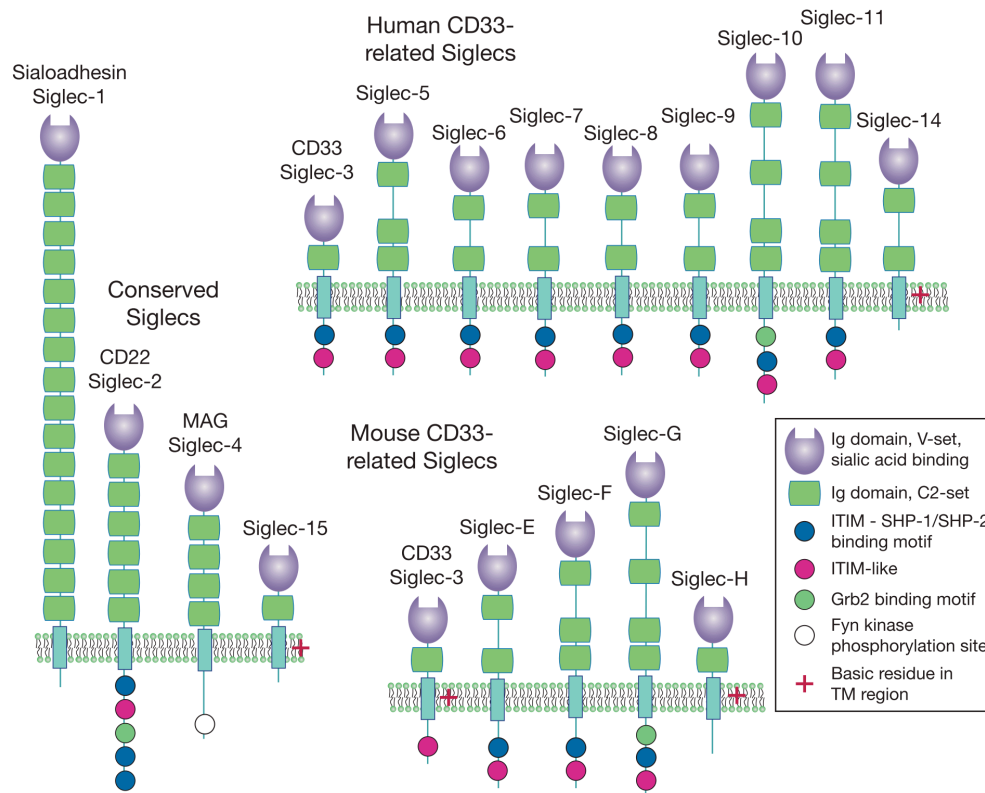

Figure 1.7 Siglec receptor family in humans and mice

Murine and human Siglec receptors can be divided into two subgroups: Evolutionary conserved Siglecs and rapidly evolving CD33-related Siglecs. Conserved Siglecs include sialoadhesin (Siglec-1), CD22 (Siglec-2), MAG (Siglec-4), and Siglec-15. The domain structures of each family member are shown. Basic residues in transmembrane (TM) regions (red cross) can interact with an adaptor protein called DAP12 containing an immunoreceptor tyrosine-based activatory motif (ITAM) domain. *C, constant; GRB2, growth factor receptor-bound protein 2; Ig, immunoglobulin; ITIM, immunoreceptor tyrosine-based inhibitory motif; MAG, myelin-associated glycoprotein; V, variable.* From (Varki, 2013).

All Siglecs are transmembrane receptors harboring an extracellular sialic acid-binding V-set domain, variable amounts of C2 Ig-like domains, and a cytosolic domain carrying intracellular signaling motifs except (Fig. 1.7). According to their signaling motifs, Siglecs can be divided into activatory, inhibitory, and non-signaling (Siglec-1 and Siglec-4) (Stanczak & Läubli, 2023). Most Siglecs are inhibitory receptors and contain immunoreceptor tyrosine-based inhibitory motifs (ITIM) or ITIM-like binding motifs in their cytosolic domain. Upon binding, the ITIM domain is phosphorylated by Src kinases, leading to the recruitment of Src-homology 2 domain (SH2)-containing phosphatases SHP-1 and SHP-2 and the subsequent

inhibition of downstream pathways by dephosphorylation (Duan & Paulson, 2020). In contrast, human Siglec-14 and Siglec-15 and murine Siglec-H contain a positively charged amino acid residue in their transmembrane domain and are considered activatory receptors. They can bind to the adaptor protein DAP12, which signals via an immunoreceptor tyrosine-based activation motif (ITAM) (Varki, 2013). Certain Siglecs (e.g., Siglec-1 and Siglec-4) bind exclusively to α2,3 linked sialic acid, whereas other Siglecs (e.g., Siglec-3, Siglec-9 and Siglec-10) have a broader binding spectrum binding to α2,3 and 2,6 linked sialic acid. Receptor-ligand binding can occur *trans*, between Siglec-expressing and neighboring cells or *cis*, on the same cell.

The function of Siglec receptors depends on their specific ligand, regulatory motifs, and the cell type expressing them (Duan & Paulson, 2020). Siglecs are mainly expressed by immune cells and are involved in immune modulation and homeostasis (Bärenwaldt & Läubli, 2019). An important feature of Siglecs is their role as pattern recognition receptors. Sialoglycans are self-associated molecular patterns (SAMPs) that provide self-recognition upon Siglec engagement and thereby limit the immune response against self-molecules (Varki, 2011). Thus, the Siglec-sialoglycan axis is important to protect against autoimmunity.

1.2.3 Siglec-sialoglycan axis in cancer

During cancer formation, various alterations can hijack the immune system leading to immune evasion, including the overexpression of SAMPs contributing to immune tolerance of cancer cells. As mentioned above, upregulation of sialoglycans is frequently found in cancer and can among other mechanisms contribute to immune evasion by engaging Siglec receptors. Recent studies highlight the importance of inhibitory Siglec receptors for regulating various immune cells in the TME, such as T cells, NK cells, DCs, and macrophages (Fig. 1.8) (Stanczak & Läubli, 2023). For example, NK cell activity can be downregulated by the interaction of sialoglycans with Siglec-7 and Siglec-9, leading to a decrease of NK cell-mediated killing *in vitro* and *in vivo*. Furthermore, increased sialoglycan levels on cancer cells inhibit NK cell engagement and antibody-dependent cellular cytotoxicity (Hudak et al., 2014; Jandus et al., 2014). High levels of ligands for inhibitory Siglec-7/9 on NK cells have been found in various cancer entities, including breast cancer and melanoma (Jandus et al., 2014). Upregulation of Siglec-9 was found on tumor-infiltrating T cells from various cancer entities and was co-expressed with several inhibitory receptors associated with an exhaustion phenotype (Haas et al., 2019; Stanczak et al., 2018). Siglec-9 ligands were highly expressed in non-small lung cancer and squamous cell carcinoma. Siglec-9 on T cells acts as an inhibitory receptor upon sialoglycan binding, leading to TCR-mediated recruitment of SHP-1/2 phosphatases (Ikehara et al., 2004; Stanczak et al., 2018). More recently, sialic acid ligands

were identified as alternative ligands for CD28 downregulating co-stimulation of T cells (Edgar et al., 2021). In addition to NK and T cells, the Siglec-sialoglycan axis can modulate myeloid cells in the TME. Myeloid cells express high numbers of several inhibitory Siglec receptors, including Siglec-9, Siglec-10, and Siglec-15 (Bärenwaldt & Läubli, 2019). Siglec-Sialoglycan interactions can lead to tumor-promoting M2 polymerization of macrophages and modulate phagocytosis. For example, macrophage differentiation was observed upon engagement of Siglec-9 and sialoglycan-containing MUC1 as well as upon interaction of Siglec-7/9 with sialic acid on pancreatic cancer *in vitro* (Beatson et al., 2016; Rodriguez et al., 2021) and pancreatic ductal adenocarcinoma cells showed increased Siglec ligand expression. Additionally, interaction of Siglec-10 with sialylated CD24 can inhibit the phagocytosis of cancer cells by macrophages (Barkal et al., 2019). On DCs, Siglec expression can modulate antigen presentation to T cells and DC activation in mice (J. Wang et al., 2022). Moreover, high levels of inhibitory Siglecs were detected on MDSCs from glioma patients, but functional relevance is currently lacking (Fig. 1.8) (Santegoets et al., 2019).
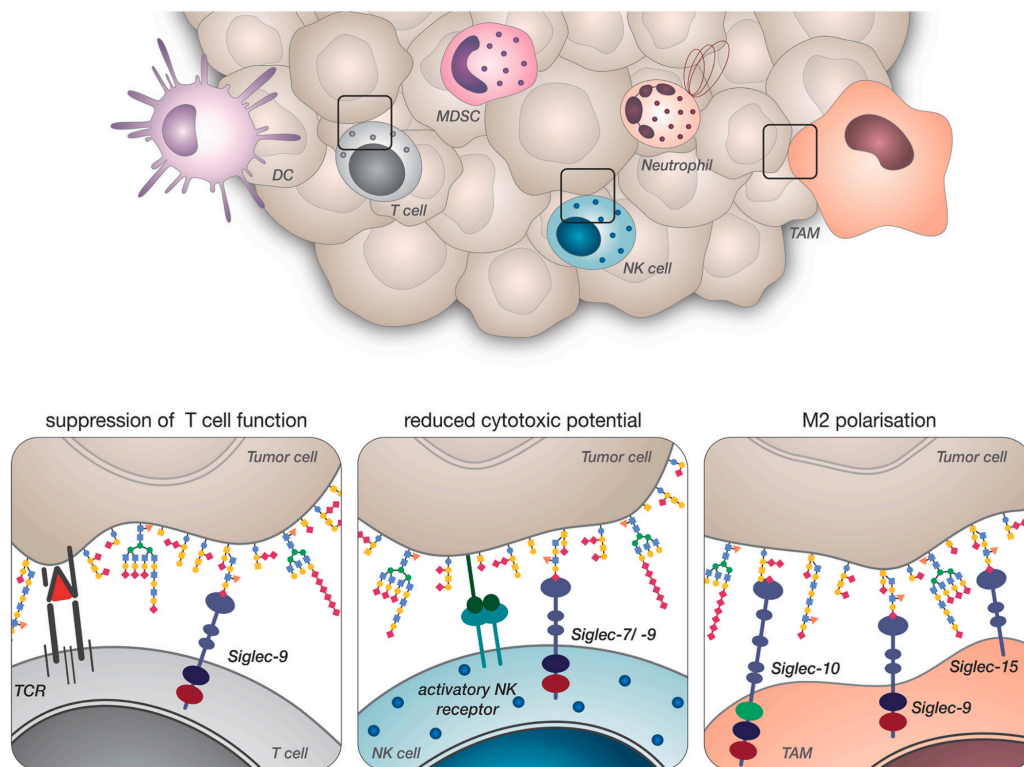
Figure 1.8: Siglec-sialoglycan interactions in the tumor microenvironment

Siglec receptors are expressed by various immune cells within the tumor microenvironment (TME). The Siglec-sialoglycan axis is involved in immune evasion and can lead to the suppression of T cell and NK cell function. The engagement of sialoglycans with Siglec receptors on macrophages can lead to pro-tumorigenic M2 polymerization. Additionally, Siglecs can be expressed by DCs, neutrophils, and MDSCs found in the TME, but further studies are needed to better understand their functional relevance. From (Stanczak & Läubli, 2023).

Given the importance of the Siglec-sialoglycan axis to modulate various immune cells and its contribution to shape an immunosuppressive TME, targeting Siglec and sialoglycan interactions is a promising new approach for cancer immunotherapy (Adams et al., 2018; Stanczak & Läubli, 2023). The Siglec-sialoglycan axis is proposed as a new immune checkpoint in cancer and is often compared to the PD-1-PD-L1 axis because both inhibit immune cell activation via intracellular ITIM signaling and facilitate immune evasion (Stanczak & Läubli, 2023). Approaches to interfere with Siglec and sialoglycan interactions include: (i) blocking antibodies, (ii) cleavage of sialic acid using sialidases, and (iii) small molecule inhibitors targeting sialic acid synthesis.

Blocking Siglecs using antagonistic antibodies is a promising approach to prevent binding. For instance, Siglec-7 and Siglec-9 blocking resulted in increased NK cell-mediated killing *in vitro* (Hudak et al., 2014; Jandus et al., 2014). In addition, Siglec-9 blocking antibody fragment led to T cell activation *in vitro* (Stanczak et al., 2018) and Siglec-9 blocking could further increase anti-tumor immune response in a human glioblastoma *in vitro* model (Schmassmann et al., 2023). In a preclinical *in vivo* model, Siglec-7 and Siglec-9 blocking increased anti-tumor immunity, highlighting the potential of Siglec blockade as a therapeutic treatment (Ibarlucea-Benitez et al., 2021). Apart from Siglec-7 and Siglec-9, Siglec-15 blocking antibody showed promising results and prolonged tumor growth *in vivo,* leading to further investigation in an early clinical trial (J. Wang et al., 2019). Further studies are needed to understand the underlying mechanism. Although Siglec blocking antibodies show some promising results, generation of highly specific Siglec antibodies that are purely blocking remains a challenge due to the similarity of CD33-related inhibitory Siglecs and absence of direct orthologous in mice (Smith & Bertozzi, 2021).

Apart from direct Siglec blocking, other approaches aim to reduce sialoglycan levels and thereby decrease Siglec ligands within the TME. These interventions mainly focus on the cleavage of sialic acid by sialidase and blockade of sialic acid synthesis and sialyltransferases (van de Wall et al., 2020). For instance, selective blockade of sialoglycan biosynthesis was achieved by *in vivo* injection of the sialic acid analog $3F_{ax}$-Neu5Ac, which led to reduced tumor growth and increased T and NK cell tumor infiltration (Büll et al., 2018). In another study, desialylation of multiple myeloma cancer cells by sialidase and sialyltransferase inhibitors resulted in an increase of NK-cell-mediated cytotoxicity (Daly et al., 2022). Desialylation on T cells facilitated CD28-mediated co-stimulation of T cells leading to increased T cell activation *in vitro* (Edgar et al., 2021). Focusing on myeloid cells, blockade of the Siglec-10 receptor CD24 could decrease tumor growth in a macrophage-dependent manner (Barkal et al., 2019). In addition, promising results were observed using a sialidase linked to a tumor-directed

antibody that selectively cleaves sialic acid from the surface of HER-2-expressing cancer cells. HER-2-directed sialidase led to better tumor control by repolarization of macrophages in the TME and enhanced immune cell infiltration *in vivo* (Gray et al., 2020; Stanczak et al., 2022). Recently, a first-in-human trial utilizing human bi-sialidase as a therapeutic strategy against solid tumors reported tolerability and desialylation of immune cells in the peripheral blood (Luke et al., 2023) (NCT05259696). Noteworthy, desialylation can not only affect Siglec-sialoglycan interactions but exposed lactosamine residues can serve as ligands for galectins that are otherwise blocked by sialylation (Mariño et al., 2023).

In summary, aberrant glycan expression is involved in various steps of carcinogenesis, including inflammation, adhesion, immunosurveillance, intracellular signaling, and protein structure (Pinho & Reis, 2015). Deciphering the changes and interaction of glycans within the TME can contribute to a better understanding of cancer dynamics and interactions with the immune system. In particular, the Siglec-sialoglycan axis seems to be a promising immune checkpoint and target for cancer therapy to shape a more permissive TME. Further studies are needed to understand the diverse role of the Siglec-sialoglycan axis within the TME and its contribution to immunosuppression. Such findings can lead to novel therapeutic strategies and might help to overcome current limitations of cancer immunotherapy.

2 AIM OF THE THESIS

The TME plays an important role in cancer immunotherapy response and resistance. Various factors influence the suppressive capacity of the TME, including suppressive myeloid cells and hypersialylation. Understanding the composition and interaction of immune cells within the TME is essential to improve current treatment regimens and increase therapy success. Apart from Siglec-3/CD33 as phenotypic marker expressed by all MDSCs, recent studies further describe the expression of Siglec-5, Siglec-7 and Siglec-9 on human glioma patient MDSCs and Siglec-E on murine MDSCs (Santegoets et al., 2019; Stanczak et al., 2022). Nevertheless, little is known about the purpose and function of Siglecs and sialoglycan ligands on MDSCs and their expression in health and disease. This thesis aims to better understand the role of the Siglec-sialoglycan axis on suppressive myeloid cells in cancer and their contribution to shape a suppressive TME. Increased understanding of immunosuppressive mechanisms within the TME is essential to overcome current limitations of cancer immunotherapy and can help to develop new treatment regimes.

The specific aims of my PhD thesis are:

- The characterization of Siglec receptor and sialoglycan ligand expression on MDSCs in humans and mice in the context of cancer
- The functional relevance of Siglec-E on myeloid cells during tumor growth *in vivo*
- The potential of targeting the Siglec-sialoglycan axis on suppressive myeloid cells utilizing Siglec blocking antibodies and Sialidase treatment that cleaves Sialoglycans

3 RESULTS

The following chapters are summarized in the manuscript below, which can be accessed as a preprint on bioRxiv: *https://doi.org/10.1101/2023.06.29.547025*

Engagement of sialylated glycans with Siglec receptors on suppressive myeloid cells inhibit anti-cancer immunity via CCL2

Ronja Wieboldt[1], Emanuele Carlini[1], Chia-wei Lin[2], Anastasiya Börsch[3], Andreas Zingg[1], Didier Lardinois[4], Petra Herzig[5], Leyla Don[5], Alfred Zippelius[5,6], Heinz Läubli[1,6†*] and Natalia Rodrigues Mantuano[1†*]

[1]Laboratories for Cancer Immunotherapy, Department of Biomedicine, University Hospital and University of Basel, Basel, Switzerland

[2]Functional Genomics Center Zurich, ETH Zurich, Zurich, Switzerland

[3]Bioinformatics Core Facility, Department of Biomedicine, University of Basel and Swiss Institute of Bioinformatics, Basel, Switzerland

[4]Department of Thoracic Surgery, University Hospital Basel, Basel, Switzerland

[5]Laboratory of Cancer Immunology, Department of Biomedicine, University Hospital and University of Basel, Basel, Switzerland

[6]Division of Oncology, University Hospital Basel, Basel, Switzerland

[†] These authors contributed equally to this work as co-senior authors

[*] Corresponding authors: HL (heinz.laeubli@unibas.ch) and NRM (natalia.rodriguesmantuano@unibas.ch)

Manuscript under review

3.1 Myeloid cells express inhibitory CD33-related Siglecs in cancer

Although no exclusive MDSC markers are known, MDSCs can be identified by co-expression of phenotypic markers that vary between murine and human. All murine MDSCs express Gr1 and CD11b and can be subdivided into $Ly6G^+Ly6C^{low}$ gMDSCs and $Ly6C^{high}$ mMDSCs (Bronte et al., 2016). In humans, gMDSCs are phenotypically characterized as $CD33^+CD11b^+HLA-DR^{low/-}CD15^+CD14^-$ and mMDSCs as $CD33^+CD11b^+HLA-DR^{low/-}CD15^-CD14^+$ (Cassetta et al., 2019). All human MDSCs express Siglec-3/CD33 as a phenotyping marker (Cassetta et al., 2019), but little is known about the expression of additional Siglec receptors on MDSCs in human cancer patients and their functional relevance (Santegoets et al., 2019).

Here, we investigated the expression of Siglec receptors found on lung patient-derived MDSCs as well as on myeloid cells from healthy donors identified as lineage$^-$ $CD33^+CD11b^+HLA-DR^{low/-}$ cells (fig. S1 A, C). Human MDSCs from lung cancer patients expressed high levels of Siglec-5, Siglec-7, Siglec-9 and Siglec-10 in the periphery and within the tumor (Fig. 3.1 A, fig. S1 C). Increased levels of Siglec-9 and Siglec-10 were expressed on patient MDSCs in the periphery compared to myeloid cells from healthy donors (Fig. 3.1 B, C). Siglec-5 and Siglec-7 showed similar expression patterns on MDSCs derived from cancer patients and myeloid cells from healthy controls in peripheral blood (fig S1 D, E).

Next, we investigated whether our findings were similar in mice by analyzing mouse CD33-related inhibitory Siglec receptors on tumor-bearing and naïve MDSCs including Siglec-E, Siglec-F and Siglec-G, which resemble potential functional paralogs of human Siglec-9, Siglec-8 and Siglec-10, respectively (Siew et al., 2022). To this end, Siglec expression of tumor-infiltrating and spleen-derived MDSCs in tumor-bearing and naïve mice was analyzed by assessing $CD11b^+Ly6G^+$ and $CD11b^+Ly6C^+$ populations, which in the tumor context are described as gMDSCs and mMDSCs, retrospectively (Bronte et al., 2016) (fig. S1 F). High levels of Siglec-E were identified across infiltrating MDSCs in different tumor types, intermediate levels of Siglec-F were only found on gMDSCs and Siglec-G was rarely expressed on both MDSC types (Fig. 3.1 D, fig S1 G). Siglec-E mean fluorescence intensity (MFI) was the highest expressed on gMDSCs compared to all other tumor-infiltrating immune cells in B16F10, followed by mMDSCs and TAMs ($CD11b^+F4/80^+$) (Fig. 3.1 E, F). Furthermore, Siglec-E expression was increased on $CD11b^+Ly6G^+$ and $CD11b^+Ly6C^+$ populations from tumor-bearing mice in the spleen compared to naïve littermates in B16F10 and EL4-bearing mice (Fig. 3.1 G, fig S1 H). These results show an increased expression of inhibitory Siglecs in humans and mice in the cancer context.
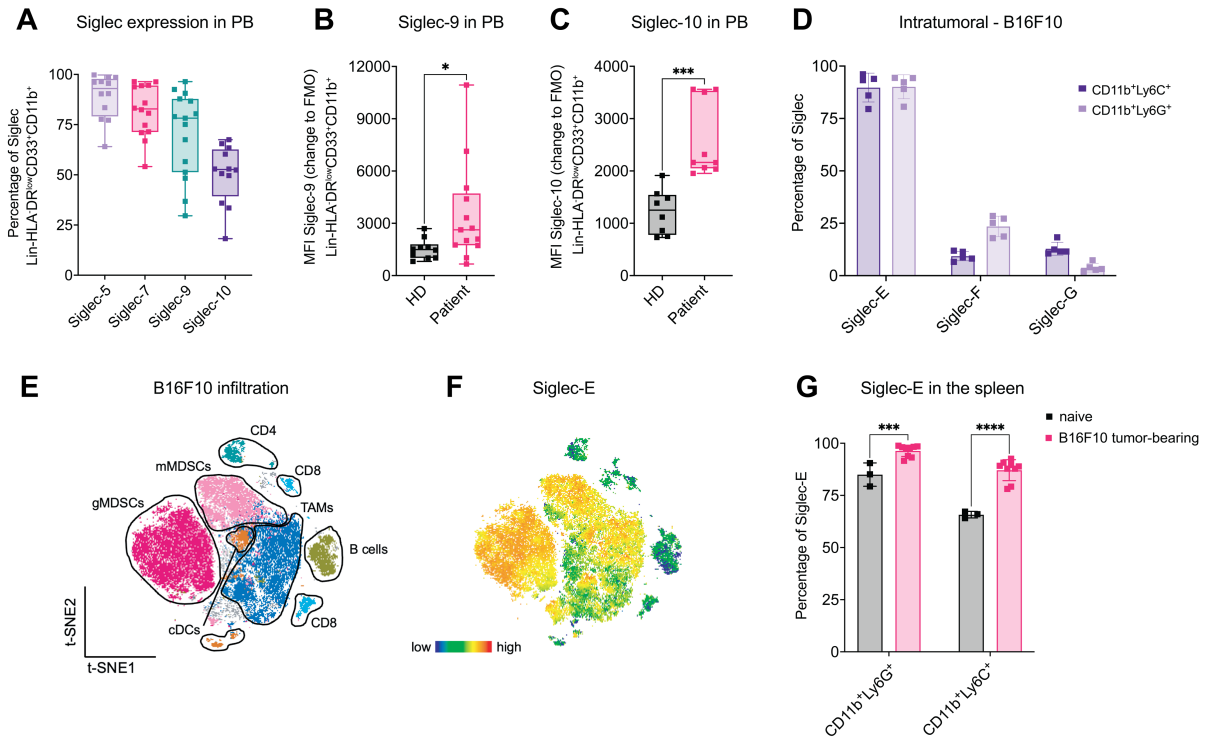
Figure 3.1: Myeloid cells express Siglecs in humans and mice

(A) Percentage of Siglec-5, Siglec-7, Siglec-9 and Siglec-10 expressed on Lin⁻HLADR^{low}CD33⁺CD11b⁺ cells detected in peripheral blood (PB) from lung cancer patients by flow cytometry. *N=12-14 donors from N=4 experiment*. **(B)** MFI of Siglec-9 and **(C)** Siglec-10 on CD45⁺Lin⁻HLADR^{low}CD33⁺CD11b⁺ cells derived from healthy donor and lung cancer patient PB from (A). MFI is shown as change to FMO and was determined by flow cytometry. *N=8-13 donors with at least N=2 experiments.* **(D)** Subcutaneously injected endpoint tumors from B16F10 melanoma-engrafted mice were harvested, digested, and immune cell infiltration was assessed by multicolor flow cytometry. Siglec-E, Siglec-F, and Siglec-G expression was assessed on CD45⁺CD11b⁺Ly6G⁺ and CD45⁺CD11b⁺Ly6C cells. *N=5 mice.* **(E)** T-distributed stochastic neighbor embedding (t-SNE) projection of multicolor flow cytometry immunophenotyping of pooled infiltrating immune cells from B16F10 tumors. *N=5 mice.* **(F)** Siglec-E expression intensity is shown as a color gradient from blue (low) to red (high). **(G)** Spleens from naïve and B16F10 melanoma tumor-bearing mice at endpoint were collected and analyzed for Siglec-E expression via flow cytometry. *N=3-9 mice per group*.

Data are presented as mean. Error bar values represent SD. Two-tailed unpaired Student's t-test or multiple unpaired t-tests (G) were used. *P<0.05, **P<0.01, ***P<0.001, and ****P<0.0001.

3.2 Myeloid cells in cancer are hypersialylated

Binding of Siglec receptors to their sialoglycan ligands has been described before and is involved in immune cell interactions with cancer cells but also during antigen presentation and formation of adaptive immunity (Läubli & Varki, 2020). Although hypersialylation is a common hallmark of cancer and is mainly studied on cancer cells, sialoglycans can additionally be expressed on secreted glycoproteins, glycolipids and the cell surface of immune cells themselves (Adams et al., 2018; van Houtum et al., 2021). To investigate the potential interactions of Siglec receptors with ligands on the surface of MDSCs, we further assessed the sialylation pattern of MDSCs in the TME. Lectin staining was performed to assess surface sialoglycan ligands including Sambucus Nigra Lectin (SNA) detecting α-2,6-linked sialic acids and Maackia Amurensis Lectin II (MALII) detecting α-2,3-linked sialic acids. Both lectins showed a significantly increased staining on peripheral MDSCs derived from lung cancer patients compared to myeloid cells from healthy donors (Fig. 3.2 A, B). No changes were detected in Peanut Agglutinin (PNA) levels, a galactosyl (β-1,3) N-acetylgalactosamine structure that is usually masked by sialic acid-binding (fig. S2 A). In addition, mass spectrometry (MS)-based analysis on released N-glycans from peripheral patient-derived CD33$^+$ cells showed a clear increase of terminally sialylated N-glycans containing multiple sialic acids when compared to myeloid cells from healthy donors (Fig. 3.2 C, D). The main N-glycan structure found on healthy donor CD33$^+$ cells were core-fucosylated N-glycans with mono sialic acid and PolyLacNAc. In addition, N-glycans containing more than 2 fucoses were also observed, indicating the presence of Lewis structures.

We further studied the expression of ligands on the surface of murine myeloid cells by lectin staining. Similar to the human setting, increased levels of SNA were detected on both, CD11b$^+$Ly6G$^+$ and CD11b$^+$Ly6C$^+$ populations in the blood of tumor-bearing mice compared to naïve littermates (Fig. 3.2 E, F). No significant differences could be observed on MALII or PNA level (fig. S2 B, C). This data shows differential expression of sialoglycans on cancer-associated suppressive myeloid cells in humans and mice.
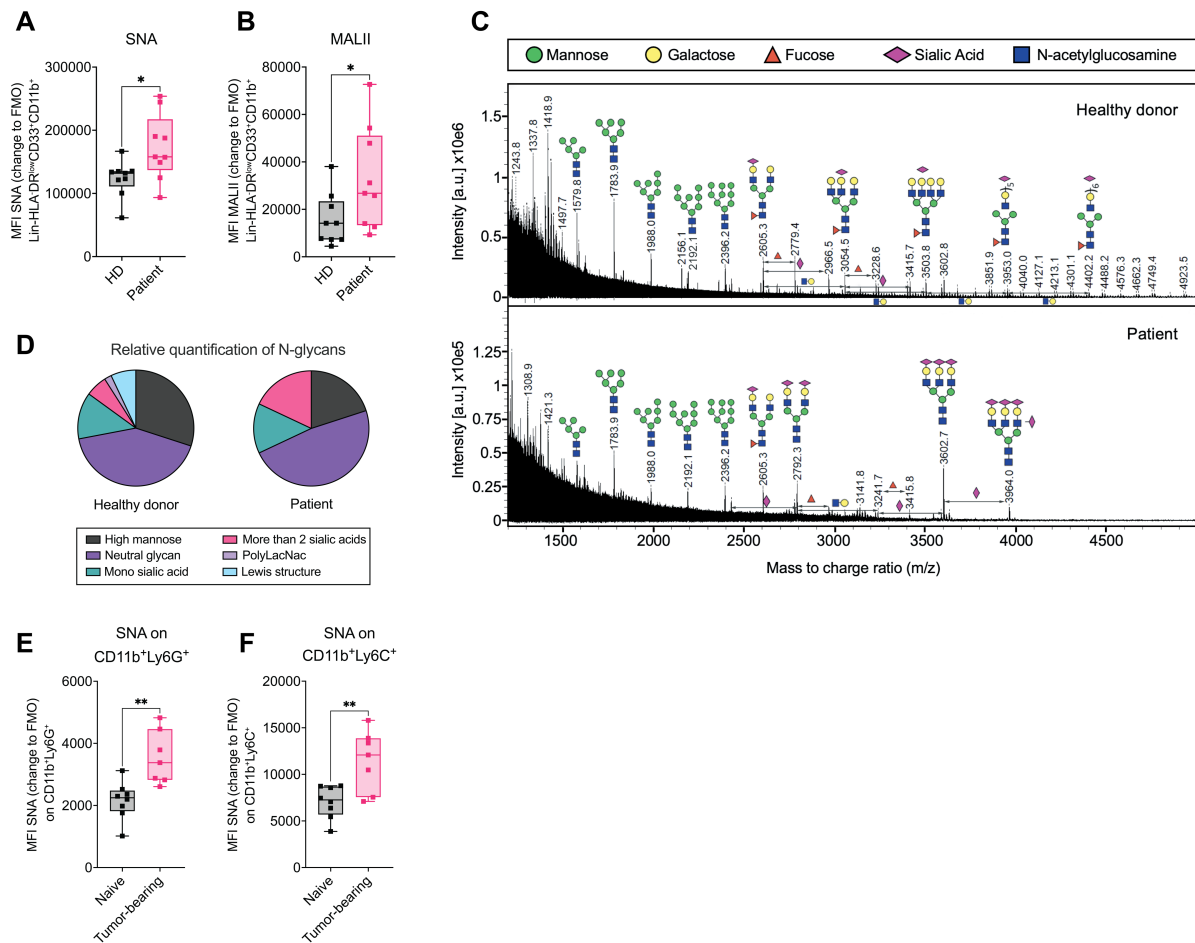
Figure 3.2: Myeloid cells in cancer are highly sialylated

(A) MFI of SNA or **(B)** MALII gated on PB-derived Lin⁻HLADR^low^CD33⁺CD11b⁺ cells from lung cancer patient and healthy controls. MFI is shown as change to FMO and was determined by flow cytometry. *N=8-13 donors with at least N=2 experiments.* **(C)** MALDI-TOF mass spectra (m/z 1200–5000) of N-glycans isolated from CD33⁺ cells of healthy donor and lung cancer patient-derived from fresh blood. The N-glycans were released by PNGaseF and permethylated prior to MALDI-TOF-TOF profiling. Main structures are depicted above the corresponding peaks. Assignments are based on composition and knowledge of biosynthetic pathways. All molecular ions are [M + Na]⁺. Residues above a bracket have not had their location unequivocally defined. **(D)** Relative quantification of N-Glycans detected in cancer patient and healthy donor derived CD33⁺ cells from **(C)**. *N=1.* **(E)** Fresh blood from B16F10 tumor-bearing mice and naïve wild type mice was collected at day 14 after tumor inoculation and analyzed for SNA gated on **(E)** CD45⁺CD11b⁺Ly6C⁺ or **(F)** CD45⁺CD11b⁺Ly6G⁺ cells. MFI is shown as change to FMO. *7-8 mice per group with N=2 experiments*.

Data are presented as mean. Error bar values represent SD. Two-tailed unpaired Student's t-test was used. *P<0.05, **P<0.01, ***P<0.001, and ****P<0.0001.

3.3 Depletion of Siglec-E on myeloid cells prolongs survival

To further investigate the role of Siglec-E on myeloid cells in the TME, Siglec-E^{loxP} mice were crossed with LysMCre to specifically target Siglec-E on LysM expressing cells in mice (SigE$^{\Delta LysM}$). SigE$^{\Delta LysM}$ were compared to Siglec-E wild type (SigE^{WT}) littermates in terms of tumor growth, survival and immune infiltration upon subcutaneous tumor injection (Fig. 3.3 A). As we were focusing on suppressive myeloid cells, models of cancer-induced emergency myelopoiesis were used, including B16F10 melanoma and EL4 lymphoma syngeneic tumor models (Youn et al., 2008). During emergency myelopoiesis, myeloid cells are rapidly increased which leads to accumulation of immature, suppressive cells including MDSCs.

Subcutaneous injection of both tumor cell lines resulted in increased numbers of CD11b$^+$Ly6G$^+$ and CD11b$^+$Ly6C$^+$ in the spleen of tumor-bearing mice compared to naïve littermates (fig. S3 A, B). Additionally, high numbers of MDSCs were found within B16F10 and EL4 tumors, making them suitable models to study the effect of Siglec-E in myeloid-driven tumors (fig. S3 C). To confirm deletion of Siglec-E in our model, Siglec-E expression was accessed by flow cytometry on myeloid cells from tumor digests and spleens of EL4 and B16F10 tumor-bearing mice (Fig. 3.3 B, fig. S3 D, E). Siglec-E was significantly decreased on gMDSCs, mMDSCs and macrophages in the tumor and spleen of SigE$^{\Delta LysM}$ compared to SigE^{WT} mice. Siglec-E was the highest expressed on gMDSCs followed by mMDSCs and macrophages in wild type mice within the tumor and the spleen (Fig. 3.3 B, fig S3 D, E) as observed before (Fig. 3.1 E, F). Deletion of Siglec-E on myeloid cells resulted in prolonged survival and decreased tumor growth of SigE$^{\Delta LysM}$ mice compared to SigE^{WT} littermate mice in B16F10 and EL4 tumor models (Fig. 3.3 C-F). We observed increased CD8$^+$ T cell infiltration in SigE$^{\Delta LysM}$ mice associated with an increased number of proliferation and expression of functional T cell markers including Granzyme B (GzmB), Ki67 and CD25 (Fig. 3.3 G-J). To avoid cancer model-dependent effects, we confirmed our findings using EL4 lymphoma tumor cells. Increased CD8$^+$ T cell infiltration was also found in EL4-bearing mice strengthening the importance of our findings (fig. S3 F-I).

As the highest expression of Siglec-E was found on gMDSCs, we hypothesized that Siglec-E depletion mainly affects gMDSCs in our model. To test this hypothesis, Ly6G depletion was performed to eliminate Ly6G-expressing gMDSCs in SigE$^{\Delta LysM}$ mice and SigE^{WT} littermates upon B16F10 tumor cell injection (Fig. 3.3 K). Depletion of gMDSC in SigE^{WT} mice prolonged their survival and tumor growth but did not affect SigE$^{\Delta LysM}$ mice lacking Siglec-E on myeloid cells (Fig. 3.3 L, fig. S3 J). Thus, Siglec-E expression on gMDSCs was likely involved in tumor progression *in vivo*. The numbers of myeloid cells within the tumor and spleen were not altered (fig. S3 K-N) suggesting a qualitative change rather than a quantitative

change of myeloid cells upon Siglec-E depletion, which possibly resulted in a less suppressive TME leading to effector T cell infiltration. These results show that Siglec-E on myeloid cells inhibits tumor growth in different murine tumor models, mainly due to Siglec-E expression on gMDSCs.
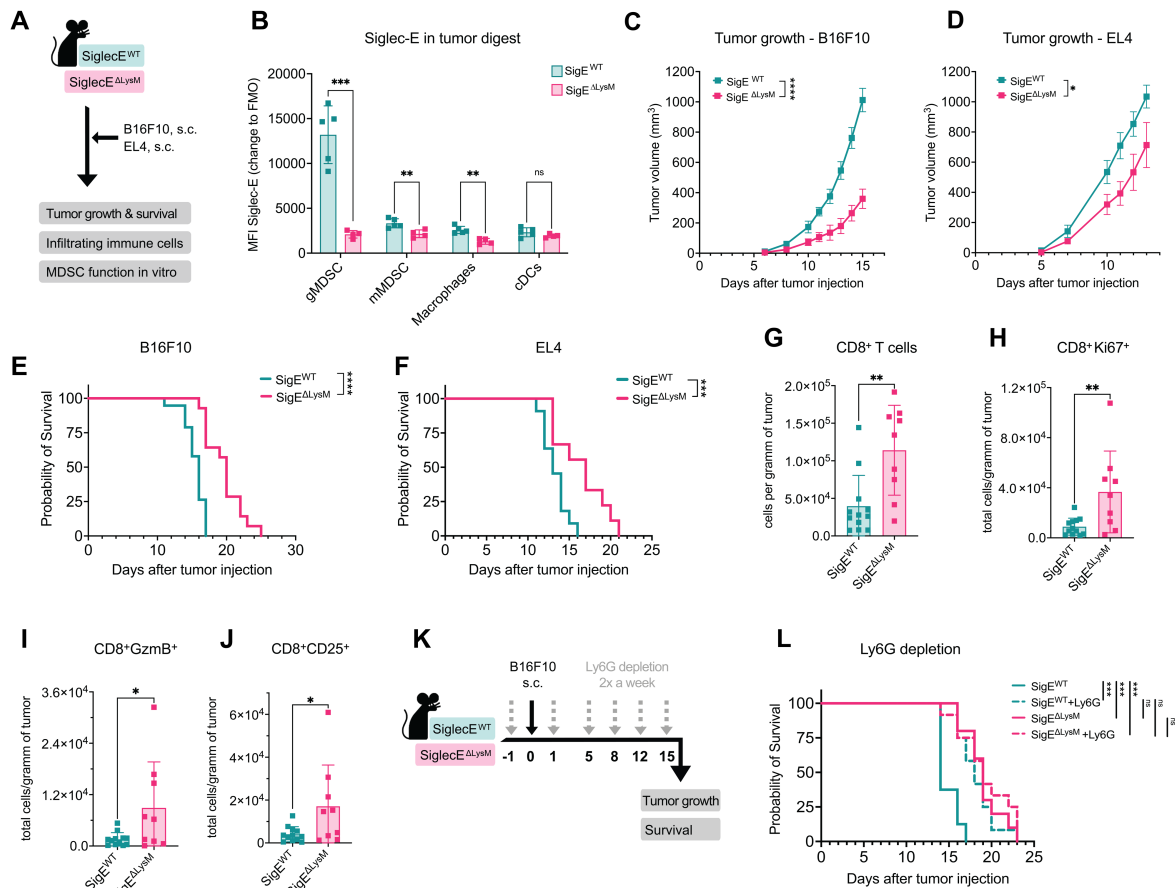
Figure 3.3: Siglec-E depletion on myeloid cells decreases tumor growth in mice

(A) Experimental setup: Siglec-ExLysM-Cre mice (SigE^ΔLysM) and Siglec-E WT (SigE^WT) littermates were subcutaneously injected with B16F10 or EL4 cells. Tumor growth, probability of survival, tumor immune cell infiltration and suppressive capacity of Gr1⁺CD11b⁺ *in vitro* were analyzed. **(B)** MFI of Siglec-E expression was assessed on myeloid cells in tumor digest at endpoint of SigE^ΔLysM mice and SigE^WT littermates. MFI of Siglec-E is shown as a change to FMO. Cells were identified as gMDSCs (CD45⁺CD11b⁺Ly6G⁺), mMDSCs (CD45⁺CD11b⁺Ly6C⁺), macrophages (CD45⁺CD11b⁺F4/80⁺), dendritic cells (DCs) (CD45⁺CD11c⁺MHCII⁺F4/80⁻). *N=4-5 mice per group.* **(C)** Tumor growth from pooled data of B10F10 and **(D)** EL4 subcutaneously injected mice. *N=9-12 mice per group from at least 2 independent experiments.* **(E)** Kaplan-Meier survival curves from pooled data of mice injected subcutaneously with B16F10. *N=9-12 mice per group from at least 2 independent experiments.* **(F)** Kaplan-Meier survival curves from pooled data from 2 experiments injected with EL4. *N=9 mice per group* **(G)** B16F10 tumors at endpoint **(C)** were digested and analyzed by flow cytometry. Intratumoral CD8⁺ cells (CD45⁺CD19⁻NKp46⁻CD3⁺CD8⁺), **(H)** Ki67⁺CD8 T cells, **(I)** GranzymeB⁺CD8 T cells⁺ (GzmB⁺), **(J)** CD25⁺CD8 T cells were quantified as cells per gram of tumor at the endpoint of the experiment. Pooled data from 2 independent experiments. *N=9-12 mice per group.* **(K)** Experimental setup: Depletion of Ly6G positive cells using depletion antibody in SigE^ΔLysM mice and SigE^WT littermates bearing B16F10 tumors. Mice were injected up to 6 times (grey arrow) with Ly6G depletion antibody starting 1 day before subcutaneous B16F10 tumor injection (black arrow). Tumor growth and survival were monitored. **(L)** Kaplan-Meier survival curves from pooled data from 2 independent experiments. *N=9-11 mice per group. (continued on next page)*

Data are presented as mean. Error bar values represent SD. Two-tailed unpaired Student's t-test or multiple unpaired t-tests (B) was used. For survival analysis, log-rank test was used followed by Šidák correction for multiple comparisons. Tumor growth was compared by mixed-effects analysis followed by Bonferroni's multiple comparisons test. *P<0.05, **P<0.01, ***P<0.001, and ****P<0.0001.

3.4 Siglec-E and sialoglycans shape the immunosuppressive capacity of murine MDSCs

Although MDSCs are involved in various pro-tumorigenic mechanisms, the key feature remains their ability to inhibit T cell response (Bronte et al., 2016). To test whether the suppressive function of MDSCs lacking Siglec-E is impaired, MDSCs were isolated by CD11b$^+$Gr1$^+$ negative selection from the spleen of B16F10 tumor-bearing mice and their suppressive capacity was tested against highly stimulated naïve T cells *in vitro* (Fig. 3.4 A). Stimulation of T cells by IL-2 and anti-CD3/28 led to high proliferation of T cells (Fig. 3.4 B). MDSCs from SigE^{WT} mice highly suppressed CD8 T cell proliferation but SigE^{ΔLysM} MDSCs were significantly less suppressive shown by an increased T cell proliferation (Fig. 3.4 C, D). This suggests that the reduced suppressive function of MDSCs lacking Siglec-E could generate a less suppressive TME *in vivo* leading to increased T cell infiltration and prolonged survival that is observed in SigE^{ΔLysM} mice.

To further evaluate if suppressive MDSCs can be altered by interfering with the Siglec-sialoglycan axis, we either added Siglec-E blocking antibody to the co-cultures or pretreated MDSCs with bacterial sialidase to reduce the level of both α2,3- and α2,6-sialoglycans on the surface of MDSCs. Using a Siglec-E blocking antibody, we could decrease the suppression by SigE^{WT} MDSCs but no significant difference was observed by blocking Siglec-E on SigE^{ΔLysM} MDSCs or T cells alone (Fig. 3.4 B-D). Pretreatment of MDSCs with sialidase strongly reduced MDSC suppressive activity of both, SigE^{ΔLysM} and SigE^{WT}-derived MDSCs (Fig. 3.4 C, D). This data shows that sialoglycan ligands and Siglec-E on murine MDSCs are important players in the suppressive effect of MDSCs against murine T cells.

To further address the effect of sialidase treatment and lack of Siglec-E *in vivo*, we generated B16F10 cells stably expressing *H1N1* viral sialidase (B16F10-sia) and compared tumor growth with B16F10 wild type in SigE^{ΔLysM} and SigE^{WT} mice (fig. S4 A+B). In accordance with *in vitro* experiments, sialidase expression highly decreased tumor growth in SigE^{ΔLysM} and SigE^{WT} mice (fig S4 C+D). Mice injected with B16F10-sia that additionally were SigE^{ΔLysM} showed the highest survival benefit and resulted in 50% tumor free-survival. However, SigE^{WT} mice injected with B16F10-sia eventually reached tumor endpoint. Taken together, Siglec-E as well as sialoglycan ligands on murine MDSCs are involved in the suppression of CD8$^+$ T cells.
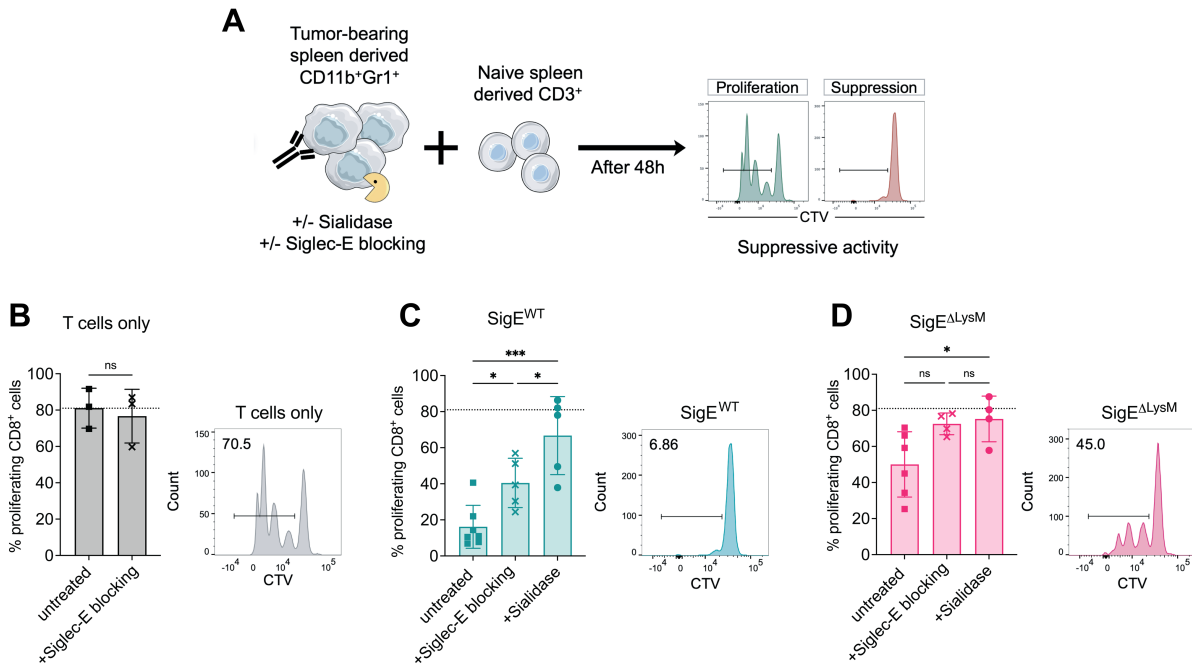
Fig. 3.4: Reduced suppressive function of MDSCs lacking Siglec-E and upon sialidase or Siglec-E blocking antibody treatment

(A) Experimental setup to assess the suppressive capacity of Gr1+CD11b+ (MDSCs) cells against naïve CD3+ (T cells) cells. MDSCs were isolated from spleens of B16F10 tumor-bearing SigE^ΔLysM mice and SigE^WT littermates. T cells were isolated from naïve littermates, stained with CTV and co-cultured with MDSCs for 48 hours in the presence of aCD3, aCD28 and IL-2. MDSCs were used immediately or pretreated with sialidase. Siglec-E blocking antibody was added to the co-cultures as indicated. **(B)** Percentage of proliferation of CD8+ T cells co-cultured without MDSCs, **(C)** with MDSCs from SigE^WT mice or **(D)** MDSCs from SigE^ΔLysM mice. Exemplary results for each untreated condition are shown on the right. Pooled data from at least 2 independent experiments. *N=3-7 mice per group from N=3 experiments.*

Data are presented as mean. Error bar values represent SD. Two-tailed unpaired Student's t-test or multiple unpaired t-tests (C, D) was used. *P<0.05, **P<0.01, ***P<0.001, and ****P<0.0001.

3.5 Sialoglycans modulate the generation of human suppressive myeloid cells generated *in vitro*

Next, we were wondering if targeting the Siglec-sialoglycan axis on human MDSCs affects their suppressive capacity. To test this, we used an *in vitro* model to generate suppressive tumor-educated myeloid-derived CD33$^+$ cells further referred to as MDSC-like cells by adapting the protocol from Lechner et al. (Lechner et al., 2011) (Fig. 3.5 A). Using lung adenocarcinoma A549 and cervix adenocarcinoma HeLa cell lines, we generated highly immunosuppressive MDSC-like cells from fresh peripheral blood mononuclear cells (PBMCs) that were able to decrease CD8$^+$ T cell proliferation in an effector:target (E:T) ratio-dependent manner (fig. S5 A). This model was used to test the role of the Siglec-sialoglycan axis during MDSC generation and function with suppression of autologous T cells as a functional read-out similar to the previous murine studies.

To determine the role of the glycosylation of cancer cells during generation of MDSC-like cells, we compared the potential of parental A549, A549 cells expressing sialidase (A549-sia) and A549-GNE Knockout (KO) cell lines to generate MDSC-like cells. A549-GNE K cells have a deficiency of UDP-N-acetylglucosamine 2-epimerase/N-acetylmannosamine kinase (GNE), a key enzyme of sialic acid biosynthesis leading to decreased sialoglycan expression (Hinderlich et al., 2015). A549-sia stably express membrane-bound viral sialidase, which cleaves α2,3- and α2,6-sialic acid from the surface of A549 cells and also surrounding cells. To test the sialidase activity, A549 cells were stained for lectins indicating effective desialylation by an increase in PNA and decrease in SNA and MALII levels (fig. S5 B). Generation of MDSC-like cells with parental cancer cells as well as GNE KO cells resulted in strong suppressive capacity. In contrast, co-culture with sialidase-expressing cancer cells induced a significantly less suppressive phenotype shown by an increased T cell proliferation (Fig. 3.5 B). To avoid a cell line-specific effect, we used HeLa and HeLa cells expressing sialidase (HeLa-sia) and observed similar results (fig. S5 D). To test the effect of sialidase expression on MDSC-like cells, we assessed the lectin levels of MDSC-like cells in A549-sia co-cultures. Co-culture with A549-sia led to desialylation of MDSC-like cells as shown by a decrease in SNA and MALII levels as well as an increase in PNA compared to MDSC-like cells generated with parental cancer cell lines (Fig. 3.5 C+D, fig. S5 C). These findings suggest that the sialoglycan levels on MDSC-like cells are important for their suppressive function against T cells, but the level of sialoglycan ligands on cancer cell lines does not impact their suppressive potential. This indicates an interaction of Siglecs and sialoglycan ligands on the surface of MDSC-like cells rather than *cis* interaction with cancer cells.

To better understand the differences of *in vitro* generated MDSC-like cells and the role of sialoglycans during MDSC generation, transcriptomics analysis was performed by bulk RNA sequencing of MDSC-like cells generated with A549 and A549-sia cancer cell lines. Suppressive myeloid cells created with A549-sia resulted in a downregulation of various functional markers previously described as MDSC markers or pro-tumor function MDSC-related genes on RNA level including S100A8/9, PTGS2, IL10 and IL1beta (Bronte et al., 2016; Veglia, Sanseviero, et al., 2021) (Fig. 3.5 E, fig. S5 E). Additionally, generation of MDSC-like cells by A549-sia co-culture significantly inhibited chemokine and chemotaxis molecules on RNA level including CCL2, CCL13, CXCL7 and CXCL2 and led to an increase in many genes involved in adhesion and attachment. These results show that desialylation of MDSC-like cells during their generation leads to downregulation of MDSC-functional markers on RNA level and decreased suppressive capacity *in vitro*.

3.6 Sialidase treatment and Siglec-9 blocking attenuate the suppressive activity of myeloid cells

Next, we wanted to address the effect of sialidase treatment and Siglec-9 blocking as a therapeutic approach to treat *in vitro* generated human suppressive myeloid cells. To this end, we generated MDSC-like cells as described in the previous section and pretreated them either with bacterial and viral sialidase to cleave surface sialoglycan ligands or added Siglec-9 blocking antibody to the co-cultures (Fig. 3.5 A+F, fig. S5 F). Sialidase pretreatment and blocking of Siglec-9 with an antibody resulted in a significant decrease of the suppressive capacity of MDSC-like cells against autologous T cells (Fig. 3.5 F, fig. S5 F). Successful desialylation of cells by sialidase treatment was demonstrated by a significant increase in PNA staining (fig. S5 G). Similar results were obtained using HeLa-generated MDSC-like cells (fig. S5 H).

To further corroborate our findings, we used cancer patient-derived CD33^{+} cells from primary tumor cell suspensions together with autologous CD8^{+} T cells isolated from PBMCs (Fig. 3.5 G). The addition of tumor-derived CD33^{+} cells from colon and lung cancer patients could significantly decrease the proliferation of CD8^{+} T cells (Fig. 3.5 H). Pretreatment of suppressive myeloid cells with sialidase led to significant reduction of their inhibitory effect on CD8^{+} T cell proliferation (Fig. 3.5 H). Although a trend towards downregulation of suppressive capacity was observed, addition of Siglec-9 blocking antibody did not lead to significant changes compared to untreated CD33^{+} cells, suggesting that other sialic acid-binding receptors including other Siglec receptors could be involved. Our experiments using human MDSC-like cells and intratumoral patient-derived suppressive CD33^{+} cells support our finding

that the interactions of Siglec receptors with cell surface sialoglycan ligands on MDSCs can regulate their suppressive potential which is an interesting target to attenuate MDSC's suppressive function.
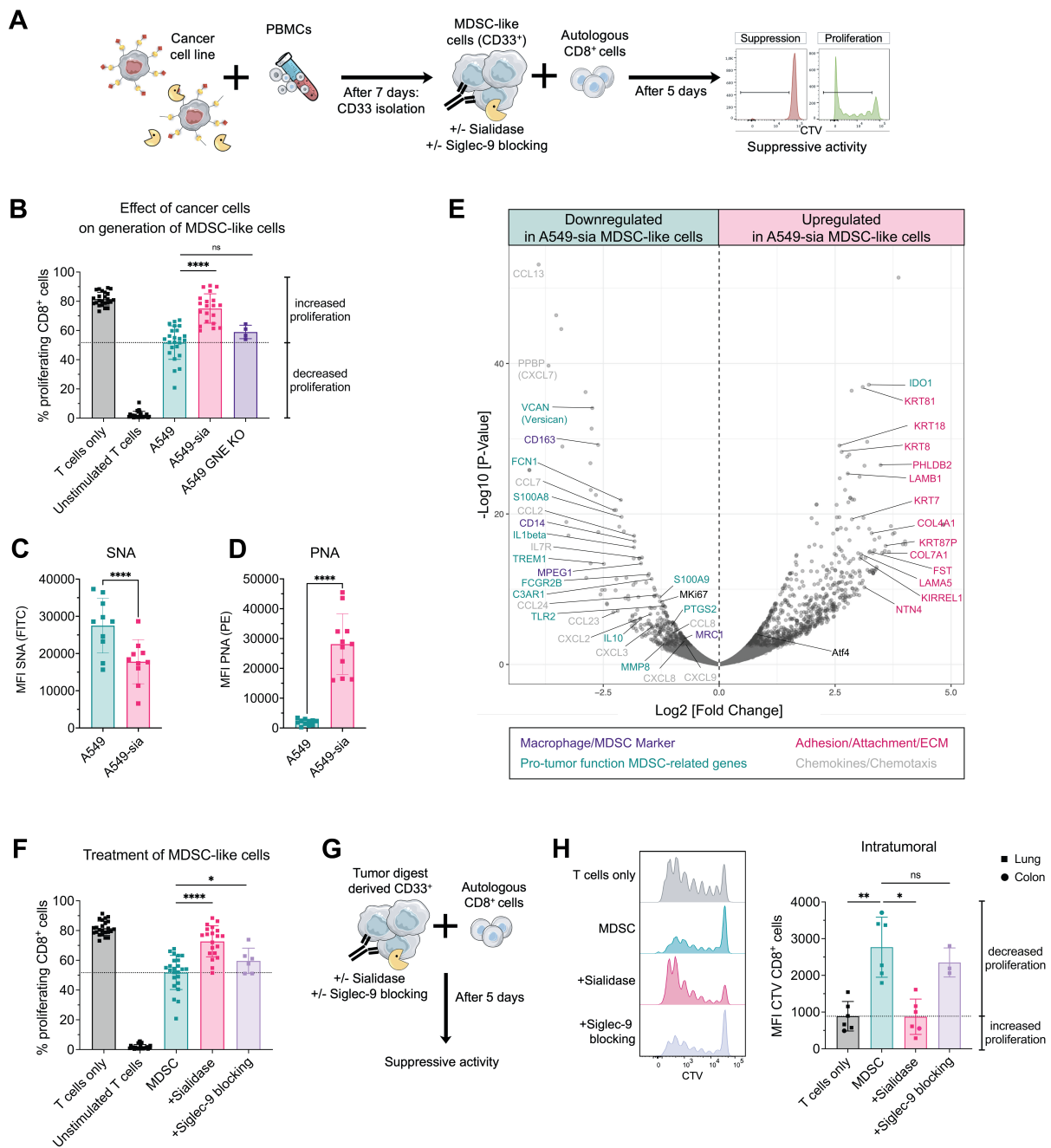
Figure 3.5: Targeting sialoglycans and Siglec-9 on suppressive human CD33⁺ cells attenuates their function

(**A**) Experimental setup to generate suppressive myeloid cells *in vitro*. Fresh PBMCs were isolated from buffy coats from healthy donors and co-cultured with indicated cancer cells lines at a ratio of 100:1. On day 7, CD33⁺ cells were isolated by magnetic positive selection and their suppressive capacity was assessed against autologous CD8⁺ T cells. Suppressive CD33⁺ cells were immediately used, pretreated with sialidase or Siglec-9 blocking antibody was added to the co-culture. CD8⁺ T cells were stained with CTV and stimulated by addition of IL-2 and anti-CD3/28 microbeads. After 5 days, CD8⁺ T cell proliferation was assessed by FACS *(continued on next page)*

(B) Percentage of proliferating CD8$^+$ cells upon co-culture with indicated suppressive CD33$^+$ cells. Suppressive myeloid cells were generated using A459, A549 stably expressing sialidase (A549-sia) or A549-GNE KO cancer cell lines. N=4-24 donors in at least n=3 experiments **(C)** Lectin staining was performed on suppressive CD33$^+$ cells on day 7 of the experiment assessing SNA and **(D)** PNA. *N=10 donors from N=5 experiments.* **(E)** Volcano plot of differentially expressed genes of suppressive CD33$^+$ cells generated with A549 or A549-sia cancer cell lines. CD33$^+$ cells were isolated on day 7 and processed for bulk RNA Sequencing. *N=4 per group.* **(F)** Percentage of proliferating CD8$^+$ cells upon co-culture with suppressive CD33$^+$ cells generated by A549 co-culture. CD33$^+$ cells were used immediately, pretreated with sialidase or Siglec-9 blocking antibody was added to the co-culture. *N=6-24 donors from at least n=4 experiments* **(G)** Assay setup to test the suppressive capacity of tumor digest-derived CD33$^+$ cells. CD33$^+$ cells were isolated freshly from tumor digest of lung or colon cancer patients, pretreated with sialidase or Siglec-9 blocking antibody was added to the co-cultures. CD8$^+$ cells were isolated from fresh PBMCs and stained with CTV. The suppressive activity was assessed on day 5 by flow cytometry. **(H)** MFI of CTV staining of CD8$^+$ cells is shown upon co-culture with tumor-derived CD33$^+$ cells. MDSCs were untreated, pretreated with sialidase or Siglec-9 blocking antibody was added to the co-culture. Exemplary results for each condition are shown on the left. *N=3-6.*

Data are presented as mean and error bar values represent SD. Paired t-test or one-way ANOVA (H) was used. *P<0.05, **P<0.01, ***P<0.001, and ****P<0.0001.

3.7 Reduction of sialoglycan ligands on MDSCs reduces immune-inhibitory CCL2 production and enhances anti-cancer immunity

Suppressive myeloid cells are involved in various pro-tumorigenic mechanisms which can be mediated by the production of suppressive cytokines or chemokines (Yang et al., 2020). To better understand the underlying mechanism responsible for changes of MDSC function influenced by Siglec-sialoglycan interactions, we analyzed the cytokines and chemokines in MDSC-T cell co-culture supernatants by ELISA. By checking murine co-culture supernatants (from Fig. 3.4 B-D), we found various cytokines in co-cultures compared to T cells alone, including CCL2, IL1β, IL-6 and IL-10 (fig. S6 A). CCL2 was highly increased in supernatants of suppressive SigE^{WT} supernatants compared to SigE$^{\Delta LysM}$ and sialidase treated conditions (Fig. 3.6 A, fig. S6 A). Furthermore, the suppressive capacity of MDSCs strongly correlated with CCL2 detected in the supernatant, indicating a relevant role of CCL2 in MDSC function (fig S6 B).

CCL2 is widely described in the context of MDSCs and can act as a chemoattractant which is involved in the migration of myeloid cells and contributes to intratumoral MDSC accumulation (Gschwandtner et al., 2019). Apart from its role as a chemoattractant, CCL2 facilitates immunosuppression of T cells by regulating suppressive functions of MDSCs via STAT3 in colorectal cancer (Chun et al., 2015) and is not only expressed by cancer cells, but also by TAMs and MDSCs (Lee et al., 2018; Y. Wang et al., 2018). To further evaluate the role of CCL2 as a mediator of MDSC suppression, the effect of CCL2 neutralization on tumor growth in SigE$^{\Delta LysM}$ and SigE^{WT} mice was addressed (Fig. 3.6 B). Importantly, CCL2 neutralization *in vivo* lead to a prolonged survival in SigE^{WT} mice, but did not significantly alter the survival of SigE$^{\Delta LysM}$ indicating an involvement in Siglec-E signaling on myeloid cells (Fig. 3.6 C). To test whether CCL2 was directly involved in the suppressive capacity of MDSCs, we analyzed the effect of CCL2 blocking antibody on MDSCs function against T cells *in vitro* (Fig. 3.6 D-F). In accordance with the *in vivo* results, CCL2 blocking significantly decreased the suppressive function of SigE^{WT} MDSCs (Fig. 3.6 E), but did not impact SigE$^{\Delta LysM}$ MDSCs (Fig. 3.6 F).

Similar to murine cell co-culture, the CCL2 transcript was significantly downregulated in conditions when MDSC-like cells were generated with A549-sia (Fig. 3.5 E). To further investigate the effect of sialidase treatment on chemokine and cytokine expression by human MDSCs, cytokine levels were measured in primary human co-culture from intratumoral suppressive myeloid cells (from Fig. 3.5 H). As observed in mice, high amounts of CCL2 were detected in supernatants of suppressive myeloid cells but pretreatment of primary human intratumoral CD33$^+$ cells with sialidase showed significantly diminished CCL2 secretion (Fig.

3.6 G, fig S6 C). Additionally, high levels of IL1β, IL-6 and IL-10 were detected in suppressive CD33$^+$ cells supernatants (Fig. 3.6 G). Sialidase treated CD33$^+$ cells and T cells alone showed low to no expression. These results suggest that interactions of cell surface sialoglycan ligands with Siglec receptors induce a suppressive phenotype in myeloid cells that inhibit sufficient anti-cancer immunity by secretion of immune-inhibitory CCL2.
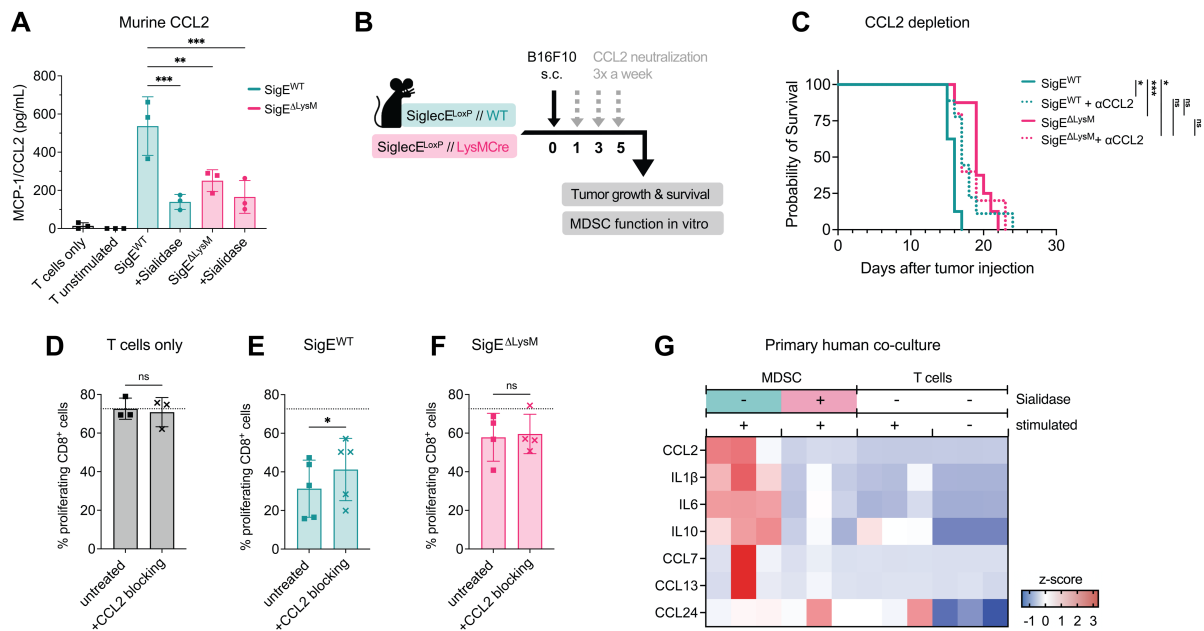
Figure 3.6: CCL2 is involved in T cell suppression via Siglec-sialoglycan axis on suppressive myeloid cells

(A) MCP-1/CCL2 found in the supernatant of murine MDSC:T cell co-cultures at endpoint of the experiment from figure 3.5 B-D. MDSCs were untreated, pretreated with sialidase or Siglec-E blocking antibody was added to the co-culture. *N=3 donors per group.* **(B)** Experimental setup: Neutralization of CCL2 using neutralization antibody in SigE$^{\Delta LysM}$ mice and SigE^{WT} littermates bearing B16F10 tumors. Mice were injected with CCL2 neutralization antibody up to 3 times a week (grey arrow) starting 1 day after subcutaneous B16F10 tumor injection (black arrow). Tumor growth and survival were monitored and suppressive capacity of MDSCs was analyzed *in vitro*. **(C)** Kaplan-Meier survival curves from pooled data from 2 independent experiments. *N=5-8 mice per group.* **(D)** Suppressive capacity of MDSCs against naïve T cells. Percentage of proliferation of CD8$^+$ T cells co-cultured without MDSCs, **(E)** with MDSCs from SigE^{WT} mice or **(F)** MDSCs from SigE$^{\Delta LysM}$ mice with or without CCL2 blocking antibody. *N=3-5 mice from N=3 experiments* **(G)** Cytokine expression found in the supernatant of human primary CD33$^+$:CD8$^+$ cell co-cultures at endpoint of the experiment from Fig. 3.6 H. CD33$^+$ cells were untreated or pretreated with sialidase. Z-scores were calculated for each cytokine and are shown on a color scale from blue to red. *N=3 donors per group.*

Data are presented as mean and error bar values represent SD. Paired t-test was used. *P<0.05, **P<0.01, ***P<0.001, and ****P<0.0001.

4 DISCUSSION

Although the Siglec-sialoglycan axis is gaining attention as a potential glyco-immune checkpoint, little is known about the expression and function of Siglecs and sialoglycan ligands on suppressive myeloid cells in cancer (van de Wall et al., 2020). Here, we show that targeting cell surface sialoglycan ligands and Siglec receptors on MDSCs can decrease their suppressive capacity by downregulation of cytokines and chemokines mainly via CCL2.
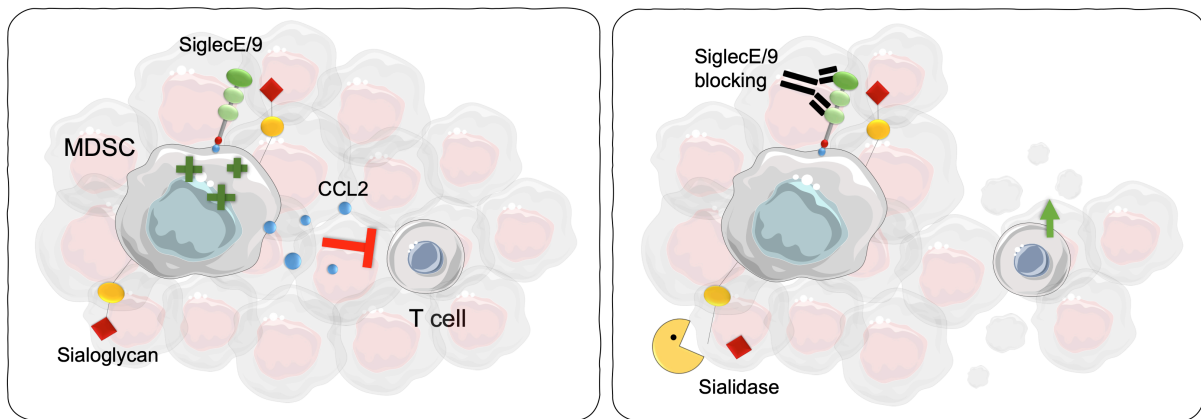

Figure 4.1 Graphical summary

Previous preclinical studies have demonstrated anti-cancer effects of blocking Siglec receptors and/or sialidase treatment on various immune cell types including T cells, NK cells and myeloid cells such as TAMs, resulting in a TME permissive towards successful cancer immunotherapy (Barkal et al., 2019; Beatson et al., 2016; Gray et al., 2020; Ibarlucea-Benitez et al., 2021; Jandus et al., 2014; Schmassmann et al., 2023; Stanczak et al., 2018, 2022). Here, we advance the understanding how Siglec-sialoglycan interactions on myeloid cells can shape an immunosuppressive environment via secretion of inhibitory CCL2 in the context of cancer across different human and murine models. Knockout of Siglec-E on myeloid cells led to prolonged tumor growth and survival in lymphoma and melanoma models of emergency-myelopoiesis and supports findings made in the glioma context (Schmassmann et al., 2023). Although we observed a strong effect of Siglec-E deletion and blocking on decreasing the suppressive capacity of suppressive myeloid cells in mice, blocking of a single inhibitory Siglec receptor on suppressive myeloid cells by Siglec-9 blocking antibody resulted in a less pronounced effect in human cell culture models. This could potentially be explained by the fact that human suppressive myeloid cells express different, maybe redundant inhibitory CD33-related Siglec receptors compared to murine suppressive myeloid cells that mainly express Siglec-E in cancer. It is possible that other Siglec family members like Siglec-5, Siglec-7 or Siglec-10 are involved in modulating the suppressive capacity of human MDSCs and that their importance might be variable or interchangeable between different tumors (Gray

et al., 2020). Sialidase treatment might be able to circumvent this by cleaving ligands for multiple Siglec receptors. A strong effect of sialidase pretreatment on the suppressive capacity of myeloid cells was observed across all assays, which supports this hypothesis. A first-in-human trial using a human bi-sialidase as cancer immunotherapy against solid tumors showed tolerability and desialylation of immune cells in the peripheral blood (Luke et al., 2023) (NCT05259696). Additional work will be needed to investigate the effect of sialidase treatment on MDSCs in this setting, but it seems encouraging to affect various players generating a suppressive TME including MDSCs and TAMs (Stanczak et al., 2022).

Reduction of sialoglycans on cancer cells did not affect the suppressive capacity of MDSC-like cells, but strong effects were observed upon constant expression of sialidase by cancer cells resulting in desialylation of MDSC-like cells. Similarly, the suppressive capacity of MDSCs was strongly reduced in human and murine MDSC:T cell co-culture models upon pretreatment of MDSCs with sialidase. These data support the hypothesis that interaction of Siglec receptors with sialoglycan ligands on myeloid cells plays a more important role as *cis* interaction than the previously propagated *trans* interactions of Siglec receptors with sialoglycan ligands on cancer cells. Expression of *cis*-ligands on various immune cells has been described before and proposed as a possible mechanism on MDSCs and immature DCs (Jenner et al., 2006; Santegoets et al., 2019). However, further studies are needed to investigate whether Siglecs and sialoglycan ligands on MDSCs interact *cis* on the same cell or *trans* between neighboring MDSCs.

Most Siglec receptors are classified as inhibitory receptors that harbor tyrosine-based signaling motifs, called ITIM domains, that can recruit and activate tyrosine phosphates including SHP-1 and SHP-2 (MacAuley et al., 2014). We identified the interaction of sialoglycan ligands and Siglecs on MDSCs as a stimulus for MDSCs leading to the release of suppressive cytokines (CCL2, IL-6, IL-10). Blockade of this interaction resulted in a decreased suppressive function. In line with our findings, others demonstrated activating signaling of macrophages and monocytes upon Siglec-9 engagement via the MEK/ERK pathway (Beatson et al., 2016). Additionally, binding of CD33/Siglec-3 by the S100A9 family on MDSCs is involved in MDSC expansion and accumulation, resulting in a release of suppressive cytokines (Chen et al., 2013). Therefore, it seems like the expression of Siglecs and sialoglycan ligands is highly context- and cell type-specific and can on one hand cause "classical" engagement and ITIM domain signaling and on the other hand result in a positive feedback loop maintaining signaling of suppressive myeloid cells. However, it is not yet clear what exact type of sialoglycan ligand is involved and further studies are needed to understand the exact mechanism by which sialoglycans can support immunosuppressive properties of suppressive

myeloid cells in cancer. Nevertheless, we see strong effect utilizing different types of sialidases, including *H1N1* viral sialidase and *Vibrio cholerae* bacterial sialidase, indicating the importance of α-2,3- and α-2,6-linked sialic acids for the suppressive function of MDSCs. Thus, it might be an advantage to utilize sialidases that cleave both linkages instead of sialidases cleaving α-2,3-linked sialic acid only (Stanczak et al., 2022). Nevertheless, it remains unclear what role other lectins play after using sialidase. Exposed lactosamine residues might bind to other immunomodulatory lectins, including galectins (Mariño et al., 2023).

Additionally, we identified CCL2 as an important immune-inhibitory chemokine released upon interactions of inhibitory Siglec receptors and sialoglycan ligands on suppressive myeloid cells. Previously, CCL2 was described to impact the secretion of effector molecules and contribute to T cell suppression via STAT3 signaling in MDSCs (Chun et al., 2015; Gschwandtner et al., 2019). Additionally, myeloid cells express high levels of CCR2, which is a promising target to interfere with MDSC migration to the TME and can also express CCL2 themselves (Barry et al., 2023; Lee et al., 2018; Y. Wang et al., 2018). Therefore, it is not surprising that we found a strong association between the suppressive capacity of MDSCs and CCL2 and that blocking of CCL2 led to an improved T cell proliferation. Nevertheless, we are the first to propose a linkage of the Siglec-sialoglycan axis on MDSCs with CCL2 expression. Further investigation is needed to better understand the molecular mechanism and role of other cytokines involved, including IL1β, IL-6 and IL-10.

Various strategies aim to target MDSCs against cancer and are under clinical investigation with some promising results (Law et al., 2020; K. Li et al., 2021). Nevertheless, due to heterogeneity, plasticity, and context-dependent functions of MDSCs, therapeutic options targeting MDSCs remain a challenge. Current therapies fail to show robust clinical activity and the selection of suitable patients and combinational therapies remains unclear (Barry et al., 2023). Here, we provide novel mechanistic insight into MDSC-mediated immunosuppression and propose targeting of MDSCs by sialidase as promising approach to reduce their suppressive potential. In addition, we developed an assay to assess the suppressive capacity of tumor-infiltrating MDSCs, which is rarely investigated and can be used to better understand MDSC subtypes and their unique functions (K. Li et al., 2021). Thus, our results help to better understand the suppressive function of MDSCs and can guide new combinational approaches in the future.

Our study contains some limitations. By using human CD33^{+} cells and murine LysM-Cre models, we target a variety of myeloid cells and it would be desirable to specifically target each of the suppressive myeloid cell subtypes to unveil their individual contribution to

immunosuppression. However, suppressive myeloid cells are closely related and recent publications utilizing in-depth transcriptional, biochemical and phenotypical characterization reveal the high complexity and plasticity of these cells (Alshetaiwi et al., 2020; Barry et al., 2023; Tcyganov et al., 2018; Veglia, Hashimoto, et al., 2021). A clear distinction and definition by phenotype as well as the functional relevance of subtypes of myeloid cells is still lacking, but would be necessary to specifically target MDSC subtypes and understand their specific functions (K. Li et al., 2021). Additionally, our assays focus on the suppressive function of MDSCs against T cells, which is described as the gold standard (Bronte et al., 2016). Interaction of Siglecs and sialoglycans on MDSC may also have additional functions on other immune cells, which need to be addressed as well.

Taken together, cancer-associated suppressive myeloid cells express high levels of inhibitory Siglec receptors and cognate sialoglycan ligands inducing an immunosuppressive phenotype. We also identified CCL2 as a major inhibitory mediator of this effect. Blocking of the Siglec-sialoglycan axis using sialidase or another broader approach targeting different Siglec receptors could potentially render an immunosuppressive TME permissive for cancer immunotherapy including immune checkpoint inhibition. Targeting sialoglycans or Siglec receptors could therefore be used to treat cancers with a significant infiltration of suppressive myeloid cells.

5 MATERIALS AND METHODS

Cell lines

HeLa and B16F10 cell lines were obtained from ATCC. A549, HeLa and EL4 were kindly provided by Zippelius Lab and HEK293T by the Bentires Lab, both from the Department of Biomedicine, Basel. *H1N1* viral sialidase expressing cell lines, A549-sia, HeLa-sia, B16F10-sia as well as EL4 GFP cells were generated by lentiviral transduction as described below. A549-GNE KO cells were generated as described before using CRISPR/CAS9 (Stanczak et al., 2018).

Mouse strains

Experiments were performed in accordance with the Swiss federal regulations and approved by the local ethics committee, Basel-Stadt, Switzerland (Approval 3036 and 3099). All animals were bred in-house at the Department of Biomedicine facility (University of Basel, Switzerland) in pathogen-free, ventilated HEPA-filtered cages under stable housing conditions of 45-65% humidity, a temperature of 21-25°C, and a a gradual light–dark cycle with light from 7:00 am to 5 pm. Mice were provided with standard food and water without restriction (License: 1007-2H).

Siglec-E^{loxP} mice were generated in collaboration with Biocytogen Company and LysM-Cre mice were generated as described before (Clausen et al., 1999). To study the role of Siglec-E KO on LysM-Cre expressing cells, Tm(Siglec-E x LysM-Cre) C57BL/6 were generated by crossing LysMCre mice with Siglec-E^{loxP} mice.

Patient samples

Tumor and blood samples were collected at the University Hospital Basel and buffy coats from healthy donors were obtained from the Blood Bank (University Hospital Basel, Switzerland). Sample collection and use of corresponding clinical data were approved by the local ethics committee in Basel, Switzerland (Ethikkommission Nordwestschweiz, EKNZ, Basel-Stadt. Switzerland) and written informed consent was obtained from all donors before sample collection.

Cell culture

Cell lines and primary cells were cultured at 37°C and 5% CO_2 and regularly checked for mycoplasma contamination. All cell lines except HEKT293T were maintained in Dulbecco's Modified Eagle Medium (DMEM, Sigma), supplemented with 10% heat-inactivated fetal bovine serum (FBS, PAA Laboratories), 1x MEM non-essential amino acid solution (Sigma) and 1% penicillin/streptomycin (Sigma). HEK293T, all primary cells and co-cultures were

maintained in Roswell Park Memorial Institute Medium (RPMI, Sigma) supplemented with 10% heat-inactivated fetal bovine serum (FBS, PAA Laboratories), 1x MEM non-essential amino acid solution (Sigma), 1 mM sodium pyruvate (Sigma), 0.05 mM 2-mercaptoethanol (Gibco) and 1% penicillin/streptomycin (Sigma).

Tumor digest, splenocyte and PBMC isolation

To obtain single cell suspension, human and mouse tumors were mechanically dissociated and subsequently enzymatically digested using accutase (PAA Laboratories), collagenase IV (Worthington), hyaluronidase (Sigma) and DNase type IV (Sigma) for 1 h at 37°C under constant agitation. Afterwards, samples were filtered using a 70 µM cell strainer and washed. Precision counting beads (BioLegend) were added to all mouse tumors to calculate the number of cells per gram of tumor.

Human peripheral blood mononuclear cells (PBMCs) were isolated from buffy coats by density gradient centrifugation using Hisopaque-1077 (Millipore) and SepMate PBMC isolation tubes (StemCell) according to the manufacturer's protocol followed by red blood cell lysis using RBC lysis buffer (eBioscience) for 2 min at RT. Subsequently, cells were washed with PBS and ready for further analysis.

For splenocyte isolation, freshly harvested murine spleens were mechanically dissociated by filtering them through a 100 µM filter. After washing, red blood cells were lysed as described above.

For murine PBMC analysis, blood from the tail vein of mice was collected on day 14 of the experiment by tail vein puncture. After washing, red blood cells were lysed as described above and samples were used immediately for lectin staining.

Single cells suspensions were used immediately or frozen for later analysis in liquid nitrogen (in 90% FBS and 10% DMSO).

Tumor models

Siglec-ExLysM-Cre mice (SigE$^{\Delta LysM}$) were injected subcutaneously into the right flank with 500 000 B16F10 melanoma, B16F10-sia, EL4 lymphoma or EL4 GFP cells in phenol red-free DMEM without additives. Siglec-E WT (SigE^{WT}) sex-matched littermates were used as control. Mice were between 8-12 weeks of age at the beginning of the experiment and conditional knockout was confirmed by flow cytometry.

Tumor size was measured 3 times a week using a caliper. Animals were sacrificed before reaching a tumor volume of 1500 mm^3 or when they reached an exclusion criterion. Tumor volume was calculated according to the following formula: Tumor volume (mm^3) = (d^2*D)/2 with D and d being the longest and shortest tumor parameter in mm, respectively.

In vivo treatment

For *in vivo* Ly6G depletion, mice were injected intraperitoneally twice per week with 100 µg/mouse Ly6G depletion antibody (Clone: 1A8, BioXCell) in PBS. Injections were started one day before tumor injection and administered twice a week till mice reached the experimental endpoint.

For neutralization of CCL2 *in vivo*, mice were injected intraperitoneally 3 times a week with 200 µg/mouse CCL2 neutralization antibody (Clone: 2H5, BioXCell) in PBS. Antibody treatment was started one day after tumor injection and continued until the endpoint of the experiment.

Multiparameter flow cytometry

Multicolor flow cytometry was performed on single cell suspension of cell lines, PBMCs, splenocytes or tumor digest. To avoid unspecific antibody binding, cells were blocked using rat anti-mouse FcγIII/II receptor (CD16/CD32) blocking antibodies (BD Bioscience) for murine and Fc Receptor Binding Inhibitor Polyclonal Antibody (Invitrogen) for human samples and subsequently stained with live/dead cell exclusion dye (Zombie Dyes, BioLegend). Surface staining was performed with fluorophore-conjugated antibodies (Table S1) or lectins for 30 minutes at 4°C in FACS buffer (PBS, 2% FCS, 0.5 mM EDTA). Stained samples were fixed using IC fixation buffer (eBioscience) until further analysis. For intracellular staining, cells were fixed and permeabilized using the Foxp3/transcription factor staining buffer set (eBioscience) and 1x Permeabilization buffer (eBioscience) according to the manufacturer's instruction. All antibodies were titrated for optimal signal-to-noise ratio. Compensation was performed using AbC Total Antibody Compensation Bead Kit (Invitrogen) or cells.

Samples were acquired on LSR II Fortessa flow cytometer (BD Biosciences), CytoFLEX (Beckmann Coulter) or Cytek Aurora (Cytek Biosciences) and analyzed using FlowJo 10.8 (TreeStar Inc). Cell sorting was performed using a BD FACSAria III or BD FACSMelody (BD Bioscience). Doublets, cell debris and dead cells were excluded before performing downstream analysis. Fluorescence-minus-one (FMO) samples were used to define the gating strategy and calculate mean fluorescence intensity (MFI).

To access desialylation status, cells were stained with lectins as described above. Fluorophore-coupled lectins - PNA-PE (GeneTex) and SNA-FITC (GeneTex) - and biotinylated lectins – MALII (GeneTex) were used at a final concentration of 10 µg/mL. Biotinylated lectins were detected using PE-Streptavidin (Biolegend).

In vitro generation of human suppressive myeloid cells

To generate suppressive human myeloid cells, we used an adapted version of the protocol established by Lechner et al. (Lechner et al., 2011).

A. Generation of MDSC-like cells

For *in vitro* MDSC induction, freshly isolated PBMCs from healthy donor buffy coats were co-cultured for 7 days with different cancer cell lines (A549, A549-GNE KO, A549-sia, HeLa, HeLa-sia) at a ratio of 1:100 in complete RPMI medium supplemented with 10 ng/mL GM-CSF (PeproTech). Cancer cells were seeded at an initial concentration of 1x10e4 cells/mL and the same amount of medium supplemented with GM-CSF was added at day 4 of the experiment. After one week, all confluent and adherent cells were collected using 0.05% trypsin-EDTA (Gibco).

B. Isolation of MDSC-like cells

For MDSC isolation, CD33 magnetic isolation was performed using the human CD33-positive selection kit II (StemCell) was used following the manufacturer's instructions. Isolated cells were resuspended in complete RPMI medium used freshly for the suppression assay.

C. Isolation of autologous CD8 T cells

Autologous CD8 T cells were obtained from frozen PBMCs from the same donor using the CD8+ Microbeads human T cell isolation Kit (Miltenyi Biotec). To monitor cell proliferation, cells were labeled with 1.25 µM CellTraceViolet (Invitrogen) according to the manufacturer's instructions. Washed cells were resuspended in complete RPMI and used for the suppression assay.

D. Suppression assay

Isolated MDSC-like cells and autologous CD8 T cells were co-cultured at indicated ratios for 5 days in a U-bottom plate in complete RPMI. T cells were stimulated by the addition of 100 IU/mL IL-2 (Proleukin) and anti-CD3/CD28 stimulation using loaded MACSiBead particles (Miltenyi Biotec) in a proportion of 1:1 of beads to cell. Unstimulated T cells and stimulated T cells without MDSC addition were used as controls. After five days, supernatants were frozen at -80°C, and the cells were stained for flow cytometry.

For Siglec-9 blocking, Siglec-9 blocking antibody (Clone 191240, R&D Systems) was added at a final concentration of 10 µg/mL. For sialidase treatment, MDSC were pretreated and washed before being added to the assay as described below.

Human intratumoral-derived MDSC suppression assay

PBMCs and tumor digests were used freshly immediately after isolation as described above. MDSCs were isolated from tumor digest and CD8 T cells from PBMCs using CD33 Microbeads (Miltenyi) or CD8 Microbeads (Miltenyi), respectively. Cells were co-cultured at a MDSC:target ratio of 1:4 in a U-bottom plate for 5 days in complete RPMI in the presence of 30 IU IL-2 (Proleukin) and human CD2/CD3/CD28 T cell activator at a final concentration of 25 µL/mL (Immunocult, StemCell). For Siglec-9 blocking, Siglec-9 blocking antibody (Clone 191240, R&D Systems) was added at a final concentration of 10 µg/mL. For sialidase

treatment, MDSC were pretreated and washed before being added to the assay as described below. Supernatants were frozen at -80°C, and the cells were stained for flow cytometry.

Murine MDSC suppression assay

Murine T cells were enriched from wild type mouse splenocytes by negative selection using the murine pan T cell isolation Kit (EasySep, StemCell). To monitor T cell proliferation, isolated T cells were stained with 2.5 µM CellTraceViolet (Invitrogen) according to the manufacturer's instructions.

Murine MDSCs were isolated from splenocytes of tumor-bearing mice by negative selection using a murine MDSCs isolation Kit (EasySep, StemCell). As indicated, obtained MDSCs were used immediately or pretreated with sialidase as described below. Isolated MDSCs and T cells were plated in a ratio of 1:1 on a 96 well flat bottom plate and co-cultured for 48 hours in complete RPMI in the presence of 50 IU IL-2 (Proleukin). For T cell stimulation, the plate was coated with anti-CD3 (clone 17A2, BioLegend) and anti-CD28 (clone 37.51, BD Biosciences). Supernatants were frozen at -80°C, and the cells were stained for flow cytometry.

For Siglec-E blocking, purified anti-mouse Siglec-E antibody (M1305A02, BioLegend) was added at a final concentration of 10 µg/mL. CCL2 blocking was performed by the addition of 50 µg/mL CCL2 (Clone 2H5, BD).

Sialidase treatment

To cleave terminal sialic acid residues, cells were treated with bacterial sialidase (*Vibrio cholerae*, Sigma) at a concentration of 10 µM for 20 minutes in PBS. Subsequently, cells were washed with complete medium and used for downstream analysis. Additionally, viral sialidase (active *H1N1*, Sino Biological) and bacterial sialidase (*Arthrobacter ureafaciens*, Roche) were used for pretreatment which is indicated in the figure legends. If not stated otherwise, *Vibrio cholerae* bacterial sialidase was used.

Lentivirus production and lentiviral transduction of cells lines

To generate cell lines expressing *H1N1* viral sialidase and GFP, A549, HeLa, B16F10 and EL4 were stably transduced with lentivirus.

For lentiviral production, 14x10e6 HEK293T cells were seeded 24 hours before transfection in 18 mL complete RPMI medium in a 15-cm culture dish. For the transfection mix, 1.9 µg pMD2.G, 3.5 µg pCMVR8.74 and 5.4 µg pLV transfer vector were mixed in 1.8 ml jetOPTIMUS buffer (Polyplus). 16.2 µl jetOPTIMUS (Polyplus) was added followed by 10 minutes of incubation and finally the addition of the prepared transfection mix. Medium was exchanged after 16 hours and lentiviral particles were collected 24 and 48 hours after medium

exchange. The pooled supernatant was concentrated with 4x in-house made PEG-8000 solution and resuspended in PBS with 1% human serum albumin. Aliquots of the produced virus were stored at -80°C until further use. pMD2.G and pCMVR8.74 were kindly provided by Didier Trono (Addgene plasmid #12259 & #22036).

For lentiviral transduction, 50 000 cancer cells were seeded in a 24-well plate in 500 µL complete RPMI medium and rested overnight. Media was renewed with addition of 100 µL concentrated lentivirus and 8 µg/mL polybrene (Sigma). To increase transduction efficiency, spinoculation was performed and cells were centrifuged for 90 minutes at 800xg. Afterwards, cells were incubated at standard cell culture conditions and transduction efficiency was frequently checked by flow cytometry staining assessing sialidase expression, PNA, MALII and SNA levels.

Cytokine and chemokine analysis

Collected supernatants from murine and human co-cultures were thawed on ice and aliquots were sent on dry ice to Eve Technologies (Canada). Cytokine and chemokine concentrations were analyzed and calculated by Eve Technology. For visualization, normalized values (z-scores) of each cytokine were calculated based on the mean and standard deviation of each marker.

Bulk RNA Sequencing

MDSC-like cells generated with A549 and A549-sia cancer cells from 4 different healthy donors were harvested after 7 days of co-culture as described above. For purification of MDSCs, cells were stained with CD33-PE (Miltenyi) followed by CD33-positive selection using the EasySep human PE positive selection Kit II (StemCell). To increase purity, cells were further sorted for PE positivity by Aria III (BD Bioscience) flow cytometer. For RNA purification, sorted cells were washed and RNA isolated using the RNeasy Plus Micro Kit (Qiagen) including a gDNA elimination step by QIAshredder spin columns (Qiagen).

Quality control (QC length profiling and concentration using RiboGreen) and library preparation (TruSeq stranded mRNA HT Kit by Illumina) were performed by the Genomics Core Facility of the University Basel. Sequencing was performed on four lanes of the Illumina NextSeq 500 instrument resulting in 38nt-long paired-end reads. The dataset was analyzed by the Bioinformatics Core Facility, Department of Biomedicine, University of Basel. cDNA reads were aligned to 'hg38' genome using Ensembl 104 gene models with the STAR tool (v2.7.10a) with default parameter values except the following parameters: outFilterMultimapNmax=10, outSAMmultNmax=1, outSAMtype=BAM SortedByCoordinate, outSAMunmapped=Within. At least 40M read pairs were mapped per sample. The software R (v4.1.1) and the tool featureCounts from Subread (v2.0.1) package from Bioconductor

(v3.14) were used to count aligned reads per gene with default parameters except: -O, -M, --read2pos=5, --primary, -s 2, -p, -B. Further analysis steps were performed using R (v4.2.0) and multiple packages from Bioconductor (v3.15). The package edgeR (v3.38.1) was used to perform differential expression analysis. A gene was included in the analysis only if it had at least 1 count per million (CPM) in at least any four samples. Gene set enrichment analysis was performed using the tool camera from the edgeR package and the Gene Ontology gene set (category C5) from MSigDB (v7.5.1).

N-Glycomics analysis

For N-glycomic profiling, harvested cells were extracted with lysis buffer containing 7 M urea, 2 M thiourea, 10 mM dithioerythreitol in 40 mM Tris buffer with 1% protease inhibitor (Roche). The cell membranes were disrupted by High Intensity Focused Ultrasound with 10 times 10 s sonication with 16 amplitudes and 1 minute on ice in between, and subsequent shaking for 4 hours at cold room. The protein extracts were alkylated with 100 mM iodoacetamide in the dark for 4 hours at 37°C. Ice-cold trichloroacetic acid was added to a final 10% w/v concentration and left for one hour. After centrifugation at 20000 g for 30 minutes at 4°C, precipitated sample pellets were washed twice with ice-cold acetone and then lyophilized. Dry protein pellets were redissolved in 50 mM ammonium bicarbonate buffer (pH 8.5), 250 unit of benzonase nuclease (Sigma-Aldrich) was added and incubated for 30 minutes at 37°C, following by trypsin digestion overnight. After deactivating the activity of trypsin, protein mixtures were further treated with PNGaseF (New England Biolab). The released glycans were cleaned up according to previous studies (Lin et al., 2011).

For MALDI-MS analyses, the glycan samples were permethylated using the sodium hydroxide/dimethyl sulfoxide slurry method, as described by Dell et al (Dell et al., 1994). The samples were dissolved in 20 μL of acetonitrile. 1 μL sample mixed with 10 mg/mL 2,5-Dihydroxybenzoic acid (Bruker) in 70% Acetonitrile with 1mM sodium chloride was spotted on MALDI target plate and analyzed by Bruker RapiFlex™ MALDI-TOF-TOF. Permethylated high mannose N-glycans and glycans from fetuin were used to calibrate the instrument prior the measurement. The laser energy for each analysis was fixed and the data were accumulated from 10 000 shots. The data was analyzed by GlycoWorkbench (Ceroni et al., 2008) and inspected manually. For relative quantification, the data was first deisotoped and the peak height was used for the calculation based on the following equation:

$$Percentage\ of\ groupped\ structures = \frac{sum\ of\ peak\ height\ from\ groupped\ structures}{sum\ of\ peak\ height\ from\ all\ structures} \times 100\%$$

Statistical Analysis

All statistical analysis were performed using GraphPad Prism9. Used statistical tests as well as sample sizes are indicated in the figure legend. p values > 0.05 were considered not significant, p values < 0.05 were considered significant. Asterisks indicate: * p value < 0.05, ** p value < 0.01, *** p value < 0.001, **** p value < 0.0001. n indicates the number of biological replicates, all bars within the graphs represent mean values, and the error bars represent standard errors of the mean (SEM) or standard deviation (SD) as indicated.

6 ADDITIONAL PROJECTS

6.1 DARPin-fused T cell engager (DATE) for adenovirus-mediated cancer therapy

Patrick C. Freitag[1‡], Jonas Kolibius[1‡], **Ronja Wieboldt[2]**, Remi Weber[1], Patricia Hartmann[1], Merel van Gogh[4], Dominik Brücher[1], Heinz Läubli[2,3], Andreas Plückthun[1]*

[1] Department of Biochemistry, University of Zurich, Winterthurerstrasse 190, 8057 Zurich, Switzerland

[2] Laboratories for Cancer Immunotherapy, Department of Biomedicine, University Hospital and University of Basel, Basel, Switzerland

[3] Department of Biomedicine and Division of Medical Oncology, University Hospital Basel, Hebelstrasse 20, 4031 Basel, Switzerland

[4] Department of Physiology, University of Zurich, Comprehensive Cancer Center Zurich, 8057 Zurich, Switzerland

‡ These authors contributed equally

* Corresponding author: AP (plueckthun@bioc.uzh.ch)

Manuscript submitted

This version represents a shortened summary to highlight the overall aim and my main contribution to the manuscript.

6.1.1 Summary

The summary was written by PF and JK.

Bispecific T cell engagers are a promising class of therapeutic proteins for vector-delivered tumor therapy. They are potent yet with some systemic toxicity, and small, thus having a short half-life, all of which make intravenous administration cumbersome. But if expressed *in situ*, these properties allow high local accumulation with low systemic concentrations due to the fast filtration in the bloodstream. However, encoding fusions between two single-chain fragments of antibodies (scFv-scFv) in viral or non-viral vectors and expressing these therapeutics *in situ* ablates all forms of quality control involved during recombinant protein production. It is therefore vital to design constructs which reduce potential mispairing and increase the homogeneity of the therapeutic product. Here, we report a new T cell engager architecture for vector-mediated immunotherapy. It is based on a fusion of a designed ankyrin repeat protein (DARPin) to a CD3-targeting scFv, termed DATE for DARPin-fused T cell engager. We show potent T cell-mediated killing of HER-2$^+$ cancer cells upon the addition of both recombinantly produced DATE and effector cells, as well as by a HER-2$^+$-retargeted high-capacity adenoviral vector coding for *in situ* DATE expression. We report remarkable tumor remission, DATE accumulation, and T cell infiltration through *in situ* expression via HER-2-retargeted helper-dependent adenoviral vectors *in vivo*. Our results support further investigations and developments of DATEs as payloads for vector-mediated tumor therapy.

6.1.2 Contribution and results

My part of the project aimed to evaluate the effect of adenovirally-delivered DARPin-fused T cell engagers *in vivo*. A xenograft mouse model was utilized to investigate different infusion routes (intravenous and intratumoral injections) of constructs of interest and their effect on tumor growth and survival. Additionally, I provided tumor and blood samples that were used to assess T cell infiltration, intratumoral DATE accumulation and serum markers.

To determine the *in vivo* efficacy of DATE secreted by high-capacity human adenovirus (HC-HAdV) delivery, HER-2-retargeted HC-AdVs encoding E08-G3 (DATE-AdV) was intratumorally injected into NSG mice subcutaneously injected with HER-2-expressing SKOV3 tumor cells (Fig 6.1 A). Additionally, all mice received human T cells isolated from healthy donors by intravenous injection. Control groups received GFP-AdV, purified DATE protein, or no treatment (Fig. 6.1 A). Treatment groups were compared in terms of survival and tumor growth. No significant reduction in tumor growth was observed in GFP-AdV-treated mice compared to the PBS-control group (Fig. 6.1 B, C). Injections of purified DATE protein resulted in prolonged tumor growth, whereas DATE delivery by HC-AdVs and continuous *in situ*

expression of DATE protein led to a more drastic reduction of tumor growth resulting in tumor clearance (Fig. 6.1 B, C). In addition, 50 % of DATE-AdVs treated mice went into complete remission and remained tumor-free for over 90 days until the endpoint of the experiment, resulting in significantly increased overall survival (Fig. 6.1 D). Administration of DATE protein resulted in slightly prolonged survival compared to untreated mice. No effects were observed upon GFP-AdV injection (Fig. 6.1 D). Assessment of T cell infiltration at tumor endpoint by immunohistochemistry indicated high T cell infiltration in DATE-AdV injected mice and intermediate accumulation in mice treated with DATE protein (Fig. 6.1 E). No T cell accumulation was observed in untreated or GFP-AdV treated mice, indicating DATE-dependent T cell infiltration. HC-AdV genomes were assessed by qPCR at the endpoint of the experiment and indicated successful virus transduction of mice injected with DATE-AdV and GFP-AdV (Fig. 6.1 F). To further assess the potential of DATE-AdV for intravenous application, mice were treated by intravenous DATE-AdV injection and compared to untreated control mice (Fig. 6.2 A). Although intravenous DATE-AdV injection led to a slight reduction in tumor growth, it did not result in tumor cure and was not as efficient as intratumoral injection (Fig. 6.2 B). Nevertheless, intravenous DATE-AdV treatment resulted in T cell infiltration and increased levels of proinflammatory TNF-α at tumor endpoint (Fig. 6.2 C, D).

Our study demonstrates the successful development of DATE-AdV as a new approach for anti-cancer vector therapy. My part of the project highlights the potential of DATE-AdV usage *in vivo* against HER-2-expressing SKOV3 cells. Intratumoral DATE-AdC injection led to the reduction of tumor growth and complete curve in 50% of the treated mice. The observed DATE expression within the tumor seemed stable and was detected even 45 days after the last vector injection leading to sustained T cell infiltration. Our current results encourage the local administration of DATE-AdV because the intravenous injection resulted in a less pronounced anti-tumor effect. Further studies are needed to evaluate the effect of DATE-AdV in immunocompetent hosts with cross-reactive targets (Day et al., 2015). In summary, our data indicate that DATE-AdV treatment is suitable for tumor-targeted vector therapy *in vivo,* resulting in local secretion of DATE protein, T cell infiltration, and a sustained anti-tumor response. Thus, DATE-AdVs represent an interesting tool for effective vector immunotherapy.
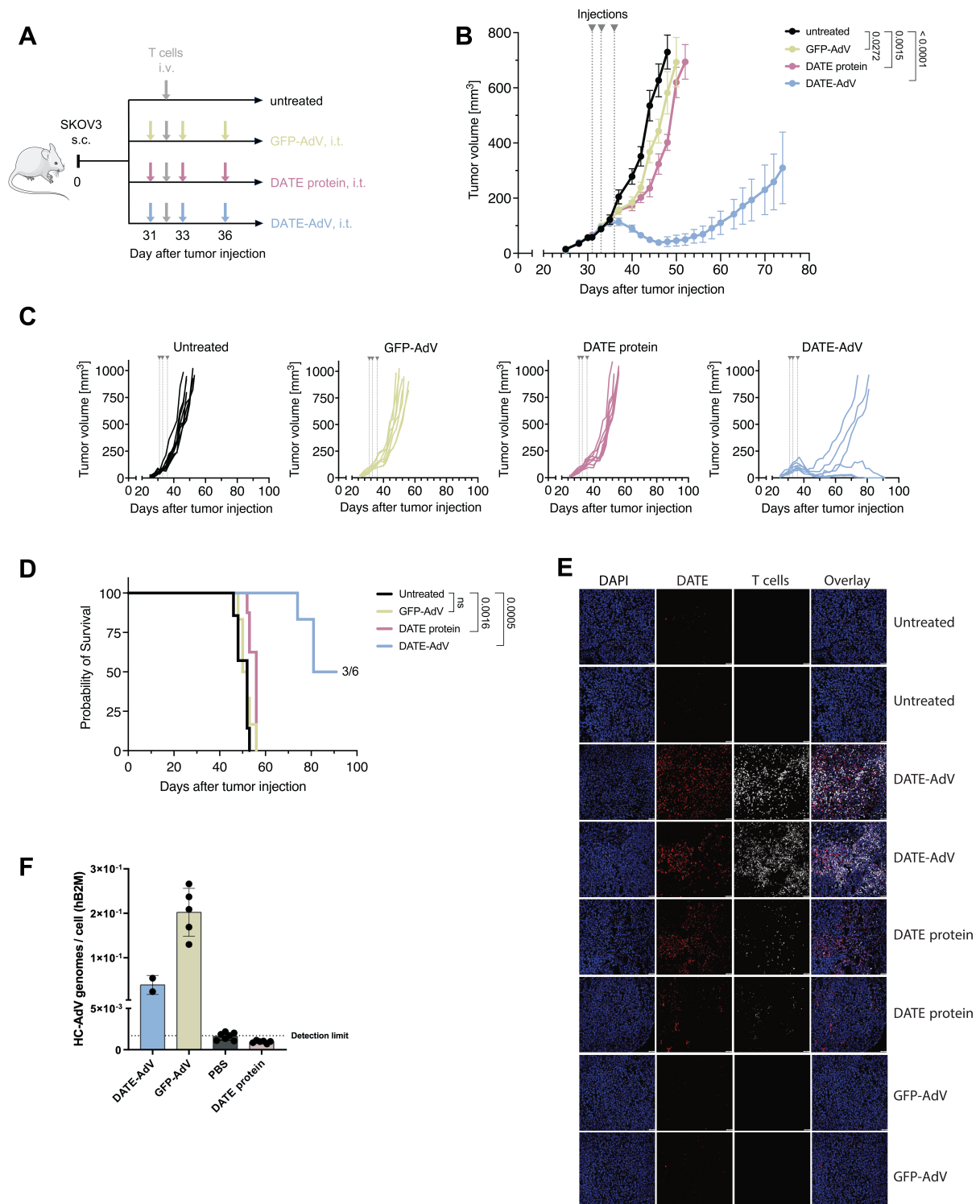
Figure 6.1: DATE-AdVs reduce tumor growth *in vivo* and induce tumor infiltration of T cells

(A) Female NSG mice were subcutaneously injected with 3×10^6 human ovarian HER-2-expressing SKOV3 cancer cells. SKOV3 tumor-bearing mice were treated with three intratumoral injections of the indicated constructs and a single intravenous injection of 7×10^6 human T cells. Mice were assessed for tumor growth and survival. Serum was collected on day 42 of the experiment and tumors were collected at endpoint for DATE detection and T cell infiltration (B) Combined tumor growth, (C) single tumor

growth curve of untreated, GFP-AdV, DATE protein and DATE-AdV-treated mice and (C) Kaplan-Meier survival curves are shown. N=6-8 mice per group. Data are shown from a representative experiment; two experiments were performed in total. Data are presented as mean. Error bar values represent SD. For survival analysis, log-rank test was used followed by Šidák correction for multiple comparisons. Tumor growth was compared on day 48 by mixed-effects analysis followed by Bonferroni's multiple comparisons test. ns = p > 0.05. (E) Immunohistochemistry analysis of representative tumor slices of optimal cutting temperature compound (OCT) embedded tumor tissue at endpoint. (F) qPCR analysis of vector DNA in tumor tissue collected at endpoint. Bar graphs represent mean ± SD.
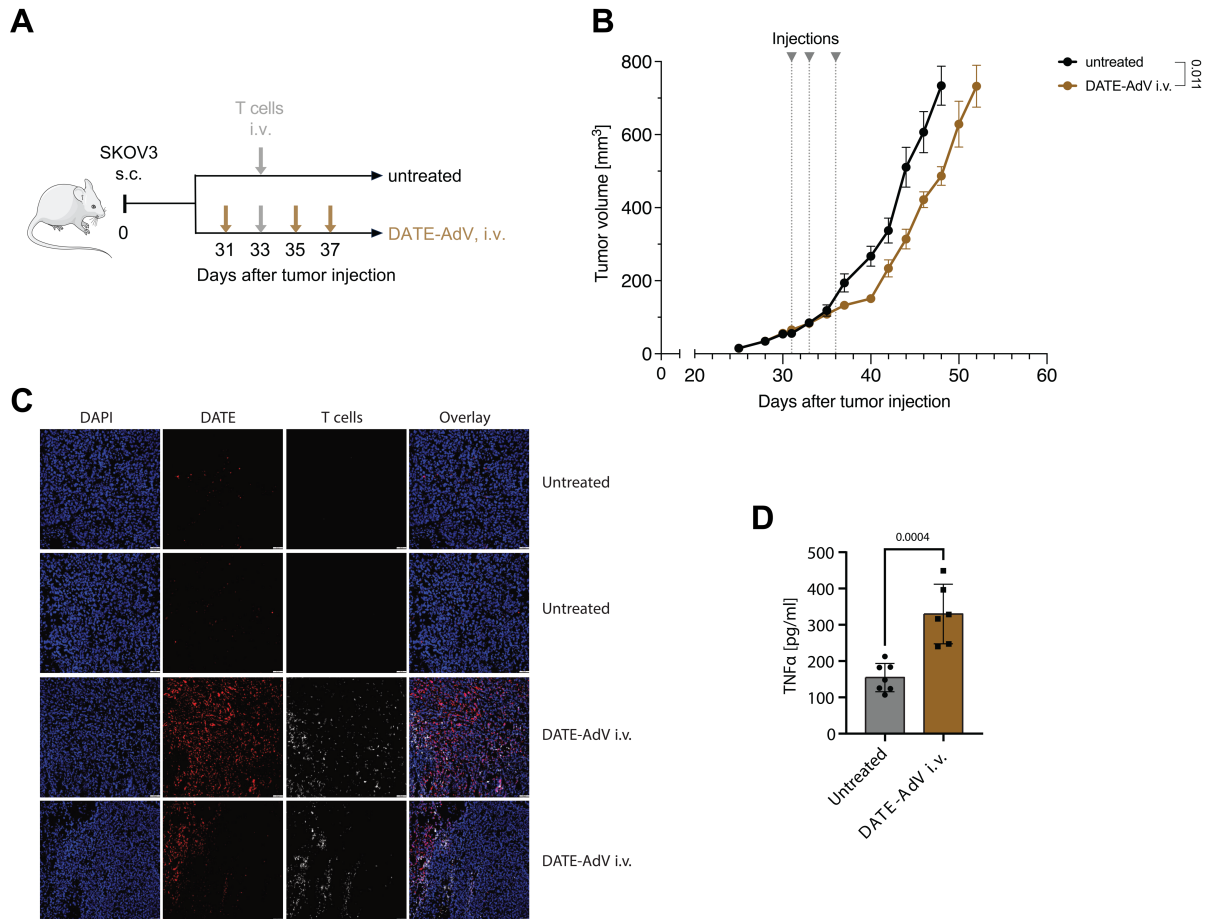
Figure 6.2: Intravenous DATE-AdV treatment of human T cell reconstituted NSG mice

(A) Female NSG mice were subcutaneously injected with human ovarian HER-2-expressing SKOV3 cancer cells. SKOV3 tumor-bearing mice were treated with three intravenous injections of DATE-AdV every 2-4 days and a single injection of 7×10^6 human T cells. (B) Tumor growth of untreated and DATE-AdV treated mice. Statistical analysis was performed on day 48 by a mixed-effect model multiple with Dunnett's multiple comparison test (n = 7 - 8 mice per group, dots represent mean ± SD) (C) Immunohistochemistry analysis of OCT-embedded tumor section of two representative mice per group. Dots represent mean ± SD (D) TNFα concentrations detected in lysed tumor tissue. Statistical analysis was performed by an unpaired two-tailed t-test (n = 7 - 8, bar graphs represent mean ± SD).

6.1.3 Methods and material

Mouse strains

Experiments were performed in accordance with the Swiss federal regulations and approved by the local ethics committee, Basel-Stadt, Switzerland (Approval 3099). NSG mice (NOD.Cg-Prkdc<scid>Il2rg < tm1Wjl>SzJ,RRID:IMSR_JAX:005557) were bred in-house at the Department of Biomedicine facility (University of Basel, Switzerland) in pathogen-free, ventilated HEPA-filtered cages under stable housing conditions of 45-65% humidity, a temperature of 21-25°C, and aa gradual light–dark cycle with light from 7:00 am to 5 pm. Mice were provided with standard food and water without restriction (License: 1007-2H).

Patient samples

Buffy coats from healthy donors were obtained from the Blood Bank (University Hospital Basel, Switzerland). Sample collection and use of corresponding clinical data was approved by the local ethics committee in Basel, Switzerland (Ethikkommission Nordwestschweiz, EKNZ, Basel-Stadt. Switzerland) and written informed consent was obtained from all donors before sample collection.

PBMC isolation

Human PBMCs were isolated from buffy coats by density gradient centrifugation using Hisopaque-1077 (Millipore) and SepMate PBMC isolation tubes (StemCell) according to manufacturer's protocol followed by red blood cell lysis using RBC lysis buffer (eBioscience) for 2 min at RT. Subsequently, the cells were washed with PBS and ready for further analysis. Single cell suspensions were stored in liquid nitrogen until further use (in 90% FBS and 10% DMSO).

T cell isolation

Human T cells were isolated from frozen healthy donor PBMCs using the EasySep Human T cell isolation Kit (StemCell) according to the manufacturer's instructions. Purity was tested by flow cytometry and was greater 95%. Freshly isolated T cells were rested overnight in in Roswell Park Memorial Institute Medium (RPMI, Sigma) supplemented with 10% heat-inactivated fetal bovine serum (FBS, PAA Laboratories), 1x MEM non-essential amino acid solution (Sigma), 1 mM sodium pyruvate (Sigma), 0.05 mM 2-mercaptoethanol (Gibco), 1% penicillin/streptomycin (Sigma) and 50 IU of IL-2 (Proleukin).

Tumor models

To validate the anti-cancer efficacy of adenovirally-delivered DARPin-fused T cell engagers *in vivo,* we established a xenograft mice model using female NOD/SCID mice that were injected subcutaneously with 3×10^6 human ovarian HER-2-expressing SKOV3 cancer cells. Mice were between 8-12 weeks of age at the beginning of the experiment. The virus was administered intratumorally once the tumors reached a tumor volume of 30-100 mm^3. Each mouse received 3 doses of virus with 1.7×10^8 transducing units every 2-3 days. Human T cells (7×10^6) isolated from healthy donors were injected intravenously one day after the first virus administration and 50 µL IL-2 (Proleukin) was given every week intraperitoneally at a dose of 2.75 mg/ml for 4 weeks. For i.v. DATE-AdV injection, 1.7×10^8 transducing units of virus were injected i.v. 3 times every 2-3 days. The tumor size was assessed 3 times a week by caliper. Animals were sacrificed before reaching a tumor volume of 1500 mm^3 or when reaching an exclusion criterion. Tumor volume was calculated according to the following formular: Tumor volume (mm^3) = $(d^2{*}D)/2$ with D and d being the longest and shortest tumor parameter in mm, respectively.

Murine tumor and serum collection

For virus detection, tumors at endpoint were collected and either snap-frozen in liquid nitrogen or embedded in OCT Embedding Matrix (CellPath). Samples were stored at -80°C until further use.

For serum collection, blood from the tail vein of mice was collected 11 days after the first virus injection by tail vein puncture. Blood was transferred to Microvette® coated with EDTA (Microvette® 200 K3E, Sarstedt) and centrifuged at 10 000 x g for 5 min at RT. The collected serum was frozen down for later analysis and stored at -80°C.

6.2 Dynamics of Natural Killer cells during clinical-grade expansion for adoptive transfer

This project is part of an ongoing clinical trial [NCT03300492] in collaboration with the Hematology Department of the University Hospital Basel. The principial Investigator of the study is Prof. Dr. med. Jakob R. Passweg and the study titled: *A Phase I/II single center study to assess the safety, tolerability, and feasibility of pre-emptive immunotherapy with in vitro expanded natural killer cells in patients treated with haploidentical stem cell transplantation for AML/MDS*.

6.2.1 Summary

Natural Killer (NK) cells are effectors of the innate immune system and play a key role in the first line of defense against viral infections neoplastic cells (Vivier et al., 2008). They can recognize and rapidly eliminate abnormal cells without prior priming and are phenotypically characterized by CD56 expression and a lack of CD3. NK cell function is tightly regulated by a complex system of activating receptors such as natural cytotoxicity receptors, DNAM-1 and NKG2D, and inhibitory receptors, which are largely represented by members of the killer immunoglobulin-like receptors (KIRs) (Vivier et al., 2008). Somatic cells are protected from killing by the expression of human leukocyte antigen (HLA) class I molecules recognized as self by KIRs. In the absence of this self-recognition and the presence of molecules interacting with activating receptors, NK cells trigger cytotoxicity and eliminate target cells by releasing cytotoxic granules like perforin and granzymes B. Moreover, NK cells can exert antibody-dependent cellular cytotoxicity (ADCC) via the CD16 receptor (Guillerey et al., 2016). Apart from direct cytotoxicity, NK cells can also trigger cytokine release and thereby bridge the innate with the adaptive immune system (Vivier et al., 2008). A tight regulation of activating and inhibitory receptors is necessary to allow NK cells to distinguish between healthy and target cells. Nevertheless, NK cells are often deregulated by the cancer microenvironment, decreased in number or show impaired cytotoxicity, which correlates with an increased risk for the patient to develop cancer (Guillerey et al., 2016; Veluchamy et al., 2017). This makes NK cells a great target in the clinical setting and various approaches aim to exploit NK cells for cancer therapy including antibodies or cytokines that directly modulate NK cell activity as well as adoptive immunotherapy with autologous or allogeneic NK cells to restore NK cell number and function (Veluchamy et al., 2017).

Important evidence on the anti-tumor potential of NK cells comes from the field of allogeneic hematopoietic stem cell transplantation. In the setting of leukemia, early reconstitution of NK cells, activation status, and NK cell counts are linked to a decreased risk

of relaps (Porrata et al., 2008; Rueff et al., 2014). Furthermore, they seem to favor transplant engraftment and promote the graft versus leukemia effect without an observed graft versus host disease and are tolerated in high doses (Ruggeri et al., 2002; Stern et al., 2013). Considering these benefits, several ongoing clinical trials are focused on the transfusion of NK cells and aim to expand large numbers of NK cells with a high anti-tumor function and a long life span (Koehl et al., 2016). Often, these protocols are time-consuming and expensive and need to be optimized, always with respect to good manufacturing process (GMP) compliance (Veluchamy et al., 2017). Therefore, it is desirable to automate parts of the process to standardize it and save resources and time.

Here, we aim to further investigate the potential of NK cell adoptive immunotherapy in the setting of hematological cancer. The overall goal is to understand and improve the current clinical-grade NK cell expansion protocol that was previously established at the University Hospital of Basel under GMP.

6.2.2 NK expansion protocol at the University Hospital of Basel

A clinical-grade NK cell expansion protocol was successfully established under GMP conditions in the laboratory of Diagnostic Hematology at the University Hospital of Basel as described previously (Fig. 6.3).
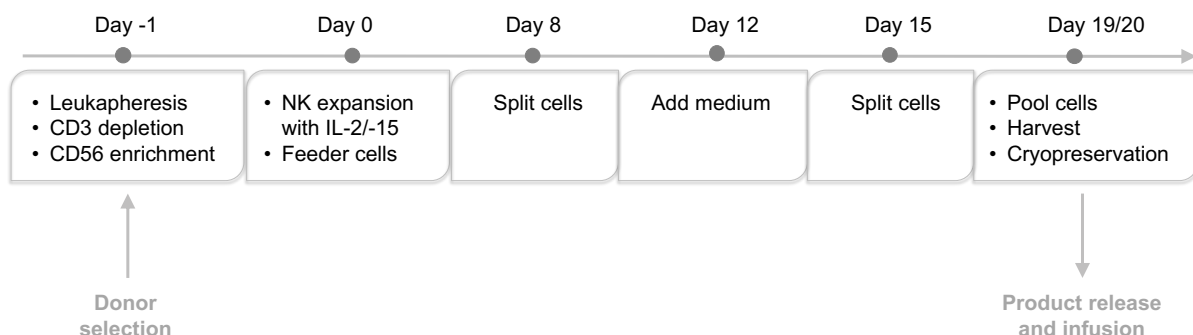
Figure 6.3: Current clinical-grade protocol to expand and manufacture NK cells for adoptive transfer

During manufacturing, NK cells are purified from the peripheral blood of healthy donors using a CliniMACS device by isolating CD56+CD3- NK cells. Subsequently, NK cells are expanded for 19 days in air-permeable tissue culture bags in the presence of human serum, IL-2/IL15, and autologous feeder cells. Autologous feeder cells consist of irradiated peripheral blood mononuclear cells collected as leftover from the purification procedure on day 0. At the end of the expansion, cells are characterized for NK cell content, T cell content, and viability and frozen in liquid nitrogen in multiple doses of injections.

Based on this NK expansion protocol, a phase I-II clinical trial in multiple myeloma with multiple infusions of NK cells expanded from haploidentical donors was recently concluded.

Patients received increasing NK cell doses after autologous hematopoietic stem-cell transplantation and high-dose Melphalan chemotherapy. The treatment was safe and well-tolerated and demonstrated the feasibility of NK cell adoptive immunotherapy in a quite complex logistic setting that requires tight coordination between cell manufacturing and clinical practice (Tschan-Plessl et al., 2021).

A second, ongoing clinical trial aims to investigate the safety and feasibility of pre-emptive immunotherapy with NK cells in AML patient treated with haploidentical stem cell transplant following post-transplantation cyclophosphamide (PT-Cy) administration [NCT03300492]. PT-Cy is a promising approach in the transplantational setting due to the fact that it removes most alloreactive donor T cells allowing the use of T cell-replete grafts without the risk of GVHD. Recently, it was demonstrated that PT-Cy treatment can eliminate mature NK cells with anti-tumor potential (Russo et al., 2018). The current clinical trial protocol aims to investigate the effect of expanded NK cells to modulate the immunological empty space after transplantation and PT-Cy in AML patients. Currently, 4/10 patients were included in the study.

6.2.3 Contribution and results

My part of the project was focused on the phenotypic and functional characterization of the NK cell product during manufacturing. A 19-color phenotype panel was established to characterize common NK cell activating and inhibitory receptors, degranulation capacity against target cells, cytokine release, proliferation capacity, and exhaustion status. Furthermore, a NK cytotoxicity assay was established to investigate the killing capacity of NK cells against the MHC class I deficient target cell line K562. Target cell death and apoptosis state serve as major read-out.

Analysis of six different time points (day 0, 8, 12, 15, 19 and 20) of the current NK expansion protocol gave insights into the dynamics of the expanded NK cell product. We observed an increase in the inhibitory receptor NKG2A as well as upregulation of NK activating receptors NKG2C, NKG2D, and NKp44 and downregulation of CD16 (Fig. 6.4 A, B). On functional levels, expanded NK cells showed a decreased in Perforin expression and an increase of granzyme B (GzmB) (Fig. 6.4 C). The exhaustion marker TIM-3 was stable upon expansion, whereas PD-1 was not detected in our NK cell product. Expanded NK cells displayed a less differentiated phenotype, with only a small subset of cells expressing the differentiation marker CD57 (Fig. 6.4 D). Proliferation of cells assessed by Ki67 was highly increased upon NK expansion and remained stable between days 12 to 20. No changes were detected in CXCR4 and KIR inhibitory receptor levels (Fig. 6.4 A, D). Stimulation of NK cells

with MHC class I negative K562 cells resulted in an increase in cytokine release and degranulation capacity upon NK expansion, as demonstrated by Interferon-γ (IFN-γ) and CD107a staining, retrospectively (Fig. 6.4 E, F). A decrease in functional activation of NK cells was observed from day 19 to 20, which includes an overnight rest of the NK product. Similar dynamics were observed in a killing assay were apoptotic and necrotic K562 target cells served as read-out (Fig. 6.4 G). Although expanded NK cells showed an increased initial killing capacity on days 8, 12, 15 and 19, we observed a decline in the final NK cell product at day 20.

Current results indicate a decline in NK cell function at the end of the manufacturing process. Most likely, overnight storage on day 19 before cryopreservation highly affects the NK product and should be avoided. Automatization of the pooling process using a Lovo cell processing system can reduce the work load and could eliminate the need for overnight rest. Additional automatization steps including the Xuri Bioreactor for cell expansion could further reduce the amount of manual work. Given the stable expression of various NK cell markers between days 15 and 19, it could also be interesting to shorten the current expansion protocol. Analysis of NK cells generated with an adapted protocol and correlation of patient outcomes with infused NK cells could be interesting objectives for additional analysis.

In summary, the phenotypic and functional analysis of NK cells during GMP expansion provided insights on the dynamics of the current NK cell product, which can guide novel clinical expansion protocols. Implementation of automatization steps and shortening of the expansion process should be tested to reduce the workload of the personnel and increase the quality of the expanded NK cell products. The established protocols to analyze NK phenotype and function can be used to evaluate the benefit of these changes. Optimization of the current NK cell protocol can help to treat more patients and might improve therapy outcome.
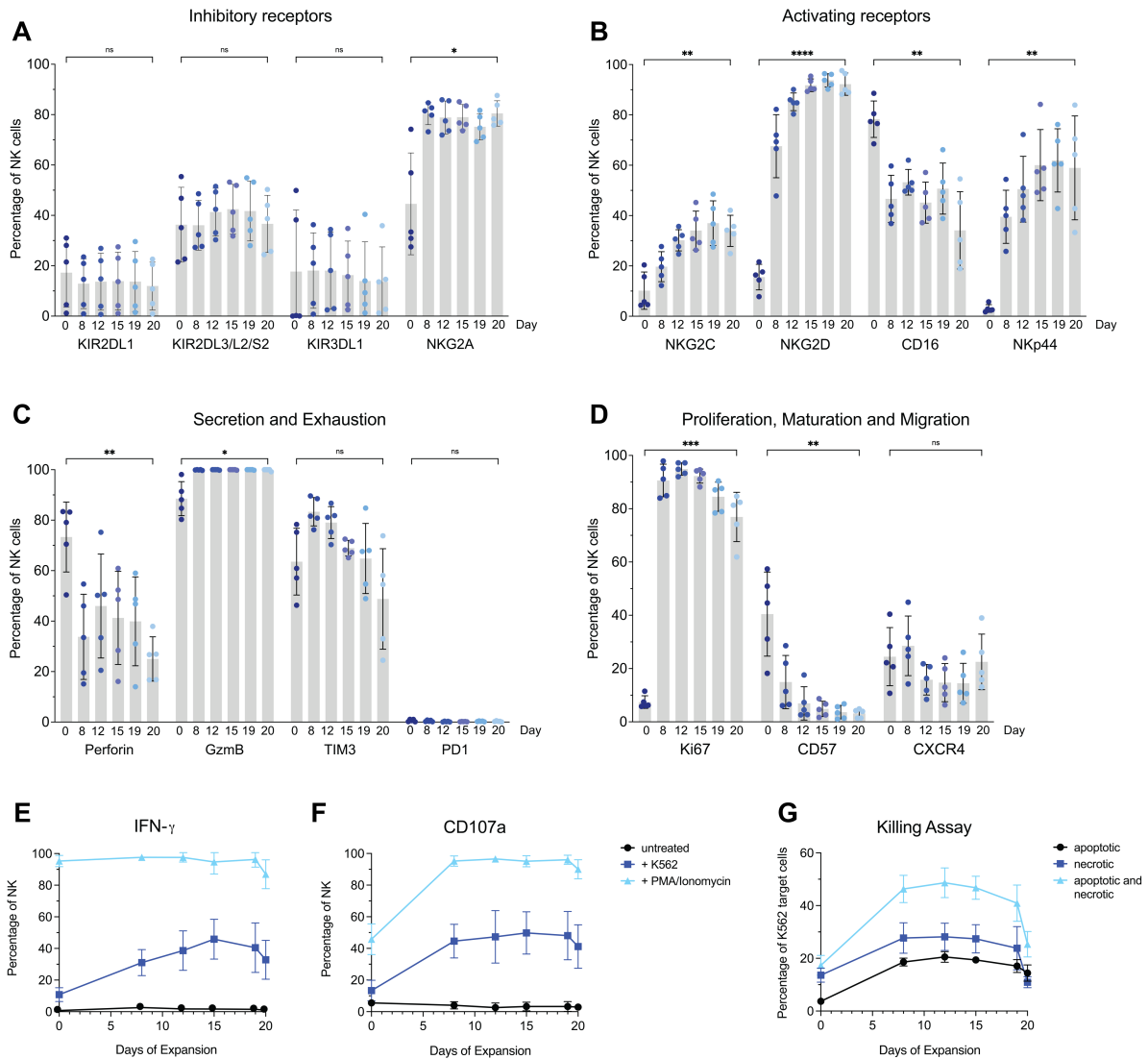
Figure 6.4: Multiparametric flow cytometry analysis of NK cells during clinical-grade *in vitro* expansion

(A) NK cells on day 0, day 8, day 12, day 15, day 19 and at endpoint of the clinical-grade expansion protocol (day 20) were analyzed by multicolor flow cytometry. Expression of (A) activating receptors, (B) inhibitory receptors, (C) secretion and exhaustion markers and (D) proliferation, maturation and migration markers are shown as percentage of bulk NK cells at indicated time points. Brackets indicate the statistical comparison of day 0 and day 20 for each marker. *N=5 donors*. (D) NK cells from all 6 times points shown in (A-D) were cultured alone, in the presence of K562 target cells or stimulated with PMA/Ionomycin. (D) Interferon-γ (IFN-γ) and (E) CD107a were assessed by flow cytometry. *N=5 donors*. (F) Killing assay using expanded NK cells from 6 different time points against K562 target cells at a ratio of 5:1. Percentage of apoptotic (Caspase-3 positive) and necrotic (dead) K562 are shown as percentage of total K562 and were assessed by flow cytometry. *N=5 donors, each donor was run in duplicates.* Data are presented as mean. Error bar values represent SD and SEM (G). Paired t-test was used. *P<0.05, **P<0.01, ***P<0.001, and ****P<0.0001.

6.3.4 Methods and material

NK cryopreservation

NK cells were collected at 6 different time points during GMP expansion (day 0, 8, 12, 15, 19 and 20) and immediately cryopreserved. The cryopreservation solution contained phosphate-buffered saline, 2% human serum albumin and 7.5% dimethyl sulfoxide. Samples were stored in liquid nitrogen.

For functional and phenotyping analysis, NK cells were thawed and rested for 2 h in Roswell Park Memorial Institute Medium (RPMI, Sigma) supplemented with 10% heat-inactivated fetal bovine serum (FBS, PAA Laboratories), and 1% penicillin/streptomycin (Sigma) in the incubator (37°C, 5% CO_2). All assays were performed in complete RPMI medium.

NK killing assay

K562 target cells were labeled using CellTrace™ Far Red Cell Proliferation Kit (Invitrogen) according to the manufacturer's instructions. NK cells and labelled K562 cells were co-cultured at a ratio of 5:1 in a 96 U-bottom plate. Killing assay was performed in duplicates for each condition and K562 cells only were used as a control. After 4 hours, cells were washed and stained for flow cytometry analysis. Precision counting beads (BioLegend) were added to each well to assess total cell numbers.

NK phenotyping and functional analysis

To assess phenotype and function of expanded NK cells, NK cells were seeded alone, co-cultured with K562 target cells at a ratio of 1:1 or stimulated with PMA (final concentration of 1 µM) and Ionomycin (final concentration of 50 nM). CD107 antibody was added to all co-cultures. After 1 hour of incubation, Monensin (GolgiSTOP, 1:1500) and Brefeldin (GolgiPLUG, 1:1000) were added and cells were incubated for another 4 hours at 37°C and 5% CO_2. Phenotype and function were evaluated by flow cytometry staining.

Multi parameter flow cytometry

Multicolor flow cytometry was performed as read-out for NK killing, phenotyping and functional assays. Cells were washed and stained with Live/dead cell exclusion dye (Live/DEAD Fixable Dead Cell Stain, Invitrogen).

Surface staining was performed with fluorophore-conjugated antibodies (Table 4.1) for 30 minutes at 4°C in FACS buffer (PBS, 2% FCS, 0.5 mM EDTA). For intracellular staining, cells were fixed and permeabilized using the Foxp3/transcription factor staining buffer set (eBioscience) and 1x Permeabilization buffer (eBioscience) according to the manufacturer's

instruction. All antibodies were titrated for optimal signal-to-noise ratio. Compensation was performed using AbC Total Antibody Compensation Bead Kit (Invitrogen) or cells.

Samples were analyzed on the Cytoflex S (Beckmann) or Aurora Spectra Analyzer (CyTek). SpectraFlow Data were collected using Beckmann Culture CytExpert (for Cytoflex) and SpectraFlow (for Aurora) and further analyzed with FlowJo (Tree Star Inc.). Doublets, cell debris and dead cells were excluded before performing downstream analysis. Fluorescence-minus-one (FMO) samples were used to define the gating strategy.

Table 6.1: Flow cytometry antibodies

Target	Clone	Fluorochrome	Manufacturer	Catalog Number
NKG2D	1D11	BUV395	BD Biosciences	743561
CD16	3G8	BUV496	BD Biosciences	612945
Ki67	B56	BUV737	BD Biosciences	567130
CD56	NCAM16.2	BUV805	BD Biosciences	749086
CXCR4	12G5	BV421	BioLegend	306518
GzmB	GB11	Pacific Blue	BioLegend	515408
CD3	UCHT1	V500	BD Biosciences	561416
CD14	M5E2	V500	BD Biosciences	561391
CD19	HIB19	V500	BD Biosciences	561121
CD57	QA17A04	BV605	BioLegend	393304
TIM3	F38-2E2	BV650	BioLegend	345028
CD107a	H4A3	BV711	BioLegend	328640
NKp44	p44-8	BV786	BD Biosciences	744304
NKG2C	REA205	Vio515	MiltenyiBiotech	130-120-019
Perforin	dG9	PerCP-Cy5.5	BioLegend	308114
NKG2A	Z199	PE	Beckman Coulter	IM3291U
PD-1	EH12-2H7	PE/Dazzle594	BioLegend	329939
KIR2DL3/L2/S2	DX27	PE-Cy7	BioLegend	312610
IFNg	4S.B3	AF647	BioLegend	502516
KIR3DL1	DX9	AF700	BioLegend	312712
KIR2DL1	REA284	APC-Vio770	MiltenyiBiotech	130-118-345
CD56	HCD56	BV605	BioLegend	318334
Caspase3	-	PE	BD Biosciences	550914

6.3 Enhancing glioblastoma clearance: Empowering anti-EGFRvIII CAR T cells with a paracrine SIRPγ-derived CD47 blocker

Tomás A. Martins[1]*; Nazanin Tatari[1]; Deniz Kaymak[1]; Ewelina M. Bartoszek[2]; Sabrina Hogan[1]; **Ronja Wieboldt[3]**; Marie-Françoise Ritz[1]; Alicia Buck[4,5]; Marta McDaid[1]; Alexandra Gerber[1]; Aisha Beshirova[6]; Tala Shekarian[1]; Manina M. Etter[7]; Anja Heider[8]; Hayget Mohamed[1]; Ines Abel[1]; Philip Schmassmann[1]; Jean-Louis Boulay[1]; Berend Snijder[5]; Tobias Weiss[4]; Heinz Läubli[3,9]; Gregor Hutter[1,7]*

[1]Brain Tumor Immunotherapy and Biology Laboratory, Department of Biomedicine, University of Basel, Basel, Switzerland

[2]Microscopy Core Facility, Department of Biomedicine, University of Basel, Basel, Switzerland

[3]Cancer Immunotherapy Laboratory, Department of Biomedicine, University of Basel, Basel, Switzerland

[4]Department of Neurology, Clinical Neuroscience Center, University Hospital Zurich and University of Zurich, Zurich, Switzerland

[5]Institute of Molecular Systems Biology, ETH Zurich, Zurich, Switzerland

[6]Experimental Immunology Laboratory, Department of Biomedicine, University of Basel, Basel, Switzerland

[7]Department of Neurosurgery, University Hospital Basel, Basel, Switzerland

[8]Immunology Laboratory, Swiss Institute of Allergy and Asthma Research, University of Zurich, Davos Wolfgang, Switzerland

[9] Division of Oncology, University Hospital Basel, Basel, Switzerland

*Corresponding authors: gregor.hutter@usb.ch, tomas.martins@unibas.ch

Manuscript submitted

This version represents a shortened summary to highlight the overall aim and my main contribution to the manuscript. All results shown were written by TM and GH and are part of the submitted manuscript.

6.3.1 Summary

A major challenge for chimeric antigen receptor (CAR) T cell therapy against glioblastoma (GBM) is the immunosuppressive tumor microenvironment (iTME), which is densely populated and supported by protumoral glioma-associated microglia and macrophages (GAMs). Blockade of CD47, a "don't-eat-me" signal overexpressed by tumor cells, disrupts the CD47-SIRPα axis and positively regulates GAM phagocytic function. However, antibody-mediated CD47 blockade monotherapy is limited by high toxicity and low bioavailability in solid tumors. Here, we combined local CAR T cell therapy with paracrine GAM modulation for an additive elimination of GBM. To this end, we engineered a novel armored CAR T cell against EGFRvIII that constitutively secretes a SIRPγ-related protein (SGRP) with high affinity to CD47. Anti-EGFRvIII-SGRP CAR T cells eliminated EGFRvIII$^+$ GBM in a dose-dependent manner *in vitro* and eradicated orthotopically xenografted EGFRvIII-mosaic GBM by locoregional application *in vivo.* This resulted in significant tumor-free long-term survival, followed by partial tumor control upon tumor re-challenge. The combination of anti-CD47 antibodies with anti-EGFRvIII CAR T cells failed to achieve a similar therapeutic effect, underscoring the importance of sustained paracrine GAM modulation. Moreover, the plasma of anti-EGFRvIII-SGRP CAR-treated mice displayed a distinct signature of innate immune modulators CCL3 and IL13. Multidimensional brain immunofluorescence microscopy and in-depth spectral flow cytometry on GBM-xenografted brains showed that anti-EGFRvIII-SGRP CAR T cells accelerated GBM clearance, increased CD68$^+$ cell trafficking to tumor scar sites, and induced a local microglia-restricted TNF response. Additionally, in a peripheral lymphoma mouse xenograft model, anti-CD19-SGRP CAR T cell treatment resulted in superior efficacy compared to conventional anti-CD19 CAR T cells. Validation on human GBM explants revealed that anti-EGFRvIII-SGRP CAR T cells had similar tumor-killing capacity compared to anti-EGFRvIII CAR monotherapy, but showed a slight improvement in CD14$^+$ cell maintenance in 48 h co-cultures. Thus, local anti-EGFRvIII-SGRP CAR T cell therapy combines the potent antitumor effect of engineered T cells with the modulation of the surrounding innate iTME, inducing an additive clearance of GBM in a manner that overcomes known mechanisms of CAR T cell therapy resistance, such as tumor innate immune suppression and antigen escape.

6.3.2 Contribution

My part of the project aimed to evaluate the effect of aCD19-SGRP in a CD19$^+$ lymphoma model *in vivo*. A xenograft mouse model was utilized to investigate targeted (aCD19 CAR or aCD19-SGRP CAR) and non-targeted CAR T cells (aEGFRvIII CAR or aEFGRvIII-SGRP CAR) and their effects on tumor growth and survival. A repetition of the experiment is currently running.

6.3.3 Results

Anti-CD19-SGRP CAR T cells have superior efficacy over conventional aCD19 CAR T cells in a peripheral lymphoma xenograft model

To demonstrate a potential benefit of iTME-targeted secretion of SGRP in another solid tumor context, we further assessed the capacity of aCD19-SGRP CAR T cells against CD19$^+$ lymphoma xenografts. In contrast to locoregional injection as the preferred application route in brain tumors, we considered a systemic approach mirroring CAR T cell treatments currently performed against leukemia[49]. CD19$^+$ Raji cells were injected s.c. in the right flank of NSG mice followed by a single dose of systemic CAR T cell infusion 3 days after tumor implantation. Animals were monitored for survival analysis and volumetric tumor burden quantification (Fig. 6.5 A). The therapeutic setup consisted of targeted CAR T cells (aCD19 CAR or aCD19-SGRP CAR) or non-targeted CAR T cells (aEGFRvIII CAR or aEFGRvIII-SGRP CAR) serving as controls (Fig. 6.5 B). All aCD19 CAR-treated animals had a significant survival benefit compared to either Vehicle or non-targeted CAR controls (Fig. 6.5 C). Strikingly, aCD19-SGRP CAR treatment resulted in the longest survival benefit (20% overall survival) with one cured animal (undetectable tumor), trending towards a superior response compared to conventional aCD19 CAR application (*P* = 0.0731; Fig. 6.5 C, D).

Thus, the contribution of SGRP-mediated innate immune modulation is of relevance in solid cancers other than GBM. This data demonstrates that our approach could potentiallly be used for the treatment of other cancers, in which myeloid immune suppression but also heterogeneity of cancer cells are playing an important role in hindering effectiv CAR T cell therapy.
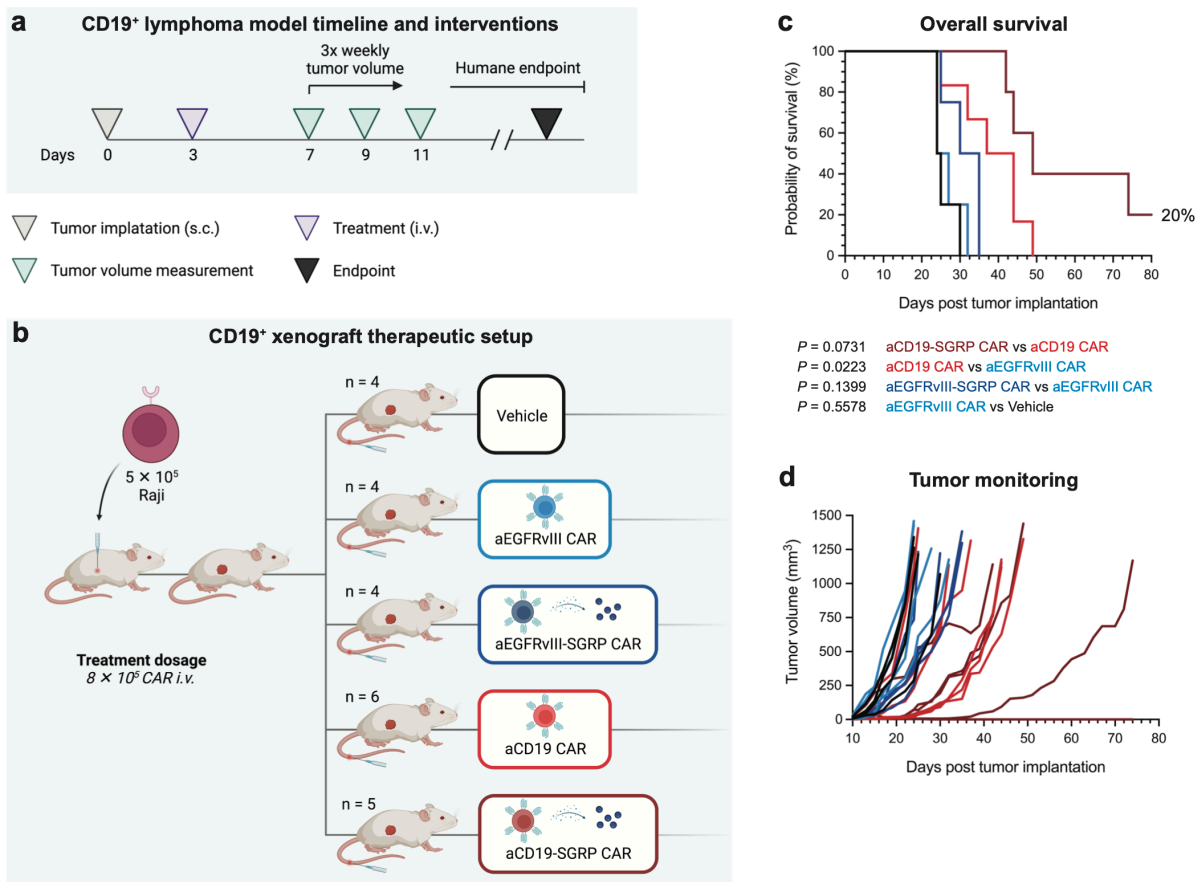
Figure 6.5: Systemic anti-CD19-SGRP CAR T cell therapy delays tumor growth and improves survival in a CD19+ lymphoma xenograft model

(A) Experimental setup and timeline of interventions of peripheral CD19+ lymphoma model treated with systemic CAR T cell infusions. Three days after tumor implantation in the right flank, mice were treated i.v. with CAR T cells, followed by 3 times weekly tumor volume assessment and clinical scoring. Mice were sacrificed upon reaching the humane endpoint. **(B)** Overview of experimental groups/therapeutic conditions and treatment dosages. **(C)** Kaplan-Meier plot of overall survival (in days). Log-rank tests were used to compare indicated treatment/control groups. **(D)** Tumor volume measurements in mm^3 of individual animals over time (in days post tumor implantation).

6.3.4 Methods and material

Mouse strains

Experiments were approved by the local ethics committee, Basel-Stadt, Switzerland (Approval 3099) and performed in accordance with the Swiss federal regulations. Animals were kept in pathogen-free, ventilated HEPA-filtered cages under stable housing conditions of 45-65% humidity, a temperature of 21-25°C, and a a gradual light–dark cycle with light from 7:00 am to 5 pm and provided with standard food and water without restriction (License 1007-2H). NSG (NOD.Cg-Prkdc<scid>Il2rg < tm1Wjl>SzJ,RRID:IMSR_JAX:005557) mice were bred in-house at the Department of Biomedicine facility (University of Basel, Switzerland).

Cell culture

Raji cells were cultured in Dulbecco's Modified Eagle Medium (DMEM, Sigma), supplemented with 10% heat-inactivated fetal bovine serum (FBS, PAA Laboratories), 1x MEM non-essential amino acid solution (Sigma) and 1% penicillin/streptomycin (Sigma). Cell lines were cultured at 37°C and 5% CO_2 and regularly checked for mycoplasma contamination.

Tumor model

To test the efficacy of the CAR constructs in a subcutaneous tumor model, NSG mice were injected with 500 000 CD19-expressing Raji cancer cells subcutaneously in the right flank. Raji cells were suspended in matrigel (BD Matrigel Basement Membrane Matrix High Concentration from Corning) diluted 1:1 in phenol red-free DMEM without additives in a total volume of 100 µL. Mice were between 8-12 weeks of age at the beginning of the experiment. Three days after tumor inoculation, mice received 0.8×10^6 CAR T cells in 100 µL PBS by intravenous injection. Tumor-bearing mice injected with T cells only were used as a control. Tumor size was measured 3 times a week using a caliper. Animals were sacrificed before reaching a tumor volume of 1500 mm^3 or when reaching an exclusion criterion. Tumor volume was calculated according to the following formular: Tumor volume (mm^3) = $(d^2 {*} D)/2$ with D and d being the longest and shortest tumor parameter in mm, respectively.

Murine serum collection

For serum collection, blood from the tail vein of mice was collected 11 days after the first virus injection by tail vein puncture. Blood was transferred to Microvette® coated with EDTA (Microvette® 200 K3E, Sarstedt) and centrifuged at 10 000 x g for 5 min at RT. The collected serum was frozen down for later analysis and stored at -80°C.

7 REFERENCES

Adams, O. J., Stanczak, M. A., Von Gunten, S., & Läubli, H. (2018). Targeting sialic acid-Siglec interactions to reverse immune suppression in cancer. In *Glycobiology* (Vol. 28, Issue 9, pp. 640–647). Oxford University Press. https://doi.org/10.1093/glycob/cwx108

Ai, L., Mu, S., Wang, Y., Wang, H., Cai, L., Li, W., & Hu, Y. (2018). Prognostic role of myeloid-derived suppressor cells in cancers: A systematic review and meta-analysis. *BMC Cancer*, *18*(1). https://doi.org/10.1186/s12885-018-5086-y

Alshetaiwi, H., Pervolarakis, N., Mcintyre, L. L., Ma, D., Nguyen, Q., Rath, J. A., Nee, K., Hernandez, G., Evans, K., Torosian, L., Silva, A., Walsh, C., & Kessenbrock, K. (2020). Defining the emergence of myeloid-derived suppressor cells in breast cancer using single-cell transcriptomics. In *Sci. Immunol* (Vol. 5). https://www.science.org

Bärenwaldt, A., & Läubli, H. (2019). The sialoglycan-Siglec glyco-immune checkpoint–a target for improving innate and adaptive anti-cancer immunity. In *Expert Opinion on Therapeutic Targets* (Vol. 23, Issue 10, pp. 839–853). Taylor and Francis Ltd. https://doi.org/10.1080/14728222.2019.1667977

Barkal, A. A., Brewer, R. E., Markovic, M., Kowarsky, M., Barkal, S. A., Zaro, B. W., Krishnan, V., Hatakeyama, J., Dorigo, O., Barkal, L. J., & Weissman, I. L. (2019). CD24 signalling through macrophage Siglec-10 is a target for cancer immunotherapy. *Nature*, *572*(7769), 392–396. https://doi.org/10.1038/s41586-019-1456-0

Barry, S. T., Gabrilovich, D. I., Sansom, O. J., Campbell, A. D., & Morton, J. P. (2023). Therapeutic targeting of tumour myeloid cells. *Nature Reviews. Cancer*. https://doi.org/10.1038/s41568-022-00546-2

Beatson, R., Tajadura-Ortega, V., Achkova, D., Picco, G., Tsourouktsoglou, T. D., Klausing, S., Hillier, M., Maher, J., Noll, T., Crocker, P. R., Taylor-Papadimitriou, J., & Burchell, J. M. (2016). The mucin MUC1 modulates the tumor immunological microenvironment through engagement of the lectin Siglec-9. *Nature Immunology*, *17*(11), 1273–1281. https://doi.org/10.1038/ni.3552

Bellis, S., Reis, C., Varki, A., Kannagi, R., Schnaar, R., & Seeberger, P. H. (2022). Glycosylation Changes in Cancer. In Varki A, Cummings RD, & Esko JD (Eds.), *Essentials of Glycobiology* (4th ed., pp. 631–644). Cold Spring Harbor Laboratory Press.

Bronte, V., Brandau, S., Chen, S. H., Colombo, M. P., Frey, A. B., Greten, T. F., Mandruzzato, S., Murray, P. J., Ochoa, A., Ostrand-Rosenberg, S., Rodriguez, P. C., Sica, A., Umansky, V., Vonderheide, R. H., & Gabrilovich, D. I. (2016). Recommendations for myeloid-derived suppressor cell nomenclature and characterization standards. In *Nature Communications* (Vol. 7). Nature Publishing Group. https://doi.org/10.1038/ncomms12150

Büll, C., Boltje, T. J., Balneger, N., Weischer, S. M., Wassink, M., Van Gemst, J. J., Bloemendal, V. R., Boon, L., Van Der Vlag, J., Heise, T., Den Brok, M. H., & Adema, G. J. (2018). Sialic acid blockade suppresses tumor growth by enhancing t-cell-mediated tumor immunity. *Cancer Research*, *78*(13), 3574–3588. https://doi.org/10.1158/0008-5472.CAN-17-3376

Burnet, M. (1957). Cancer-A Biological Approach. *British Medical Journal*, *1*(5023), 841. https://doi.org/10.1136/bmj.1.5023.841

Cao, H., & Crocker, P. R. (2011). Evolution of CD33-related siglecs: Regulating host immune functions and escaping pathogen exploitation? In *Immunology* (Vol. 132, Issue 1, pp. 18–26). https://doi.org/10.1111/j.1365-2567.2010.03368.x

Cassetta, L., Baekkevold, E. S., Brandau, S., Bujko, A., Cassatella, M. A., Dorhoi, A., Krieg, C., Lin, A., Loré, K., Marini, O., Pollard, J. W., Roussel, M., Scapini, P., Umansky, V., & Adema, G. J. (2019). Deciphering myeloid-derived suppressor cells: isolation and markers in humans, mice and non-human primates. *Cancer Immunology, Immunotherapy*, *68*(4), 687–697. https://doi.org/10.1007/s00262-019-02302-2

Cassetta, L., Bruderek, K., Skrzeczynska-Moncznik, J., Osiecka, O., Hu, X., Rundgren, I. M., Lin, A., Santegoets, K., Horzum, U., Godinho-Santos, A., Zelinskyy, G., Garcia-Tellez,

T., Bjelica, S., Taciak, B., Kittang, A. O., Höing, B., Lang, S., Dixon, M., Müller, V., … Brandau, S. (2020). Differential expansion of circulating human MDSC subsets in patients with cancer, infection and inflammation. *Journal for ImmunoTherapy of Cancer*, *8*(2). https://doi.org/10.1136/jitc-2020-001223

Ceroni, A., Maass, K., Geyer, H., Geyer, R., Dell, A., & Haslam, S. M. (2008). GlycoWorkbench: A tool for the computer-assisted annotation of mass spectra of glycans. *Journal of Proteome Research*, *7*(4), 1650–1659. https://doi.org/10.1021/pr7008252

Chen, X., Eksioglu, E. A., Zhou, J., Zhang, L., Djeu, J., Fortenbery, N., Epling-Burnette, P., Van Bijnen, S., Dolstra, H., Cannon, J., Youn, J. I., Donatelli, S. S., Qin, D., De Witte, T., Tao, J., Wang, H., Cheng, P., Gabrilovich, D. I., List, A., & Wei, S. (2013). Induction of myelodysplasia by myeloid-derived suppressor cells. *Journal of Clinical Investigation*, *123*(11), 4595–4611. https://doi.org/10.1172/JCI67580

Chockalingam, R., Downing, C., & Tyring, S. K. (2015). Cutaneous squamous cell carcinomas in organ transplant recipients. In *Journal of Clinical Medicine* (Vol. 4, Issue 6, pp. 1229–1239). MDPI. https://doi.org/10.3390/jcm4061229

Chun, E., Lavoie, S., Michaud, M., Gallini, C. A., Kim, J., Soucy, G., Odze, R., Glickman, J. N., & Garrett, W. S. (2015). CCL2 Promotes Colorectal Carcinogenesis by Enhancing Polymorphonuclear Myeloid-Derived Suppressor Cell Population and Function. *Cell Reports*, *12*(2), 244–257. https://doi.org/10.1016/j.celrep.2015.06.024

Clausen, B. E., Burkhardt, C., Reith, W., Renkawitz, R., & Förster, I. (1999). Conditional gene targeting in macrophages and granulocytes using LysMcre mice. In *Transgenic Research* (Vol. 8).

Couzin-Frankel, J. (2013). Cancer immunotherapy. In *Science* (Vol. 342, Issue 6165, pp. 1432–1433). https://doi.org/10.1126/science.342.6165.1432

Daly, J., Sarkar, S., Natoni, A., Stark, J. C., Riley, N. M., Bertozzi, C. R., Carlsten, M., & O'Dwyer, M. E. (2022). Targeting hypersialylation in multiple myeloma represents a novel approach to enhance NK cell–mediated tumor responses. *Blood Advances*, *6*(11), 3352–3366. https://doi.org/10.1182/bloodadvances.2021006805

Day, C. P., Merlino, G., & Van Dyke, T. (2015). Preclinical Mouse Cancer Models: A Maze of Opportunities and Challenges. In *Cell* (Vol. 163, Issue 1, pp. 39–53). Cell Press. https://doi.org/10.1016/j.cell.2015.08.068

Dell, A., Reason, A. J., Khoo, K.-H., Panico, M., McDowell, R. A., & Morris, H. R. (1994). Mass Spectrometry of Carbohydrate-Containing Biopolymers. In *Guide to Techniques in Glycobiology* (Vol. 230, pp. 108–132). https://doi.org/https://doi.org/10.1016/0076-6879(94)30010-0

Deng, J., & Fleming, J. B. (2022). Inflammation and Myeloid Cells in Cancer Progression and Metastasis. In *Frontiers in Cell and Developmental Biology* (Vol. 9). Frontiers Media S.A. https://doi.org/10.3389/fcell.2021.759691

Dennis, J. W., Lau, K. S., Demetriou, M., & Nabi, I. R. (2009). Adaptive regulation at the cell surface by N-glycosylation. In *Traffic* (Vol. 10, Issue 11, pp. 1569–1578). https://doi.org/10.1111/j.1600-0854.2009.00981.x

Dighe, A. S., Richards, E., Old, L. J., & Schreiber', R. D. (1994). Enhanced in vivo growth and resistance to rejection of tumor cells expressing dominant negative IFNγ receptors. In *Immunity* (Vol. 1).

Dobie, C., & Skropeta, D. (2021). Insights into the role of sialylation in cancer progression and metastasis. In *British Journal of Cancer* (Vol. 124, Issue 1, pp. 76–90). Springer Nature. https://doi.org/10.1038/s41416-020-01126-7

Dobosz, P., Stępień, M., Golke, A., & Dzieciątkowski, T. (2022). Challenges of the Immunotherapy: Perspectives and Limitations of the Immune Checkpoint Inhibitor Treatment. In *International Journal of Molecular Sciences* (Vol. 23, Issue 5). MDPI. https://doi.org/10.3390/ijms23052847

Duan, S., & Paulson, J. C. (2020). Siglecs as Immune Cell Checkpoints in Disease. *Annu Rev Immunol.* https://doi.org/10.1146/annurev-immunol-102419

Dunn, G. P., Bruce, A. T., Ikeda, H., Old, L. J., & Schreiber, R. D. (2002). Cancer immunoediting: from immuno-surveillance to tumor escape. *Nature Immunology*, *3*(11). http://www.nature.com/natureimmunology

Dysthe, M., & Parihar, R. (2020). Myeloid-Derived Suppressor Cells in the Tumor Microenvironment. In *Advances in Experimental Medicine and Biology* (Vol. 1224, pp. 117–140). Springer. https://doi.org/10.1007/978-3-030-35723-8_8

Edgar, L. J., Thompson, A. J., Vartabedian, V. F., Kikuchi, C., Woehl, J. L., Teijaro, J. R., & Paulson, J. C. (2021). Sialic Acid Ligands of CD28 Suppress Costimulation of T Cells. *ACS Central Science*, *7*(9), 1508–1515. https://doi.org/10.1021/acscentsci.1c00525

Eriksson, E., Wenthe, J., Irenaeus, S., Loskog, A., & Ullenhag, G. (2016). Gemcitabine reduces MDSCs, tregs and TGFβ-1 while restoring the teff/treg ratio in patients with pancreatic cancer. *Journal of Translational Medicine*, *14*(1). https://doi.org/10.1186/s12967-016-1037-z

Gabrilovich, D. I., Bronte, V., Chen, S. H., Colombo, M. P., Ochoa, A., Ostrand-Rosenberg, S., & Schreiber, H. (2007). The terminology issue for myeloid-derived suppressor cells. In *Cancer Research* (Vol. 67, Issue 1, p. 425). https://doi.org/10.1158/0008-5472.CAN-06-3037

Galon, J., & Bruni, D. (2019). Approaches to treat immune hot, altered and cold tumours with combination immunotherapies. In *Nature Reviews Drug Discovery* (Vol. 18, Issue 3, pp. 197–218). Nature Publishing Group. https://doi.org/10.1038/s41573-018-0007-y

Galon, J., Costes, A., Sanchez-Cabo, F., Kirilovsky, A., Mlecnik, B., Lagorce-Pages, C., Tosolini, M., Camus, M., Berger, A., Wind, P., Fridman, W.-H., & Pages, F. (2006). Type, Density, and Location of ImmuneCells Within Human Colorectal Tumors Predict Clinical Outcome. *Science*, *313*, 1960–1963. https://doi.org/10.1029/2004GL021533

Goswami, S., Anandhan, S., Raychaudhuri, D., & Sharma, P. (2023). Myeloid cell-targeted therapies for solid tumours. In *Nature Reviews Immunology* (Vol. 23, Issue 2, pp. 106–120). Nature Research. https://doi.org/10.1038/s41577-022-00737-w

Gray, M. A., Stanczak, M. A., Mantuano, N. R., Xiao, H., Pijnenborg, J. F. A., Malaker, S. A., Miller, C. L., Weidenbacher, P. A., Tanzo, J. T., Ahn, G., Woods, E. C., Läubli, H., & Bertozzi, C. R. (2020). Targeted glycan degradation potentiates the anticancer immune response in vivo. *Nature Chemical Biology*, *16*(12), 1376–1384. https://doi.org/10.1038/s41589-020-0622-x

Greten, F. R., & Grivennikov, S. I. (2019). Inflammation and Cancer: Triggers, Mechanisms, and Consequences. In *Immunity* (Vol. 51, Issue 1, pp. 27–41). Cell Press. https://doi.org/10.1016/j.immuni.2019.06.025

Gschwandtner, M., Derler, R., & Midwood, K. S. (2019). More Than Just Attractive: How CCL2 Influences Myeloid Cell Behavior Beyond Chemotaxis. In *Frontiers in Immunology* (Vol. 10). Frontiers Media S.A. https://doi.org/10.3389/fimmu.2019.02759

Guillerey, C., Huntington, N. D., & Smyth, M. J. (2016). Targeting natural killer cells in cancer immunotherapy. In *Nature Immunology* (Vol. 17, Issue 9, pp. 1025–1036). Nature Publishing Group. https://doi.org/10.1038/ni.3518

Guislain, A., Gadiot, J., Kaiser, A., Jordanova, E. S., Broeks, A., Sanders, J., van Boven, H., de Gruijl, T. D., Haanen, J. B. A. G., Bex, A., & Blank, C. U. (2015). Sunitinib pretreatment improves tumor-infiltrating lymphocyte expansion by reduction in intratumoral content of myeloid-derived suppressor cells in human renal cell carcinoma. *Cancer Immunology, Immunotherapy*, *64*(10), 1241–1250. https://doi.org/10.1007/s00262-015-1735-z

Haas, Q., Boligan, K. F., Jandus, C., Schneider, C., Simillion, C., Stanczak, M. A., Haubitz, M., Seyed Jafari, S. M., Zippelius, A., Baerlocher, G. M., Läubli, H., Hunger, R. E., Romero, P., Simon, H.-U., & von Gunten, S. (2019). Siglec-9 Regulates an Effector Memory CD8+ T-cell Subset That Congregates in the Melanoma Tumor Microenvironment. *Cancer Immunology Research*, *7*(5), 707–718. https://doi.org/10.1158/2326-6066.CIR-18-0505

Hanahan, D. (2022). Hallmarks of Cancer: New Dimensions. In *Cancer Discovery* (Vol. 12, Issue 1, pp. 31–46). American Association for Cancer Research Inc. https://doi.org/10.1158/2159-8290.CD-21-1059

Hassanpour, S. H., & Dehghani, M. (2017). Review of cancer from perspective of molecular. *Journal of Cancer Research and Practice*, *4*(4), 127–129. https://doi.org/10.1016/j.jcrpr.2017.07.001

Hernández-Ramírez, R. U., Shiels, M. S., Dubrow, R., & Engels, E. A. (2017). Cancer risk in HIV-infected people in the USA from 1996 to 2012: a population-based, registry-linkage study. *The Lancet HIV*, *4*(11), e495–e504. https://doi.org/10.1016/S2352-3018(17)30125-X

Hinderlich, S., Weidemann, W., Yardeni, T., Horstkorte, R., & Huizing, M. (2015). UDP-GlcNAc 2-epimerase/ManNAc kinase (GNE): A master regulator of sialic acid synthesis. *Topics in Current Chemistry*, *366*, 97–138. https://doi.org/10.1007/128_2013_464

Hudak, J. E., Canham, S. M., & Bertozzi, C. R. (2014). Glycocalyx engineering reveals a Siglec-based mechanism for NK cell immunoevasion. *Nature Chemical Biology*, *10*(1), 69–75. https://doi.org/10.1038/nchembio.1388

Ibarlucea-Benitez, I., Weitzenfeld, P., Smith, P., & Ravetch, J. V. (2021). Siglecs-7/9 function as inhibitory immune checkpoints in vivo and can be targeted to enhance therapeutic antitumor immunity. *PNAS*, *118*(26). https://doi.org/10.1073/pnas.2107424118/-/DCSupplemental

Ikehara, Y., Ikehara, S. K., & Paulson, J. C. (2004). Negative regulation of T cell receptor signaling by Siglec-7 (p70/AIRM) and Siglec-9. *Journal of Biological Chemistry*, *279*(41), 43117–43125. https://doi.org/10.1074/jbc.M403538200

Jandus, C., Boligan, K. F., Chijioke, O., Liu, H., Dahlhaus, M., Démoulins, T., Schneider, C., Wehrli, M., Hunger, R. E., Baerlocher, G. M., Simon, H. U., Romero, P., Münz, C., & Von Gunten, S. (2014). Interactions between Siglec-7/9 receptors and ligands influence NK cell-dependent tumor immunosurveillance. *Journal of Clinical Investigation*, *124*(4), 1810–1820. https://doi.org/10.1172/JCI65899

Jenner, J., Kerst, G., Handgretinger, R., & Müller, I. (2006). Increased α2,6-sialylation of surface proteins on tolerogenic, immature dendritic cells and regulatory T cells. *Experimental Hematology*, *34*(9), 1211–1217. https://doi.org/10.1016/j.exphem.2006.04.016

Kirchhammer, N., Trefny, M. P., Auf der Maur, P., Läubli, H., & Zippelius, A. (2022). Combination cancer immunotherapies: Emerging treatment strategies adapted to the tumor microenvironment. *Science Translational Medicine*. https://doi.org/10.1056/nejmoa2111380

Ko, J. S., Rayman, P., Ireland, J., Swaidani, S., Li, G., Bunting, K. D., Rini, B., Finke, J. H., & Cohen, P. A. (2010). Direct and differential suppression of myeloid-derived suppressor cell subsets by sunitinib is compartmentally constrained. *Cancer Research*, *70*(9), 3526–3536. https://doi.org/10.1158/0008-5472.CAN-09-3278

Koehl, U., Kalberer, C., Spanholtz, J., Lee, D. A., Miller, J. S., Cooley, S., Lowdell, M., Uharek, L., Klingemann, H., Curti, A., Leung, W., & Alici, E. (2016). Advances in clinical NK cell studies: Donor selection, manufacturing and quality control. In *OncoImmunology* (Vol. 5, Issue 4). Taylor and Francis Inc. https://doi.org/10.1080/2162402X.2015.1115178

Kumar, V., Patel, S., Tcyganov, E., & Gabrilovich, D. I. (2016). The Nature of Myeloid-Derived Suppressor Cells in the Tumor Microenvironment. In *Trends in Immunology* (Vol. 37, Issue 3, pp. 208–220). Elsevier Ltd. https://doi.org/10.1016/j.it.2016.01.004

Kusmartsev, S., Su, Z., Heiser, A., Dannull, J., Eruslanov, E., Kübler, H., Yancey, D., Dahm, P., & Vieweg, J. (2008). Reversal of myeloid cell - mediated immunosuppression in patients with metastatic renal cell carcinoma. *Clinical Cancer Research*, *14*(24), 8270–8278. https://doi.org/10.1158/1078-0432.CCR-08-0165

Labani-Motlagh, A., Ashja-Mahdavi, M., & Loskog, A. (2020). The Tumor Microenvironment: A Milieu Hindering and Obstructing Antitumor Immune Responses. In *Frontiers in Immunology* (Vol. 11). Frontiers Media S.A. https://doi.org/10.3389/fimmu.2020.00940

Läubli, H., & Varki, A. (2020). Sialic acid–binding immunoglobulin-like lectins (Siglecs) detect self-associated molecular patterns to regulate immune responses. In *Cellular and Molecular Life Sciences* (Vol. 77, Issue 4, pp. 593–605). Springer. https://doi.org/10.1007/s00018-019-03288-x

Law, A. M. K., Valdes-Mora, F., & Gallego-Ortega, D. (2020). Myeloid-Derived Suppressor Cells as a Therapeutic Target for Cancer. In *Cells* (Vol. 9, Issue 3). NLM (Medline). https://doi.org/10.3390/cells9030561

Leach, D. R., Krummel, M. F., & Allison, J. P. (1996). Enhancement of Antitumor Immunity by CTLA-4 Blockade. *Science*, *271*, 1734–1736. https://www.science.org

Lechner, M. G., Megiel, C., Russell, S. M., Bingham, B., Arger, N., Woo, T., & Epstein, A. L. (2011). Functional characterization of human Cd33+ And Cd11b+ myeloid-derived suppressor cell subsets induced from peripheral blood mononuclear cells co-cultured with a diverse set of human tumor cell lines. *Journal of Translational Medicine*, *9*. http://www.translational-medicine.com/content/9/1/90

Lee, S., Lee, E., Ko, E. Y., Ham, M., Lee, H. M., Kim, E. S., Koh, M., Lim, H. K., Jung, J., Park, S. Y., & Moon, A. (2018). Tumor-associated macrophages secrete CCL2 and induce the invasive phenotype of human breast epithelial cells through upregulation of ERO1-α and MMP-9. *Cancer Letters*, *437*, 25–34. https://doi.org/10.1016/j.canlet.2018.08.025

Li, K., Shi, H., Zhang, B., Ou, X., Ma, Q., Chen, Y., Shu, P., Li, D., & Wang, Y. (2021). Myeloid-derived suppressor cells as immunosuppressive regulators and therapeutic targets in cancer. In *Signal Transduction and Targeted Therapy* (Vol. 6, Issue 1). Springer Nature. https://doi.org/10.1038/s41392-021-00670-9

Li, T., Liu, T., Zhu, W., Xie, S., Zhao, Z., Feng, B., Guo, H., & Yang, R. (2021). Targeting MDSC for Immune-Checkpoint Blockade in Cancer Immunotherapy: Current Progress and New Prospects. In *Clinical Medicine Insights: Oncology* (Vol. 15). SAGE Publications Ltd. https://doi.org/10.1177/11795549211035540

Lin, C. W., Chen, J. M., Wang, Y. M., Wu, S. W., Tsai, I. H., & Khoo, K. H. (2011). Terminal disialylated multiantennary complex-type N-glycans carried on acutobin define the glycosylation characteristics of the Deinagkistrodon acutus venom. *Glycobiology*, *21*(4), 530–542. https://doi.org/10.1093/glycob/cwq195

Liu, C., Yang, M., Zhang, D., Chen, M., & Zhu, D. (2022). Clinical cancer immunotherapy: Current progress and prospects. In *Frontiers in Immunology* (Vol. 13). Frontiers Media S.A. https://doi.org/10.3389/fimmu.2022.961805

Luke, J. J., Johnson, M., Tolcher, A., Chen, C. T., Dai, T., Curti, B. D., El-Khoueiry, A., Sznol, M., Henick, B. S., Horak, C., Jayaraman, P., Cole, C. B., Wilson, D., Cao, L., Peng, L., Feltquate, D., Lathers, D., & Sharma, M. R. (2023). Abstract CT034: GLIMMER-01: initial results from a phase 1 dose escalation trial of a first-in-class bi-sialidase (E-602) in solid tumors. *Cancer Research*, *83*(8_Supplement), CT034–CT034. https://doi.org/10.1158/1538-7445.AM2023-CT034

MacAuley, M. S., Crocker, P. R., & Paulson, J. C. (2014). Siglec-mediated regulation of immune cell function in disease. In *Nature Reviews Immunology* (Vol. 14, Issue 10, pp. 653–666). Nature Publishing Group. https://doi.org/10.1038/nri3737

Mantuano, N. R., Natoli, M., Zippelius, A., & Läubli, H. (2020). Tumor-associated carbohydrates and immunomodulatory lectins as targets for cancer immunotherapy. In *Journal for ImmunoTherapy of Cancer* (Vol. 8, Issue 2). BMJ Publishing Group. https://doi.org/10.1136/jitc-2020-001222

Mariño, K. V., Cagnoni, A. J., Croci, D. O., & Rabinovich, G. A. (2023). Targeting galectin-driven regulatory circuits in cancer and fibrosis. In *Nature Reviews Drug Discovery*. Nature Research. https://doi.org/10.1038/s41573-023-00636-2

Mereiter, S., Balmaña, M., Campos, D., Gomes, J., & Reis, C. A. (2019). Glycosylation in the Era of Cancer-Targeted Therapy: Where Are We Heading? In *Cancer Cell* (Vol. 36, Issue 1, pp. 6–16). Cell Press. https://doi.org/10.1016/j.ccell.2019.06.006

Mirza, N., Fishman, M., Fricke, I., Dunn, M., Neuger, A. M., Frost, T. J., Lush, R. M., Antonia, S., Gabrilovich, D. I., & Lee, H. (2006). All-trans-retinoic acid improves differentiation of myeloid cells and immune response in cancer patients 1. *Cancer Res.*, *66*(18), 9299–9307.

Mittal, D., Gubin, M. M., Schreiber, R. D., & Smyth, M. J. (2014). New insights into cancer immunoediting and its three component phases-elimination, equilibrium and escape. In *Current Opinion in Immunology* (Vol. 27, Issue 1, pp. 16–25). https://doi.org/10.1016/j.coi.2014.01.004

Noel, M., O'Reilly, E. M., Wolpin, B. M., Ryan, D. P., Bullock, A. J., Britten, C. D., Linehan, D. C., Belt, B. A., Gamelin, E. C., Ganguly, B., Yin, D., Joh, T., Jacobs, I. A., Taylor, C. T., & Lowery, M. A. (2020). Phase 1b study of a small molecule antagonist of human chemokine (C-C motif) receptor 2 (PF-04136309) in combination with nab-paclitaxel/gemcitabine in first-line treatment of metastatic pancreatic ductal adenocarcinoma. *Investigational New Drugs*, *38*(3), 800–811. https://doi.org/10.1007/s10637-019-00830-3

Pagès, F., Galon, J., Dieu-Nosjean, M. C., Tartour, E., Sautès-Fridman, C., & Fridman, W. H. (2010). Immune infiltration in human tumors: A prognostic factor that should not be ignored. In *Oncogene* (Vol. 29, Issue 8, pp. 1093–1102). https://doi.org/10.1038/onc.2009.416

Pearce, O. M. T., & Läubli, H. (2015). Sialic acids in cancer biology and immunity. *Glycobiology*, *26*(2), 111–128. https://doi.org/10.1093/glycob/cwv097

Peixoto, A., Relvas-Santos, M., Azevedo, R., Lara Santos, L., & Ferreira, J. A. (2019). Protein glycosylation and tumor microenvironment alterations driving cancer hallmarks. *Frontiers in Oncology*, *9*(MAY). https://doi.org/10.3389/fonc.2019.00380

Pinho, S. S., & Reis, C. A. (2015). Glycosylation in cancer: Mechanisms and clinical implications. In *Nature Reviews Cancer* (Vol. 15, Issue 9, pp. 540–555). Nature Publishing Group. https://doi.org/10.1038/nrc3982

Porrata, L. F., Inwards, D. J., Ansell, S. M., Micallef, I. N., Johnston, P. B., Gastineau, D. A., Litzow, M. R., Winters, J. L., & Markovic, S. N. (2008). Early Lymphocyte Recovery Predicts Superior Survival after Autologous Stem Cell Transplantation in Non-Hodgkin Lymphoma: A Prospective Study. *Biology of Blood and Marrow Transplantation*, *14*(7), 807–816. https://doi.org/10.1016/j.bbmt.2008.04.013

Reily, C., Stewart, T. J., Renfrow, M. B., & Novak, J. (2019). Glycosylation in health and disease. In *Nature Reviews Nephrology* (Vol. 15, Issue 6, pp. 346–366). Nature Publishing Group. https://doi.org/10.1038/s41581-019-0129-4

Rodrigues, E., & Macauley, M. S. (2018). Hypersialylation in cancer: Modulation of inflammation and therapeutic opportunities. In *Cancers* (Vol. 10, Issue 6). MDPI AG. https://doi.org/10.3390/cancers10060207

Rodriguez, E., Boelaars, K., Brown, K., Eveline Li, R. J., Kruijssen, L., Bruijns, S. C. M., van Ee, T., Schetters, S. T. T., Crommentuijn, M. H. W., van der Horst, J. C., van Grieken, N. C. T., van Vliet, S. J., Kazemier, G., Giovannetti, E., Garcia-Vallejo, J. J., & van Kooyk, Y. (2021). Sialic acids in pancreatic cancer cells drive tumour-associated macrophage differentiation via the Siglec receptors Siglec-7 and Siglec-9. *Nature Communications*, *12*(1). https://doi.org/10.1038/s41467-021-21550-4

Rueff, J., Medinger, M., Heim, D., Passweg, J., & Stern, M. (2014). Lymphocyte subset recovery and outcome after autologous hematopoietic stem cell transplantation for plasma cell myeloma. *Biology of Blood and Marrow Transplantation*, *20*(6), 896–899. https://doi.org/10.1016/j.bbmt.2014.03.007

Ruggeri, L., Capanni, M., & Velardi, A. (2002). Effectiveness of Donor Natural Killer Cell Alloreactivity in Mismatched Hematopoietic Transplants. *Science*, *295*, 2097–2100. https://doi.org/10.1126/science.1068440

Russo, A., Oliveira, G., Berglund, S., Greco, R., Gambacorta, V., Cieri, N., Toffalori, C., Zito, L., Lorentino, F., Piemontese, S., Morelli, M., Giglio, F., Assanelli, A., Lupo Stanghellini, M. T., Bonini, C., Peccatori, J., Ciceri, F., Luznik, L., & Vago, L. (2018). NK cell recovery after haploidentical HSCT with posttransplant cyclophosphamide: dynamics and clinical implications. *Blood*, *131*(2), 247–262. http://ashpublications.org/blood/article-pdf/131/2/247/1406231/blood780668.pdf

Santegoets, K. C. M., Gielen, P. R., Büll, C., Schulte, B. M., Kers-Rebel, E. D., Küsters, B., Bossman, S. A. J. F. H., ter Laan, M., Wesseling, P., & Adema, G. J. (2019). Expression profiling of immune inhibitory Siglecs and their ligands in patients with glioma. *Cancer Immunology, Immunotherapy*, *68*(6), 937–949. https://doi.org/10.1007/s00262-019-02332-w

Schjoldager, K. T., Narimatsu, Y., Joshi, H. J., & Clausen, H. (2020). Global view of human protein glycosylation pathways and functions. In *Nature Reviews Molecular Cell Biology* (Vol. 21, Issue 12, pp. 729–749). Nature Research. https://doi.org/10.1038/s41580-020-00294-x

Schmassmann, P., Roux, J., Buck, A., Tatari, N., Hogan, S., Wang, J., Rodrigues Mantuano, N., Wieboldt, R., Lee, S., Snijder, B., Kaymak, D., Martins, T. A., Ritz, M.-F., Shekarian, T., Mcdaid, M., Weller, M., Weiss, T., Läubli, H., & Hutter, G. (2023). Targeting the Siglec-sialic acid axis promotes antitumor immune responses in preclinical models of glioblastoma. *Science Translational Medicine*. https://www.science.org

Schreiber, R. D., Old, L. J., & Smyth, M. J. (2011a). Cancer Immunoediting: Integrating Immunity's Roles in Cancer Suppression and Promotion. *Science*, *331*, 1565–1570. https://www.science.org

Schreiber, R. D., Old, L. J., & Smyth, M. J. (2011b). Cancer Immunoediting: Integrating Immunity's Roles in Cancer Suppression and Promotion. *Science*, *331*, 1565–1570. https://www.science.org

Senovilla, L., Vacchelli, E., Galon, J., Adjemian, S., Eggermont, A., Fridman, W. H., Sautès-Fridman, C., Ma, Y., Tartour, E., Zitvogel, L., Kroemer, G., & Galluzzi, L. (2012). Trial watch prognostic and predictive value of the immune infiltrate in cancer. In *OncoImmunology* (Vol. 1, Issue 8, pp. 1323–1343). https://doi.org/10.4161/onci.22009

Shankaran, V., Ikeda, H., Bruce, A. T., White, J. M., Swanson, P. E., Old, L. J., & Schreiber, R. D. (2001). IFNg and lymphocytes prevent primary tumour development and shape tumour immunogenicity. *Nature*, *410*, 1107–1111.

Sharma, P., & Allison, J. P. (2015a). Immune checkpoint targeting in cancer therapy: Toward combination strategies with curative potential. In *Cell* (Vol. 161, Issue 2, pp. 205–214). Cell Press. https://doi.org/10.1016/j.cell.2015.03.030

Sharma, P., & Allison, J. P. (2015b). The future of immune checkpoint therapy. *Science*, *348*(6230), 56–61. https://www.science.org

Sharma, P., Hu-Lieskovan, S., Wargo, J. A., & Ribas, A. (2017). Primary, Adaptive, and Acquired Resistance to Cancer Immunotherapy. In *Cell* (Vol. 168, Issue 4, pp. 707–723). Cell Press. https://doi.org/10.1016/j.cell.2017.01.017

Siew, J. J., Chern, Y., Khoo, K. H., & Angata, T. (2022). Roles of Siglecs in neurodegenerative diseases. In *Molecular Aspects of Medicine*. Elsevier Ltd. https://doi.org/10.1016/j.mam.2022.101141

Smith, B. A. H., & Bertozzi, C. R. (2021). The clinical impact of glycobiology: targeting selectins, Siglecs and mammalian glycans. In *Nature Reviews Drug Discovery* (Vol. 20, Issue 3, pp. 217–243). Nature Research. https://doi.org/10.1038/s41573-020-00093-1

Stanczak, M. A., & Läubli, H. (2023). Siglec receptors as new immune checkpoints in cancer. In *Molecular Aspects of Medicine* (Vol. 90). Elsevier Ltd. https://doi.org/10.1016/j.mam.2022.101112

Stanczak, M. A., Rodrigues Mantuano, N., Kirchhammer, N., Sanin, D. E., Jacob, F., Coelho, R., Everest-Dass, A. V, Wang, J., Trefny, M. P., Monaco, G., Bärenwaldt, A., Gray, M. A., Petrone, A., Kashyap, A. S., Glatz, K., Kasenda, B., Normington, K., Broderick, J., Peng, L., … Läubli, H. (2022). Targeting cancer glycosylation repolarizes tumor-

associated macrophages allowing effective immune checkpoint blockade. *Science Translational Medicine*, *14*. https://www.science.org

Stanczak, M. A., Siddiqui, S. S., Trefny, M. P., Thommen, D. S., Boligan, K. F., Von Gunten, S., Tzankov, A., Tietze, L., Lardinois, D., Heinzelmann-Schwarz, V., Von Bergwelt-Baildon, M., Zhang, W., Lenz, H. J., Han, Y., Amos, C. I., Syedbasha, M., Egli, A., Stenner, F., Speiser, D. E., … Läubli, H. (2018). Self-associated molecular patterns mediate cancer immune evasion by engaging Siglecs on T cells. *Journal of Clinical Investigation*, *128*(11), 4912–4923. https://doi.org/10.1172/JCI120612

Stern, M., Passweg, J. R., Meyer-Monard, S., Esser, R., Tonn, T., Soerensen, J., Paulussen, M., Gratwohl, A., Klingebiel, T., Bader, P., Tichelli, A., Schwabe, D., & Koehl, U. (2013). Pre-emptive immunotherapy with purified natural killer cells after haploidentical SCT: A prospective phase II study in two centers. *Bone Marrow Transplantation*, *48*(3), 433–438. https://doi.org/10.1038/bmt.2012.162

Street, S. E. A., Cretney, E., & Smyth, M. J. (2001). *Perforin and interferon-g activities independently control tumor initiation, growth, and metastasis*. http://ashpublications.org/blood/article-pdf/97/1/192/1670448/192.pdf

Tcyganov, E., Mastio, J., Chen, E., & Gabrilovich, D. I. (2018). Plasticity of myeloid-derived suppressor cells in cancer. In *Current Opinion in Immunology* (Vol. 51, pp. 76–82). Elsevier Ltd. https://doi.org/10.1016/j.coi.2018.03.009

Tschan-Plessl, A., Kalberer, C. P., Wieboldt, R., Stern, M., Siegler, U., Wodnar-Filipowicz, A., Gerull, S., Halter, J., Heim, D., Tichelli, A., Tsakiris, D. A., Malmberg, K. J., Passweg, J. R., & Bottos, A. (2021). Cellular immunotherapy with multiple infusions of in vitro-expanded haploidentical natural killer cells after autologous transplantation for patients with plasma cell myeloma. *Cytotherapy*, *23*(4), 329–338. https://doi.org/10.1016/j.jcyt.2020.09.009

Umansky, V., Blattner, C., Gebhardt, C., & Utikal, J. (2016). The role of myeloid-derived suppressor cells (MDSC) in cancer progression. In *Vaccines* (Vol. 4, Issue 4). MDPI AG. https://doi.org/10.3390/vaccines4040036

Vajaria, B. N., & Patel, P. S. (2017). Glycosylation: a hallmark of cancer? In *Glycoconjugate Journal* (Vol. 34, Issue 2, pp. 147–156). Springer New York LLC. https://doi.org/10.1007/s10719-016-9755-2

Vajdic, C. M., & Van Leeuwen, M. T. (2009). Cancer incidence and risk factors after solid organ transplantation. In *International Journal of Cancer* (Vol. 125, Issue 8, pp. 1747–1754). https://doi.org/10.1002/ijc.24439

van de Wall, S., Santegoets, K. C. M., van Houtum, E. J. H., Büll, C., & Adema, G. J. (2020). Sialoglycans and Siglecs Can Shape the Tumor Immune Microenvironment. In *Trends in Immunology* (Vol. 41, Issue 4, pp. 274–285). Elsevier Ltd. https://doi.org/10.1016/j.it.2020.02.001

van Houtum, E. J. H., Büll, C., Cornelissen, L. A. M., & Adema, G. J. (2021). Siglec Signaling in the Tumor Microenvironment. In *Frontiers in Immunology* (Vol. 12). Frontiers Media S.A. https://doi.org/10.3389/fimmu.2021.790317

Vanhaver, C., van der Bruggen, P., & Bruger, A. M. (2021). Mdsc in mice and men: Mechanisms of immunosuppression in cancer. In *Journal of Clinical Medicine* (Vol. 10, Issue 13). MDPI. https://doi.org/10.3390/jcm10132872

Varki, A. (2001). Loss of N-glycolylneuraminic acid in humans: Mechanisms, consequences, and implications for hominid evolution. *Yearbook of Physical Anthropology*, *44*, 54–69. https://doi.org/10.1002/ajpa.10018

Varki, A. (2011). Letter to the Glyco-Forum: Since there are PAMPs and DAMPs, there must be SAMPs? Glycan 'self-associated molecular patterns' dampen innate immunity, but pathogens can mimic them. *Glycobiology*, *21*(9), 1121–1124. https://doi.org/10.1093/glycob/cwr087

Varki, A. (2013). Siglecs. In *Encyclopedia of Biological Chemistry* (pp. 229–231). Elsevier. https://doi.org/10.1016/B978-0-12-378630-2.00483-7

Varki, A., Schnaar, R. L., & Schauer, R. (2015). Sialic Acids and Other Nonulosonic Acids. In A. Varki, R. D. Cummings, J. Esko, R. L. Schnaar, & P. H. Seeberger (Eds.), *Essentials of Glycobiology*. Cold Spring Harbor (NY): Cold Spring Harbor Laboratory Press.

Veglia, F., Hashimoto, A., Dweep, H., Sanseviero, E., de Leo, A., Tcyganov, E., Kossenkov, A., Mulligan, C., Nam, B., Masters, G., Patel, J., Bhargava, V., Wilkinson, P., Smirnov, D., Sepulveda, M. A., Singhal, S., Eruslanov, E. B., Cristescu, R., Loboda, A., … Gabrilovich, D. I. (2021). Analysis of classical neutrophils and polymorphonuclear myeloid-derived suppressor cells in cancer patients and tumor-bearing mice. *Journal of Experimental Medicine*, *218*(4). https://doi.org/10.1084/JEM.20201803

Veglia, F., Sanseviero, E., & Gabrilovich, D. I. (2021). Myeloid-derived suppressor cells in the era of increasing myeloid cell diversity. In *Nature Reviews Immunology* (Vol. 21, Issue 8, pp. 485–498). Nature Research. https://doi.org/10.1038/s41577-020-00490-y

Veltman, J. D., Lambers, M. E., Van Nimwegen, M., Hendriks, R. W., Hoogsteden, H. C., Aerts, J. G., & Hegmans, P. (2010). *COX-2 inhibition improves immunotherapy and is associated with decreased numbers of myeloid- derived suppressor cells in mesothelioma. Celecoxib influences MDSC function*. http://www.biomedcentral.com/1471-2407/10/464

Veluchamy, J. P., Kok, N., van der Vliet, H. J., Verheul, H. M. W., de Gruijl, T. D., & Spanholtz, J. (2017). The rise of allogeneic Natural killer cells as a platform for cancer immunotherapy: Recent innovations and future developments. In *Frontiers in Immunology* (Vol. 8, Issue MAY). Frontiers Media S.A. https://doi.org/10.3389/fimmu.2017.00631

Vincent, J., Mignot, G., Chalmin, F., Ladoire, S., Bruchard, M., Chevriaux, A., Martin, F., Apetoh, L., Rébé, C., & Ghiringhelli, F. (2010). 5-Fluorouracil selectively kills tumor-associated myeloid-derived suppressor cells resulting in enhanced T cell-dependent antitumor immunity. *Cancer Research*, *70*(8), 3052–3061. https://doi.org/10.1158/0008-5472.CAN-09-3690

Vivier, E., Tomasello, E., Baratin, M., Walzer, T., & Ugolini, S. (2008). Functions of natural killer cells. In *Nature Immunology* (Vol. 9, Issue 5, pp. 503–510). https://doi.org/10.1038/ni1582

Wang, J., Manni, M., Bärenwaldt, A., Wieboldt, R., Kirchhammer, N., Ivanek, R., Stanczak, M., Zippelius, A., König, D., Rodrigues Manutano, N., & Läubli, H. (2022). Siglec Receptors Modulate Dendritic Cell Activation and Antigen Presentation to T Cells in Cancer. *Frontiers in Cell and Developmental Biology*, *10*. https://doi.org/10.3389/fcell.2022.828916

Wang, J., Sun, J., Liu, L. N., Flies, D. B., Nie, X., Toki, M., Zhang, J., Song, C., Zarr, M., Zhou, X., Han, X., Archer, K. A., O'Neill, T., Herbst, R. S., Boto, A. N., Sanmamed, M. F., Langermann, S., Rimm, D. L., & Chen, L. (2019). Siglec-15 as an immune suppressor and potential target for normalization cancer immunotherapy. *Nature Medicine*, *25*(4), 656–666. https://doi.org/10.1038/s41591-019-0374-x

Wang, Y., Zhang, X., Yang, L., Xue, J., & Hu, G. (2018). Blockade of CCL2 enhances immunotherapeutic effect of anti-PD1 in lung cancer. *Journal of Bone Oncology*, *11*, 27–32. https://doi.org/10.1016/j.jbo.2018.01.002

Wu, Y., Yi, M., Niu, M., Mei, Q., & Wu, K. (2022). Myeloid-derived suppressor cells: an emerging target for anticancer immunotherapy. In *Molecular Cancer* (Vol. 21, Issue 1). BioMed Central Ltd. https://doi.org/10.1186/s12943-022-01657-y

Yang, Y., Li, C., Liu, T., Dai, X., & Bazhin, A. V. (2020). Myeloid-Derived Suppressor Cells in Tumors: From Mechanisms to Antigen Specificity and Microenvironmental Regulation. In *Frontiers in Immunology* (Vol. 11). Frontiers Media S.A. https://doi.org/10.3389/fimmu.2020.01371

Youn, J.-l., Nagaraj, S., Collazo, M., Gabrilovich, D. I., & Lee, H. (2008). *Subsets of Myeloid-Derived Suppressor Cells in Tumor Bearing Mice 1*. 5791–5802. www.jimmunol.org.

Zhang, S., Ma, X., Zhu, C., Liu, L., Wang, G., & Yuan, X. (2016). The role of myeloid-derived suppressor cells in patients with solid tumors: A meta-analysis. *PLoS ONE*, *11*(10). https://doi.org/10.1371/journal.pone.0164514

Zhu, S. Y., & Yu, K. Da. (2022). Breast Cancer Vaccines: Disappointing or Promising? In *Frontiers in Immunology* (Vol. 13). Frontiers Media S.A. https://doi.org/10.3389/fimmu.2022.828386

8 SUPPLEMENTARY FIGURES

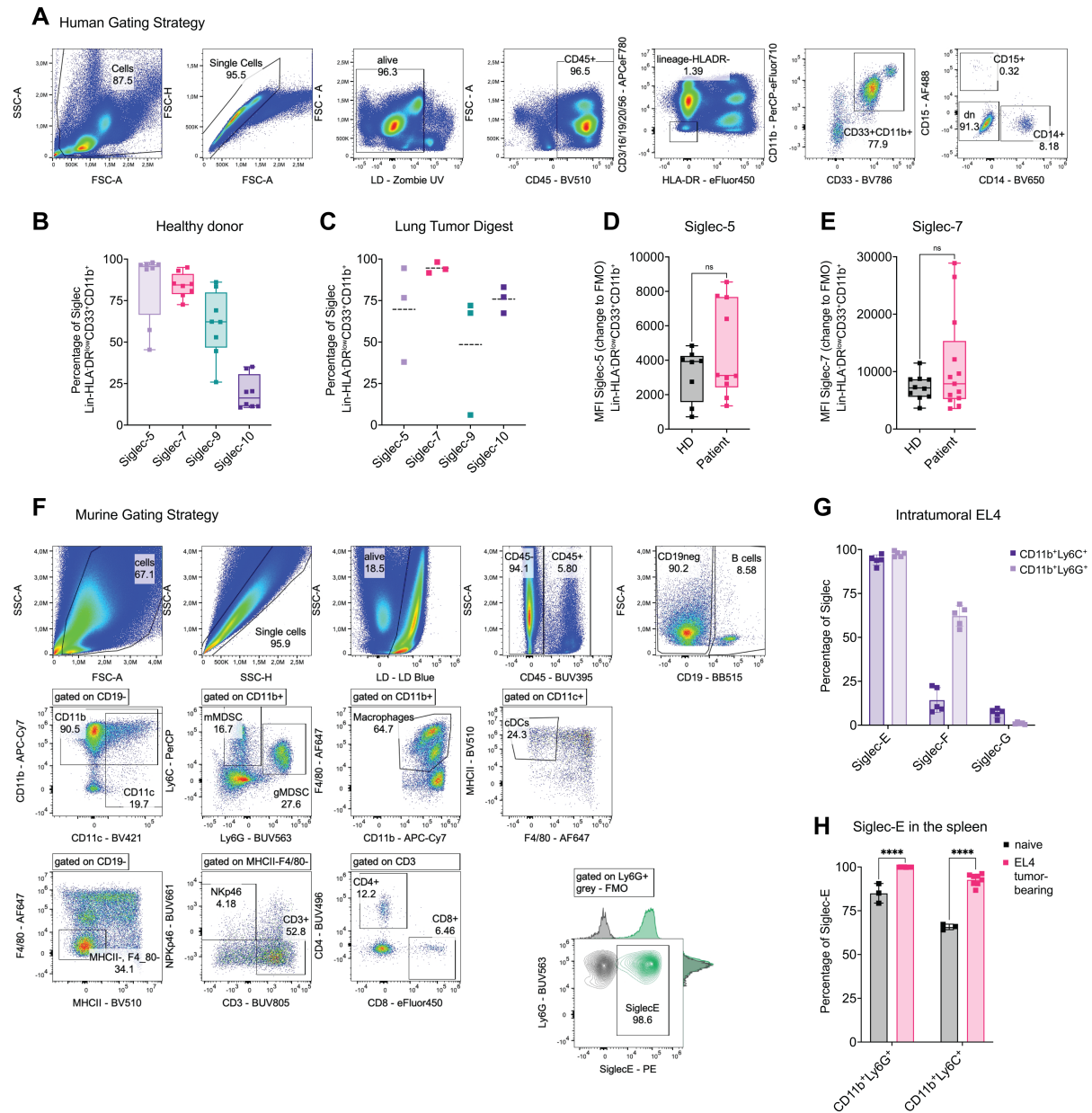The supplementary material includes:

Supplementary figures and tables

Figure S1: Expression of Siglecs on myeloid cells from various origins

(A) Exemplary gating strategy used for Fig 1A-E. MDSCs were gated as CD45$^+$Lin$^-$(CD3$^-$CD16$^-$CD19$^-$CD20$^-$CD56$^-$) HLADR^{low}CD33$^+$CD11b$^+$ cells. **(B)** Percentage of Siglec-5, Siglec-7, Siglec-9 and Siglec-10 expressed on CD45$^+$Lin$^-$HLADR^{low}CD33$^+$CD11b$^+$ cells derived from healthy donor peripheral blood (PB) or **(C)** intratumorally from lung cancer tumor digest. *N=3-8 donors with at least N=2* **(D)** MFI of Siglec-5, **(E)** Siglec-7 gated on CD45$^+$Lin$^-$HLADR^{low}CD33$^+$CD11b$^+$ cells derived from healthy donor and lung cancer patient PB. MFI is shown as change to FMO and was determined by flow cytometry. *N=8-13 donors with at least N=2 experiments.* **(F)** Representative gating strategy to identify murine immune cell types in tumor digest, peripheral blood and spleen. **(G)** Subcutaneously injected endpoint tumors from EL4 lymphoma engrafted mice were harvested, digested and immune cell infiltration was assessed by multicolor flow cytometry. Siglec-E, Siglec-F and Siglec-G expression was assessed on CD45$^+$CD11b$^+$Ly6G$^+$ and CD45$^+$CD11b$^+$Ly6C cells. *N=5 mice.* **(H)** Spleens from naïve and EL4 lymphoma tumor-bearing mice at endpoint were collected and analyzed for Siglec-E expression via flow cytometry. *N=3-8 mice per group. (continued on next page)*

Data are presented as mean. Error bar values represent SD. Two-tailed unpaired Student's t-test or multiple unpaired t-tests (H) was used. *P<0.05, **P<0.01, ***P<0.001, and ****P<0.0001
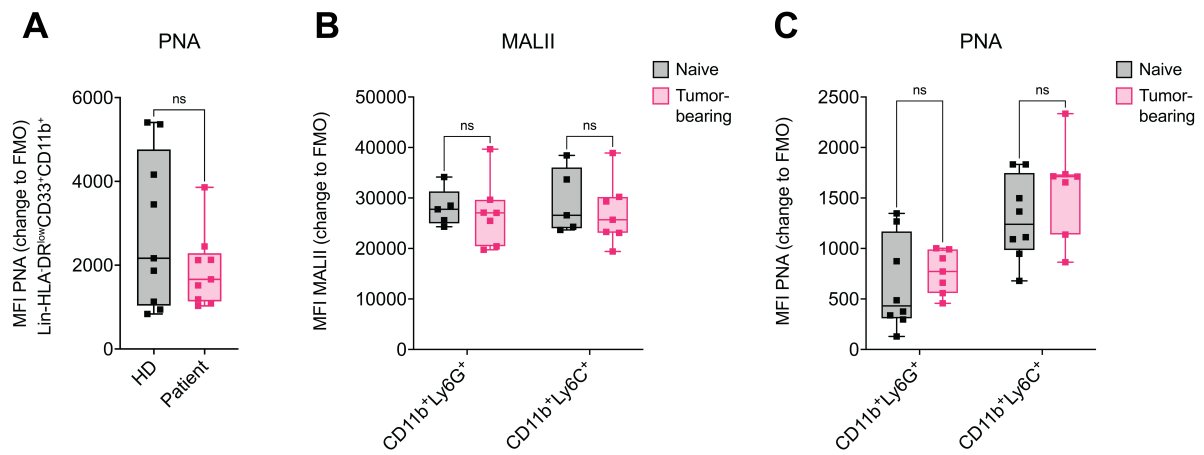
Figure S2: Sialoglycan expression on myeloid cells in human and mice

(A) PNA gated on PB-derived CD45$^+$Lin$^-$HLADR^{low}CD33$^+$CD11b$^+$ cells from primary lung cancer patient and healthy controls. MFI is shown as a change to FMO and was determined by flow. *N=8-12 donors with at least N=2.* **(B)** Fresh blood from B16F10 tumor-bearing mice and naïve wild type mice was collected at day 14 after tumor inoculation and analyzed for MALII or **(C)** PNA gated on CD45$^+$CD11b$^+$Ly6C$^+$ or CD45$^+$CD11b$^+$Ly6G$^+$ cells. MFI is shown as a change to FMO. *5-8 mice per group.*

Data are presented as mean. Error bar values represent SD. Two-tailed unpaired Student's t-test or multiple unpaired t-tests (B, C) was used. *P<0.05, **P<0.01, ***P<0.001, and ****P<0.0001.
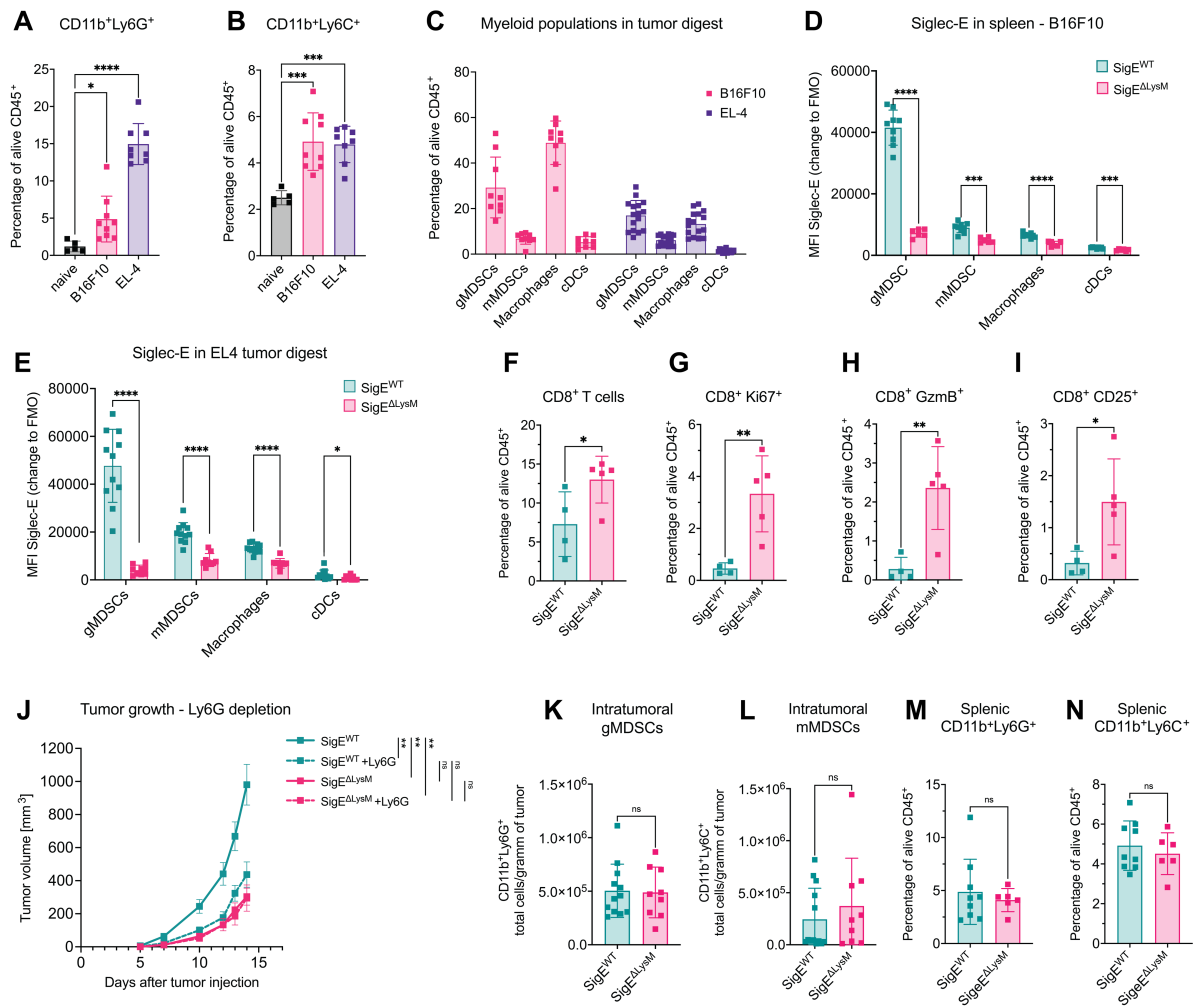
Figure S3: Siglec-E depletion on myeloid cells leads to survival benefits in tumor models of emergency myelopoiesis

(A) Spleens from naïve mice, EL4 lymphoma or B16F10 melanoma tumor-bearing mice at endpoint were collected and analyzed for CD11b$^+$Ly6G$^+$ and **(B)** CD11b$^+$Ly6C$^+$ cell infiltration. *N=5-9 mice per group*. **(C)** Tumor digest analyzed at endpoint for myeloid cell infiltration. gMDSCs (CD45$^+$CD11b$^+$Ly6G$^+$), mMDSCs (CD45$^+$CD11b$^+$Ly6C$^+$), macrophages (CD45$^+$CD11b$^+$F4/80$^+$), dendritic cells (DCs) (CD45$^+$CD11c$^+$MHCII$^+$F4/80$^-$) are shown as percentage of CD45 cells. *N=9-16 mice per group*. **(D)** MFI of Siglec-E expression in B16F10 tumor-bearing mice was analyzed on myeloid cells in the spleen at endpoint of the experiment. *N=6-9 mice per group*. **(E)** MFI of Siglec-E expression in EL4 tumor-bearing mice was analyzed on myeloid cells in tumor digest at endpoint. *N=4-5 mice per group*. **(F)** Subcutaneous EL4-GFP tumors were analyzed at endpoint via flow cytometry. Intratumoral CD8 T cells at endpoint (CD45$^+$aliveCD19$^-$NKp46$^-$CD3$^+$CD8$^+$) were further sub gated on **(G)** Ki67$^+$, **(H)** GranzymeB$^+$(GzmB$^+$) **(I)** CD25$^+$ CD8 T cells and quantified as percentage of CD45$^+$ cells. *N=4-5 mice per group*. **(J)** Tumor volume from pooled data from 2 independent experiments. Siglec-E$^{\Delta LysM}$ mice and Siglec-E^{WT} mice were treated up to 6 times with Ly6G depletion antibody as shown in Figure 2 I. *N=9-11 mice per group.* **(K)** Tumor digest analyzed at endpoint for myeloid cell infiltration. gMDSCs (CD45$^+$CD11b$^+$Ly6G$^+$) and **(L)** mMDSCs (CD45$^+$CD11b$^+$Ly6C$^+$) were quantified as cells per gram of tumor at the endpoint of the experiment. Pooled data from 2 independent experiments. *N=9-12 mice per group. (continued on next page)*

(M) Spleens from B16F10 melanoma tumor-bearing mice at endpoint were collected and analyzed for CD11b$^+$Ly6G$^+$ and **(N)** CD11b$^+$Ly6C$^+$ cells. Cells were quantified as percentage of alive CD45$^+$ cells. *N=6-9 mice per group.*

Data are presented as mean. Error bar values represent SD or SEM (F, G, L). Two-tailed unpaired Student's t-test, multiple unpaired t-tests (D, E) or one-way ANOVA followed by Dunnett's multiple comparisons test (A, B) was used. Tumor growth was compared by mixed-effects analysis followed by Bonferroni's multiple comparisons test. *P<0.05, **P<0.01, ***P<0.001, and ****P<0.0001.
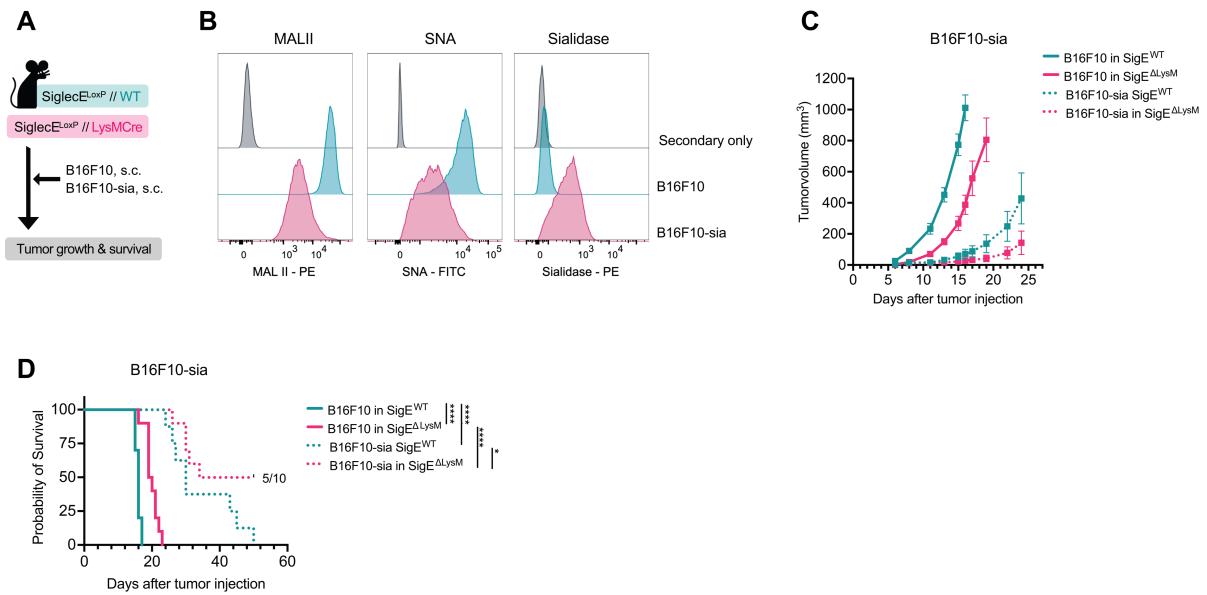
Figure S4: Combination of sialidase expression and lack of Siglec-E on myeloid cells prolongs survival *in vivo*

(A) Experimental setup: SigE$^{\Delta LysM}$ and SigE^{WT} littermates were subcutaneously injected with B16F10 or B16F10 cells expressing sialidase (B16F10-sia). Tumor growth and probability of survival were addressed as the main read-out. **(B)** B16F10 and B16F10-sia cells were stained for SNA, MALII and Sialidase expression to validate the successful generation of stable cell lines. Cell lines were stained before each experiment, representative results are shown. **(C)** Tumor volume and **(D)** Kaplan-Meier survival curves from pooled data from 2 independent experiments. *N=8-12 mice per group from 2 experiments.*

Data are presented as mean with error bars presenting SEM. Tumor growth was compared by mixed-effects analysis followed by Bonferroni's multiple comparisons test. For survival analysis, log-rank test was used followed by Šidák correction for multiple comparisons. *P<0.05, **P<0.01, ***P<0.001, and ****P<0.0001.
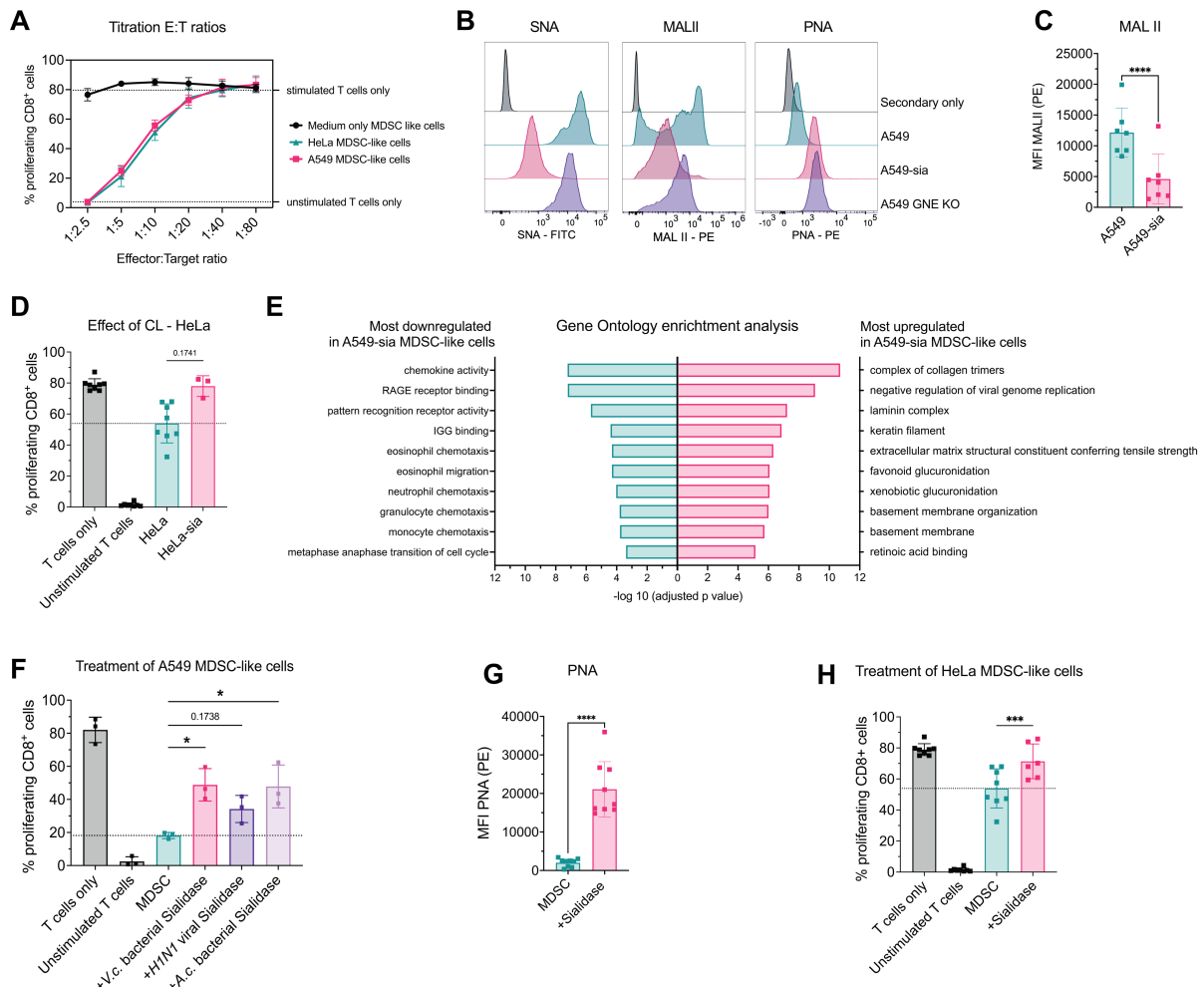
Figure S5: Sialylation modulates the suppressive potential of human CD33$^+$ cells

(A) Identification of E:T ratios to validate the suppressive capacity of CD33$^+$ cells against CD8$^+$ cells. Suppressive myeloid cells were generated by co-culture with A549 (pink), HeLa (green) or without cancer cells (black). Dotted lines indicate the proliferation of T cells alone with/without stimulation by IL-2, aCD3/28 microbeads. *N=4 donors of N=2 experiments*. **(B)** A549, A549 expressing sialidase (A549-sia) and A549-GNE KO cells were stained for SNA, MALII and PNA to validate the successful generation of stable cell lines. Cell lines were stained before each experiment, representative results are shown. **(C)** MALII staining was performed on suppressive CD33$^+$ cells on day 7 of the experiment. N=7 donors of *N=4 experiments.* **(D)** Percentage of proliferating CD8$^+$ cells upon co-culture (1:10 ratio) with indicated suppressive CD33$^+$ cells. Suppressive myeloid cells were generated using HeLa or HeLa-expressing sialidase (HeLa-sia) cancer cell lines. *N=3-8 donors.* **(E)** Gene ontology enrichment analysis of the top 10 up- and downregulated gene sets found in suppressive CD33$^+$ cells generated with A549-sia compared to parental A549 cell line. **(F)** PNA staining was assessed on suppressive CD33$^+$ cells after pretreatment with sialidase on day 7 of the experiment. *N=9 donors of N=5 experiments.***(G)** Proliferating CD8$^+$ cells in percentage co-cultured with suppressive CD33$^+$ cells generated by A549 co-culture in a ratio of 1:5. CD33$^+$ cells were used immediately or were pretreated with indicated sialidases. *N=3 donors of N=2 experiments.* **(H)** Percentage of proliferating CD8$^+$ cells upon co-culture (1:10 ratio) with suppressive CD33$^+$ cells generated by HeLa co-culture. CD33$^+$ cells were used immediately or were pretreated with sialidase.

Data are presented as mean and error bar values represent SD. Paired t-test was used. *P<0.05, **P<0.01, ***P<0.001, and ****P<0.0001.
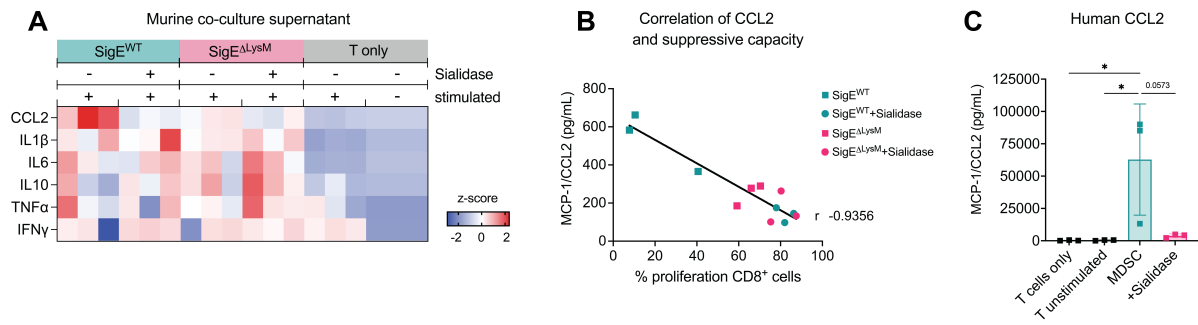
Figure S6: Suppressive myeloid cells correlate with CCL2 expression in humans and mice

(A) Cytokines found in the supernatant of murine MDSC:T cell co-cultures at endpoint of the experiment from figure 3. Z-scores were calculated for each cytokine. MDSCs were untreated, pretreated with sialidase or Siglec-E was added to the co-culture. *N=3 donors per group*. **(B)** Correlation of MCP-1 levels measured in supernatants of murine MDSC:T cell co-cultures at endpoint and percentage of proliferation of CD8+ T cells from the same condition. *N=3 donors per group*. **(C)** MCP-1/CCL2 found in the supernatant of human primary CD33+:CD8+ cell co-cultures at endpoint of the experiment from figure 3.5 H. CD33+ cells were untreated or pretreated with sialidase. Z-scores were calculated for each cytokine and are shown on a color scale from blue to red. *N=3 donors per group*.

Data are presented as mean and error bar values represent SD. One-way ANOVA was used. R shows the Pearson correlation coefficient. *P<0.05, **P<0.01, ***P<0.001, and ****P<0.0001.

Table S1: Flow cytometry antibodies

Target	Clone	Fluorochrome	Manufacturer	Catalog Number
CD11b	ICRF44	eFluor710	eBioscience	46-0118-42
CD11b	M1/70	APC-Cy7	BioLegend	101226
CD11c	N418	BV421	BioLegend	117330
CD11c	N418	FITC	BioLegend	117306
CD14	M5E2	BV650	BioLegend	301836
CD15	HI98	AF488	BioLegend	301910
CD16	B73.1	APC-Cy7	BioLegend	360709
CD19	SJ25C1	eFluor780	eBioscience	47-0198-42
CD19	6D5	BV570	BioLegend	115535
CD19	1D3	BB515	BD Biosciences	564509
CD20	2H7	eFluor780	eBioscience	47-0209-42
CD25	PC61.5	PE-Cy5.5	eBioscience	35-0251-82
CD3	SK7	eFluor780	eBioscience	47-0036-42
CD3	HIT3A	FITC	BioLegend	300306
CD3	145-2C11	BUV805	BD Biosciences	741895
CD3	145-2C11	PE	BioLegend	100308
CD33	WM53	BV786	BD Biosciences	740974
CD33	AC104.3E3	PE	Miltenyi Biotec	130-113-349
CD4	SK3	PE	eBioscience	12-0047-42
CD4	GK1.5	BUV496	BD Biosciences	612952
CD4	RM4-5	BV605	BioLegend	100548
CD45	HI30	BV510	BioLegend	304036
CD45	2D1	PerCP-Cy5.5	Invitrogen	45-9459-42
CD45	30-F11	BUV395	BD Biosciences	564279
CD56	CMSSB	eFluor780	eBioscience	47-0567-42
CD8	SK1	APC	BioLegend	344722
CD8	53-6.7	eFluor 450	eBioscience	48-0081-82
CD8a	53-6.7	PE-Cy7	eBioscience	25-0081-82
F4/80	BM8	AF647	BioLegend	123122
GzmB	NGZB	PE-eFluor610	eBioscience	61-8898-82
HLA DR	L243	eFluor450	eBioscience	9048-9952-120
Ki67	SolA15	AF532	eBioscience	58-5698-82
Ly6-C	HK1.4	PerCP	BioLegend	128028
Ly6-G	1A8	BUV563	BD Biosciences	612921
MHCII	M5/114.15.2	BV510	BioLegend	107636
NKp46	29A14	BUV661	BD Biosciences	741678
Siglec-10	5G6	PE	BioLegend	347604
Siglec-5	1A5	APC	BioLegend	352006
Siglec-7	6-434	PE	BioLegend	339204
Siglec-9	K8	AF647	BioLegend	351510
Siglec-E	M1304A01	PE	BioLegend	677104
Siglec-F	E50-2440	PE	BD Biosciences	552126
Siglec-G	SH2.1	APC	Invitrogen	17-5833-82
Siglec-H	551	PE	BioLegend	129605

9 ACKNOWLEDGEMENTS

10 APPENDIX

10.1 List of abbreviations

ADCC   Antibody-dependent cellular cytotoxicity

ATRA   All-trans-retinoic acid

CCR2   CC-chemokine receptor 2

CL   Cancer cell line

COSMC   Core 1 β3-galactosyltransferase Specific Molecular Chaperone

CTLA-4   Cytotoxic T lymphocyte-associated protein 4

CXCR2   CXC-chemokine receptor 2

DARPin   Designed ankyrin repeat protein

DC   Dendritic cell

DMEM   Dulbecco's Modified Eagle Medium

DN   Double negative

ECM   Extracellular matrix

eMDSC   Early-stage MDSCs

E:T   Effector:target

GAGs   Glycosaminoglycans

GAMs   Glioma-associated microglia and macrophages

GBM   Glioblastoma

gMDSC   Granulocytic myeloid-derived suppressor cells

GMP   Good manufacturing practice

GNE   UDP-N-acetylglucosamine 2-epimerase/N-acetylmannosamine kinase

HC-HAdV   High-capacity human adenovirus

HLA   Human leukocyte antigen

IFN-γ   Interferon-γ

IL   Interleukin

ITAM   Immunoreceptor tyrosine-based activatory motif

ITIM   Immunoreceptor tyrosine-based inhibitory motif

KIR   Killer immunoglobulin-like receptor

KO   Knockout

Le^x/Le^a sialyl-Lewis x and Lewis a

MALII   Maackia Amurensis Lectin II

MDSC   Myeloid-derived suppressor cells

MFI   Mean fluorescence intensity

MHC   Major histocompatibility complex

mMDSC   Monocytic myeloid-derived suppressor cell

MMPs	Matrix metalloproteinases
Neu5Ac	N-acetyl-neuraminic acid
Neu5Gc	N-gycolyl-neuraminic acid
NK cell	Natural Killer cell
NO	Nitric oxide
OCT	Optimal cutting temperature compound
PBMCs	Peripheral blood mononuclear cells
PD-1	Programmed death 1
PMN-MDSC	Polymorphonuclear myeloid-derived suppressor cells
PNA	Peanut Agglutinin
PT-Cy	Post-transplantation cyclophosphamide
ROS	Reactive oxygen species
RPMI	Roswell Park Memorial Institute Medium
SAMP	Self-associated molecular pattern
SHP	Src-homology 2 domain (SH2)-containing phosphatases
Siglec	Sialic acid-binding immunoglobulin-like lectins
SigE$^{\Delta LysM}$	Siglec-ExLysM-Cre; mice with KO of Siglec-E on LysM expressing cells
SigE^{WT}	Siglec-E wild type
SGRP	SIRPγ-related protein
SNA	Sambucus Nigra Lectin
TAM	Tumor-associated macrophage
TAN	Tumor-associated neutrophile
TCR	T cell receptor
TGF-β	Transforming growth factor β
TME	Tumor microenvironment
TNFα	Tumor necrosis factor alpha
Treg	CD4$^+$ regulatory T cells
V.c.	Vibrio cholerae
VEGF	Vascular Endothelial Growth Factor

10.2 List of figures and tables

10.3 Curriculum Vitae

Ronja Wieboldt

✉ ronja.wieboldt@gmail.com

Research

10/2023 – today	**Postdoctoral Researcher**, Department of Biomedicine, University of Basel, CH Group of Prof. Dr. Heinz Läubli (Cancer Immunotherapy)
08/2020 – 09/2023	**PhD student**, Department of Biomedicine, University of Basel, CH Group of Prof. Dr. Heinz Läubli (Cancer Immunotherapy)
01/2019 – 07/2023	**Marie Curie Early-Stage Researcher** University Hospital of Basel, Clinical Hematology, CH Topic: NK cell adoptive immunotherapy in hematological malignancies Research stay at Karolinska Institutet (10/2019) at the lab of Prof. Dr. Hans-Gustaf Ljunggren
2015 – 2018	**Research Assistant/Student Assistant** University Hospital Hamburg and Philipps-Universität Marburg, DE Internships in 6 different laboratories in clinical research and basic research with cancer focus (2 - 12 month)

Education

08/2020 – 09/2023	**PhD in Biomedical Research** Department of Biomedicine, University of Basel, Basel, CH Group of Prof. Dr. Heinz Läubli (Cancer Immunotherapy) Topic: Interaction of sialylated glycans with Siglec receptors on suppressive myeloid cells
10/2016 – 10/2018	**Master of Science in Biomedical Science** Philipps-Universität Marburg, Marburg, DE
Master thesis	Center for Tumor Biology and Immunology, Marburg, DE Group of Prof. Dr. Thorsten Stiewe Topic: p53 and its interaction with the cytoskeleton
10/2013 – 07/2016	**Bachelor of Science in Biomedical Science** Philipps-Universität Marburg, Marburg, DE
Bachelor thesis	Department of Visceral, Thoracic and Vascular Surgery, University Hospital Marburg, Marburg, DE at the group of Dr. Emily Slater Topic: Establishment of Glypican-1 on exosomes as a potential biomarker for the detection of familial pancreatic cancer

Additional Education

In addition to regular classes from the University Basel and the Transferable Skills Program:

2023	Mentoring Program: ZOOM@Novartis
2021	Project Management in Clinical Study Operation
2021	Laboratory Animal Course (FELASA Category B)
2020	Good Clinical Practice (GCP): Basic and Advanced Course

Conferences and Symposia

In addition to regularly presenting my work at lab meetings, institute and graduate school seminars:

04/2023	AACR Annual Meeting 2023, April 2023, Orlando, USA, *Poster presentation*
10/2022	University of Basel Immunology Community Retreat Engelberg (UBICo Meeting), Engelberg, CH, *Poster presentation*
09/2022	6th Annual Meeting of the Upper Rhine Immunology Group (URI), Karlsruhe, DE, *Poster presentation*
08/2021	33rd Meeting of the Swiss Immunology PhD student, Ermatingen, CH, *Oral presentation*

List of Publications

- Pavlakis E, Neumann M, Merle N, **Wieboldt R**, Wanzel M, Ponath V; Pogge von Strandmann E, Elmshäuser S, Stiewe T. (2023) Mutant p53-ENTPD5 control of the calnexin/calreticulin cycle: a druggable target for inhibiting integrin-α5-driven metastasis, *J. Exp. Clin. Cancer Res.* doi:10.1186/s13046-023-02785-z
- Schmassmann P, Roux J, Buck A, Tatari N, Hogan S, Wang J, Rodrigues Mantuano N, **Wieboldt R,** Lee S, Snijder B, Kaymak D, Martins T, Ritz M, Shekarian T, McDaid M, Weller M, Weiss T, Läubli H, Hutter. *(*2023) The Siglec-sialic acid-axis is a target for innate immunotherapy of glioblastoma. *Sci. Transl. Med.* doi: 10.1126/scitranslmed.adf5302
- **Wieboldt R**, Läubli H. (2022) Glycosaminoglycans in cancer therapy. *Am J Physiol Cell Physiol.* doi:10.1152/ajpcell.00063.2022
- Wang J, Manni M, Bärenwaldt A, **Wieboldt R**, Kirchhammer N, Ivanek R, Stanczak M, Zippelius A, König D, Rodrigues Manutano N, Läubli H. (2022) Siglec Receptors Modulate Dendritic Cell Activation and Antigen Presentation to T Cells in Cancer. *Front Cell Dev Biol*. doi: 10.3389/fcell.2022.828916
- Tschan-Plessl A, Kalberer CP, **Wieboldt R,** Stern M, Siegler U, Wodnar-Filipowicz A, Stern M, Siegler U, Wodnar-Filipowicz A, Gerull S, Halter J, Heim D, Tichelli A, Tsakiris D, Malmberg J, Passweg J, Bottos A. (2021) Cellular immunotherapy with multiple infusions of in vitro-expanded haploidentical natural killer cells after autologous transplantation for patients with plasma cell myeloma. *Cytotherapy*. doi:10.1016/j.jcyt.2020.09.009
- Landerer H, Arnone M, **Wieboldt R**, Goersch E, Konantz M, Lengerke C. (2020) Two Flow Cytometric Approaches of NKG2D Ligand Surface Detection to Distinguish Stem Cells from Bulk Subpopulations in Acute Myeloid Leukemia. *J. Vis. Exp*. doi:10.3791/61803
- Bartsch DK, Gercke N, Strauch K, **Wieboldt R**, Matthäi E, Wagner V, Rospleszcz S, Schäfer A, Franke F, Mintziras I, Bauer C, Grote T, Figiel J, Di Fazio P, Burchert A, Reinartz S,Pogge von Strandmann E, Klöppel G, Slater P. (2018) The combination of miRNA-196b, LCN2, and TIMP1 is a potential set of circulating biomarkers for screening individuals at risk for familial pancreatic cancer. *J Clin Med*. doi:10.3390/jcm7100295

  Unpublished work
- **Wieboldt R,** Carlini E, Lin CW, Börsch A, Zingg A, Lardinois D, Herzig P, Don L, Zippelius A, Läubli H, Rodrigues Manutano N. (2023) Engagement of sialylated glycans with Siglec receptors on suppressive myeloid cells inhibit anti-cancer immunity via CCL2, *under review, bioRxiv preprint: https://doi.org/10.1101/2023.06.29.547025*
- Freitag P, Kolibius J, **Wieboldt R**, Weber R, Hartmann P, van Gogh M, Brücher D, Läubli H, Plückthun A. (2023) DARPin-fused T cell engager (DATE) for adenovirus-mediated cancer therapy, *submitted*
- Martins T, Tatari N, Kaymak D, Bartoszek E, Hogan S, **Wieboldt R**, Ritz M-R, Buck A, Marta McDaid M, Gerber A, Beshirova A, Shekarian T, Etter M, Heider A, Mohamed H, Abel I, Schmassmann P, Boulay J-L, Snijder B, Weiss T, Läubli H, Hutter G. (2023) Enhancing anti-EGFRvIII CAR T cell therapy against glioblastoma with a paracrine SIRPγ-derived CD47 blocker, *submitted, bioRxiv preprint: https://doi.org/10.1101/2023.08.31.555122*